

X-RAY EMISSIONS FROM ACCRETING WHITE DWARFS: A REVIEW

K. MUKAI^{1,2}

¹*CRESST and X-ray Astrophysics Laboratory, NASA/GSFC, Greenbelt, MD 20771, USA*

²*Also Department of Physics, University of Maryland, Baltimore County, 1000 Hilltop Circle, Baltimore, MD 21250, USA*

(Received July 1, 2016; Revised September 27, 2016; Accepted April 8, 2018)

Submitted to PASP

ABSTRACT

Interacting binaries in which a white dwarf accretes material from a companion — cataclysmic variables (CVs) in which the mass donor is a Roche-lobe filling star on or near the main sequence, and symbiotic stars in which the mass donor is a late type giant — are relatively commonplace. They display a wide range of behaviors in the optical, X-rays, and other wavelengths, which still often baffle observers and theorists alike. Here I review the existing body of research on X-ray emissions from these objects for the benefits of both experts and newcomers to the field. I provide introductions to the past and current X-ray observatories, the types of known X-ray emissions from these objects, and the data analysis techniques relevant to this field. I then summarize of our knowledge regarding the X-ray emissions from magnetic CVs, non-magnetic CVs and symbiotic stars, and novae in eruption. I also discuss space density and the X-ray luminosity functions of these binaries and their contribution to the integrated X-ray emission from the Galaxy. I then discuss open questions and future prospects.

Keywords: accretion, accretion disks — binaries: symbiotic — stars: dwarf novae — novae, cataclysmic variables — X-rays: binaries

arXiv:1703.06171v1 [astro-ph.HE] 17 Mar 2017

1. INTRODUCTION

White dwarf is the most common endpoint of stellar evolution, and many stars are born in binary systems with sufficiently small initial separations so that they go through one or more phases of mass exchange. As a result, there are numerous accreting white dwarfs (AWDs) in the solar neighborhood (see §8.1). The wide array of phenomena exhibited by AWDs make them interesting objects of study on their own right. Their proximity and relative simplicity (relativistic effects can be neglected for most purposes) make them an excellent laboratory to study accretion physics, on their own or in comparison with other accretion-driven systems. An understanding of the long-term evolution of AWDs of all types is necessary in studying the progenitor channels of Supernovae of Type Ia (SNIa), which is one of the outstanding questions in astrophysics and cosmology. Finally, AWDs turn up in significant numbers in transient searches and in X-ray surveys, and are an important contributor to the unresolved X-ray emissions from the Galactic ridge and bulge. Thus, researchers who are interested in the X-ray sky in general, including those that are engaged in variability and X-ray surveys not specifically targeted to study AWDs, must pay attention to AWDs, and learn to recognize them.

Accretion and nuclear fusion are the two primary energy sources in AWDs. When fusion is not taking place, the accretion luminosity often dominates over those of component stars, and a significant fraction is emitted as X-rays. Nuclear fusion can take place either explosively in the form of nova eruptions, or in the form of continuous shell burning. While in progress, nuclear fusion dominates over accretion; in addition, it is also possible that total energy emitted by AWDs integrated over its life time is dominated by nuclear fusion, depending on the fraction of the accreted hydrogen burned. When the surface of the nuclear-burning white dwarf is exposed, it is a powerful source of soft X-rays (predominantly below 0.5 keV) as supersoft sources (SSSs). Finally, both accretion and fusion can lead to mass loss, with velocities as high as the escape velocity. Such flows also have kinetic energy sufficient to result in X-ray emission, if they encounter a strong shock in a sufficiently dense environment.

It is often the case that a large fraction of the luminosity of AWDs is emitted in the X-ray range. The X-ray emission mechanism is usually tied to the processes on, or immediately around, the white dwarf, while optical observations reveal the processes further out. Therefore, X-ray observations are an essential tool for us to advance our understanding of AWDs, but if and only if interpreted in the context of multiwavelength observations.

For the purpose of this review, I define X-rays as photons in the energy range 0.1–100 keV, further divided into soft (0.1–2 keV), medium energy (2–10 keV), and hard (10–100 keV) bands. The extreme ultraviolet (EUV) range, if defined as 60–1000Å, overlaps with the softest range of the soft X-rays at 0.1–0.2 keV where it is least susceptible to interstellar absorption. I include EUV observations in this band in this article, implicitly at times and explicitly at other times. Here I review the state of the art of X-ray observations of AWDs as of late 2016. I include both major classes of AWDs, cataclysmic variables (CVs) with a Roche-lobe filling donor, and symbiotic stars with a late type giant donor, in this review.

This review is intended to provide a summary of subclasses, the tools of trade for X-ray studies of AWDs, the major findings obtained to date and questions, and puzzles that remain. The intended audience includes both researchers familiar with AWDs in general but not with X-ray observations, and X-ray astronomers not intimately familiar with AWDs. If this review also proves useful to experts of this field as a reference, and provide a chance for them to reflect on larger issues that can be addressed by X-ray observations of AWDs, I will have succeeded well beyond the minimum requirements I set myself.

The rest of this review is structured as follows. In the next two subsections, I present a brief overview of X-ray observatories and the major subclasses of AWDs for the non-experts. In §2, I present a brief overview of physical processes leading to X-ray emission in AWDs. In §3, I present different methods for extracting information from X-ray data. I discuss the problem of identifying AWDs and its subclasses in §4. I present the physical and astrophysical inferences for magnetic systems, non-magnetic systems, and novae, respectively, in §5, 6, and 7. I then discuss the collective properties of AWDs in §8, followed by a discussion of the problems and questions raised in the preceding sections in §9. I conclude with a brief summary and future prospects in §10.

1.1. *Brief Overview of X-ray Observatories*

The earliest type of technology used for X-ray astronomy are the non-imaging, collimated proportional counters, operating primarily in the medium energy band. While many such instruments had a large collecting area, they also suffered from large background rates, both due to particles and to celestial X-rays from objects other than the intended targets, and hence had limited sensitivities. Non-imaging instruments are therefore useful only for bright X-ray sources

(of order 10^{-11} ergs cm $^{-2}$ s $^{-1}$ or higher), or just a few dozen X-ray brightest AWDs. Nevertheless, important results on AWDs have been obtained with non-imaging instruments, notably the large area counter (LAC) on-board (1987–1991; Turner et al. 1989) and the proportional counter array (PCA) on-board *RXTE* (1995–2012; Jahoda et al. 1996).

True imaging in X-rays started with *Einstein* (1978–1981; Giacconi et al. 1979) in the 0.1–4 keV band. Imaging soft X-ray observation continued with *ROSAT* (1990–1999; Trümper 1983), which also carried the Wide Field Camera (WFC), which was sensitive to EUV photons. *EUVE* (1992–2001; Bowyer & Malina 1991) was a mission dedicated to EUV observations. In the medium energy X-ray range, *ASCA* (1993–2000; Tanaka, Inoue & Holt 1994) was the first satellite to carry out imaging observations in energies up to 10 keV. *XMM-Newton* (1999–present; Jansen et al. 2001) and *Chandra* (1999–present; Weisskopf, O’Dell & van Speybroeck 1996) can reach flux levels below 10^{-14} ergs cm $^{-2}$ s $^{-1}$ in the 0.3–10 keV band. Other recent instruments with imaging capabilities in the soft and medium energy ranges include the X-ray Imaging Spectrometer (XIS) on-board *Suzaku* (2005–2015; Mitsuda et al. 2007) and the X-Ray Telescope (XRT) on-board *Swift* (2004–present; Gehrels et al. 2004).

The technology used to build soft and medium-energy X-ray telescopes alone is not sufficient to build hard X-ray imaging optics. One successful alternative is the coded mask aperture. Instruments based on this technology have a large field of view (FOV), require long integration times, and sources can only be “imaged” after specialized and computer-intensive processing. Coded-aperture mask instruments can then localize individual sources to several arcminutes. Two prominent examples are *INTEGRAL* (2002–present; Winkler et al. 2003) and the burst alert telescope (BAT) on-board *Swift*. More recently, X-ray telescope technology has been extended to hard X-rays using multi-layer coating. The first satellite to achieve this is the *NuSTAR* mission (2012–present; Harrison et al. 2013).

In the soft and medium energy X-rays, CCD-based detectors have become the standard. CCD data typically have energy resolution of 2–6%, which is very low in the standards of optical spectroscopy. Grating instruments provide high resolution, but have relatively low effective areas, once the efficiency of the grating is taken into account. Thus one can only observe the X-ray brightest AWDs. In the soft X-ray/EUV, the spectrometer instrument on *EUVE* and the low energy transmission grating (LETG) on *Chandra* have produced notable results on AWDs. At higher energies, results on AWDs have been published using the reflection grating spectrometers (RGS) on *XMM-Newton* in the 0.3–2 keV range, and using the high energy transmission grating (HETG) on *Chandra* in the 0.5–8 keV range.

1.2. Brief Overview of Many Object Types

CVs and symbiotic stars can be sub-classified in myriad ways. While many of the detailed divisions are beyond the scope of this review, it is impossible to describe AWDs without referring to at least some of the major subclasses.

CVs are systems in which the mass donor is a Roche-lobe filling late type star on or near the main sequence. Those with hydrogen-deficient donors are called the AM CVn stars (Solheim 2010): they are sometimes treated as a subclass of CVs, and sometimes considered a parallel class. Excluding AM CVn stars, the majority of CVs have an orbital period (P_o) in the 80 min–10 hr range, and their evolution is driven by angular momentum loss. Gravitational radiation is a mechanism that is believed to operate in all CVs (Kraft, Mathews & Greenstein 1962), while an additional mechanism, almost certainly magnetic braking, operates mostly for systems with periods longer than ~ 3 hrs (Knigge, Baraffe & Patterson 2011). CVs evolve from long period to short, temporarily detaching when the magnetic braking mechanism becomes less effective and resuming accretion at $P_o \sim 2$ hrs. Therefore, there are fewer CVs with 2–3 hr orbital periods, referred to as the period gap.

In symbiotic stars, the mass donor is a late type giant. While nuclear evolution of the giant ultimately drives the mass transfer in symbiotic stars, it is not clear how many systems operate purely by capturing the wind of the donor, how many donors overflow their Roche-lobe, and how important the hybrid “wind Roche-lobe overflow” mechanism (Mohamed & Podsiadlowski 2007) is.

Traditional classification schemes of CVs relied largely on their variability properties. I will use the term “nova eruptions” to refer to high amplitude brightening caused by violent ejection of mass powered by thermonuclear run-aways. Perhaps the only way for AWDs to avoid nova eruptions over evolutionary time scales is if the accreted matter is continuously burned: such systems are observed as SSSs, while nova eruptions lead to a temporary (weeks–years) super-soft source stage. Variability unrelated to nuclear burning includes dwarf nova outbursts, which are widely believed to be due to disk instability that operates when the mass transfer rate from the donor is low (see §6.2). Other CVs exhibit occasional low states, whose origins are less clear.

In the context of this review, the most important classification scheme is based on the magnetic field of the white dwarf primary. CVs are said to be non-magnetic when the field is not strong enough to alter the accretion flow, often

taken to mean that the accretion disk extends all the way down to the surface of the primary. In magnetic CVs, the magnetic field controls the flow at least near the primary. The latter are divided into two major subclasses. In intermediate polars (IPs, also known as DQ Her type systems; [Patterson 1994](#)), a partial accretion disk is usually present, and the spin period (P_s) of the primary is significantly shorter than P_o . In polars (or AM Her type systems; [Cropper 1990](#)), the magnetic field is so strong as to prevent the formation of an accretion disk, optical and infrared light contains a strong contribution by the cyclotron emission from the accretion region and is therefore polarized, and the spin is usually synchronized to the orbit ($P_s = P_o$). Asynchronous polars are objects in which P_s and P_o differ by $<1\%$ but otherwise have the properties of a polar. In symbiotic stars, the equivalent of polars should not exist due to the much larger binary separation, but there is no obvious reason why IP-like systems should not exist.

For further discussion of CV subclasses, their inter-relationships, and evolutionary scenarios, readers are directed to [Warner \(1995\)](#) and the upcoming review by [Patterson & Knigge \(2017\)](#).

2. TYPES OF X-RAY EMISSIONS AND BASIC PHYSICAL PROCESSES

X-rays from AWDs are mostly, if not exclusively, emitted through thermal processes. Thermal X-ray emissions are usually divided into optically thick (optical depth, τ much greater than 1) and optically thin ($\tau < 1$). This is clearly a simplification: many AWDs may have regions of intermediate optical depth ($\tau \sim 1$).

When the accretion flow hits the white dwarf surface and is shocked above the surface, the plasma must cool and further decelerate before it can settle onto the white dwarf surface. For the highest temperature, fully ionized plasma, the Bremsstrahlung continuum dominates over line emission. As the plasma cools to lower temperatures ($kT \sim 1$ keV), when many ions retain some electrons, line cooling becomes important and then dominant ([Gehrels & Williams 1993](#)).

In the case of radial accretion (either spherically symmetric or magnetically confined “accretion column¹”), accretion flow is initially cool and supersonic, and at the free-fall velocity that approaches the final value of

$$v_{ff} = \sqrt{\frac{2GM_{wd}}{R_{wd}}}$$

where M_{wd} and R_{wd} are the mass and radius of the white dwarf primary, respectively, and G is the Newtonian constant of gravity. This is a very steep function of M_{wd} because of the mass-radius relationship for white dwarfs². The strong shock condition dictates that the post-shock flow initially travels at $1/4v_{ff}$, and the difference is converted to thermal energy, leading to

$$kT_{s,ff} = \frac{3}{8} \frac{GM_{wd}\mu m_H}{R_{wd}}$$

where m_H is the proton mass and μ is the mean molecular weight of the accreting gas (here assumed to be 0.615), and k is Boltzmann’s constant. The maximum shock temperatures are 22, 36, 57, and 92 keV, respectively, for 0.6, 0.8, 1.0, and 1.2 M_\odot white dwarfs (see also [Figure 1](#)).

The Bremsstrahlung cooling time scale t_c of a single temperature, X-ray emitting plasma is

$$t_c = 6.8 \times 10^{14} \frac{\sqrt{kT}}{n} s$$

where the temperature kT is in units of keV, the number density n is in units of cm^{-3} . Therefore, a 10 keV plasma with a density of 10^{15}cm^{-3} will cool in roughly 2 seconds, numbers not atypical of those encountered in AWDs.

As first investigated by [Aizu \(1973\)](#), the resulting shock height is such that the time for the shocked plasma to reach the white dwarf surface equals the total cooling time, which has to be calculated along with the density and the temperature profile of the post-shock region. A sample profile is shown in [Figure 2](#). As can be seen, the density rises quickly towards the white dwarf surface. As a result, most of the cooling takes place near the bottom of the post-shock region, which is the origin of the lowest temperature emission, while the origin of the highest energy photons is more uniform.

A simple expectation for non-magnetic CVs is that half the available potential energy is radiated away in the Keplerian accretion disk. The disk around AWDs is never hot enough to emit X-rays; instead, they are sources of IR,

¹ Here I use this terminology without necessarily implying a specific shape of the accretion region.

² Throughout this review, I use the convenient formula due to [Webbink](#) as reported in [Pringle & Webbink \(1975\)](#) for numerical calculations. While this is not the most up-to-date mass-radius relationship for white dwarfs, and the core temperature and composition do change the relationship somewhat, the [Webbink](#) formula is sufficiently accurate for most current needs in regard to AWDs.

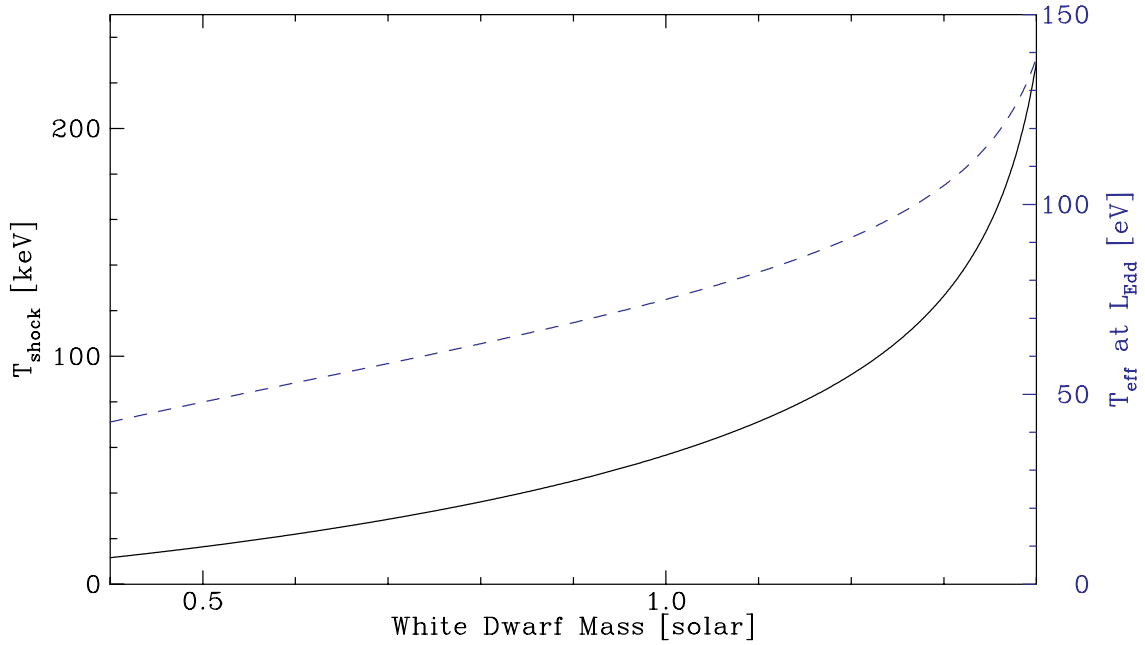


Figure 1. Expected shock temperature as a function of the white dwarf mass, assuming a radial accretion with free-fall from infinity (solid black line, left axis). Also plotted is the maximum possible effective temperature at local Eddington limit as a function of the white dwarf mass (dashed blue line, right scale).

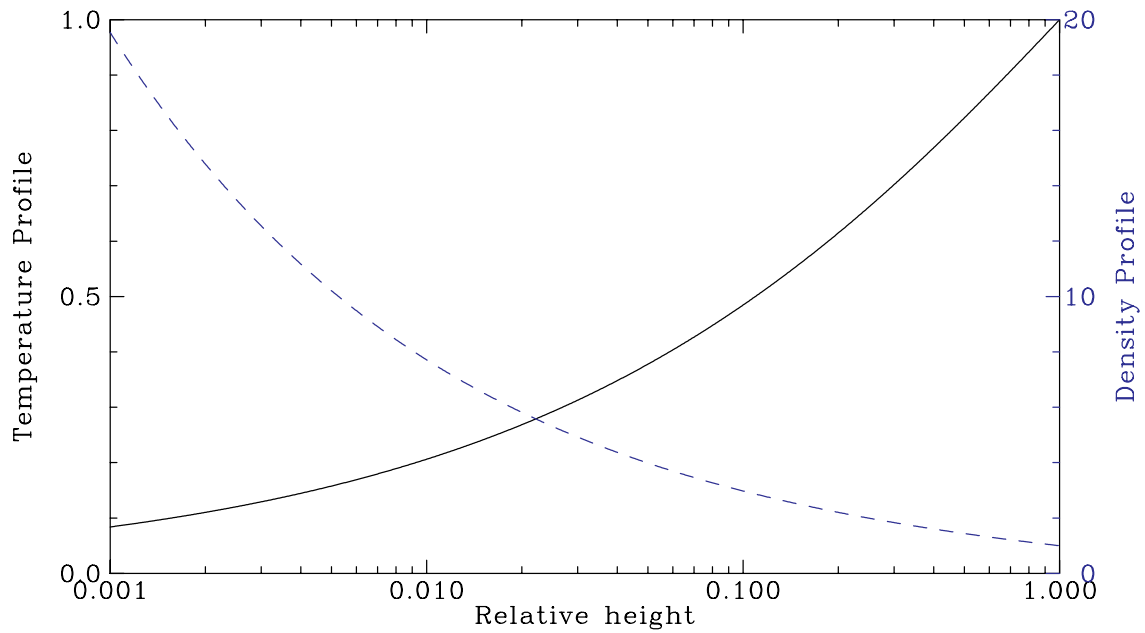


Figure 2. Relative temperature (solid black, left axis) and density (dashed blue, right axis) of the post-shock region, in an Aizu-type accretion column, normalized to the respective values at the shock.

optical, and UV photons. If the white dwarf is spinning slowly compared to the break-up rate, then the other half is available in the boundary layer between the disk proper (i.e., the Keplerian part) and the white dwarf. If the boundary layer remains optically thin, it should emit hard and medium energy X-rays broadly similar to those seen in magnetic CVs (Patterson & Raymond 1985a). However, the theory of the boundary layer is much more complex than that of

accretion column in magnetic CVs: while a one-dimensional theory is sufficient to establish the overall characteristics of an accretion column, the theory of boundary layer must be at least two dimensional. The most pressing question is whether the shock can be strong. If it is, a scaled (by a factor of 2 in available energy) version of the Aizu model might provide a good initial approximation. On the other hand, if there may be a series of weak shocks, the maximum temperature of the emitting plasma is lower still.

Optically-thin, thermal X-ray emission is also seen during nova eruptions. When the nova occurs in symbiotic stars, the ejecta are embedded in the dense wind of the mass donor. In this case, the ejecta promptly encounters the red giant wind and strongly shocked. In contrast, when the nova occurs in CVs, any shocks present must be internal, in that collisions are between multiple components of the ejecta with different velocities. The expected density is a strong function of time, as the ejecta expand. Since a 1 keV, $n = 10^6 \text{ cm}^{-3}$ plasma has a cooling time of ~ 20 yrs, X-ray emission observed several weeks after eruption may represent a small fraction of the thermal energy of the shocked plasma; the predominant cooling mechanism in this case is likely to be adiabatic expansion. Significant radiative cooling requires a high density: either the very early phase of an eruption when the ejecta occupies a small volume, or near the red giant mass donor in a relatively tight orbit around the white dwarf.

It is also possible for the accretion disk wind (Drew & Proga 2000) to collide with something else, get shocked, and emit medium energy X-rays. In both novae and in accretion disk wind shocks, non-equilibrium ionization (NEI) effect may need to be considered. In NEI plasma, the ionization state of elements have not caught up to the current temperature, a situation that is expected when the ionization time nt is less than $10^{12} \text{ cm}^{-3} \text{ s}$ (Smith & Hughes 2010). This effect is not of significant concern for the accretion powered X-rays, which is in a steady-state situation where the injection of freshly shocked material is balanced by radiative cooling in AWDs. By definition, steady-state requires a radiative shock, in which case $nt_c > 10^{14} \text{ cm}^{-3} \text{ s}$, hence the X-ray emitting plasma is in ionization equilibrium.

Soft X-ray and EUV emissions in AWDs can be from the white dwarf surface itself, or from an optically thick boundary layer (Patterson & Raymond 1985b). The former is inevitable at some level, even when the primary energy release mechanism is the optically thin X-ray emission, because it is expected to occur near the white dwarf surface. A substantial fraction (up to a half) must therefore be intercepted by the white dwarf photosphere, much of it absorbed and reprocessed (see below for a discussion of “reflection”). This is the baseline mechanism leading to the soft component in magnetic CVs (Lamb & Masers 1979). Other mechanisms include accretion of dense blobs, which liberate the kinetic energy deep within the white dwarf photosphere (Kuijpers & Pringle 1982), the accretion energy liberated within the optically-thick boundary layer (Patterson & Raymond 1985b), and nuclear burning seen in SSSs and in novae (Kahabka & van den Heuvel 1997).

The combination of the typical emitting area A (some fraction of the total surface area of the white dwarf) and the typical luminosity (L) often found in the optically-thick component in AWDs results in effective temperatures (T_{eff}) in the range $\sim 100,000\text{--}1,000,000\text{K}$ (kT of $\sim 9\text{--}90$ eV). Note, however, that the lower limit of this observed range of temperatures may well be determined by the combination of interstellar absorption and instrument sensitivity, rather than the intrinsic properties of AWDs. The upper limit, on the other hand, is constrained by radiation pressure. Although this is often considered in terms of the Eddington luminosity, the local version of the argument is also valid: accretion rate per unit area cannot be so high that the resulting radiation pressure exceeds the local gravity. This translates to an upper limit to the local accretion rate, and since $L/A \propto T_{eff}^4$, an upper limit to the temperature. The Eddington limit of white dwarf temperature is shown in, e.g., Figure 5 of Williams, King & Brooker (1987). This figure also illustrates the atmosphere limit, which is based on a higher opacity than pure electron scattering. Since matter is unlikely to be fully ionized in AWDs, this is a more realistic case and results in lower maximum temperatures than the Eddington limit.

The partially ionized nature of matter also means that the blackbody model is only an approximation. As photons emerge from deep inside the optically thick region through the $\tau \sim 1$ zone, it leaves an imprint on the outgoing spectrum in the form of absorption lines and edges; the temperature, the pressure and the bulk motion of this region determines what features are present, and how broad they are. The detailed models of such spectra are called stellar atmosphere models, but the situation in AWDs is more complex than that typically found in stars. Composition is a key issue, determined by the competition between fresh accretion and gravitational settling, and the exact mixture of pristine gas vs. nuclear burning products. Another is the temperature structure. Irradiation by X-rays results in a temperature inversion above the photosphere and a flatter temperature profile with optical depth; the edges and lines will be weak if the temperature profile is flat where these features are formed (Williams, King & Brooker 1987).

The X-ray photons that are emitted by the AWDs often interact with matter inside the binary, circum-binary matter, and the interstellar medium (ISM). For X-rays below 10 keV, photoelectric absorption is the dominant process. The strong energy dependence of photoelectric absorption is encoded the very terminology “hard” and “soft” X-rays. For reference, equivalent hydrogen column density (N_{H} ; assuming solar composition) at which the transmission is $1/e$ is $1.2 \times 10^{20} \text{ cm}^{-2}$, $1.4 \times 10^{21} \text{ cm}^{-2}$, $2.3 \times 10^{22} \text{ cm}^{-2}$ and $2.8 \times 10^{23} \text{ cm}^{-2}$, respectively for photon energies of 0.2, 0.5, 2.0, and 5.0 keV. For an assumed ISM density of 0.1 cm^{-3} , the resulting N_{H} is $1.2 \times 10^{20} \text{ cm}^{-2}$ at a distance of $\sim 400 \text{ pc}$.

However, absorption significantly in excess of the expected ISM absorption is often seen in the X-ray spectra of AWDs. The measured X-ray N_{H} is often significantly greater than that expected from optical or UV extinction (using, e.g., the calibration by [Predehl & Schmitt 1995](#) of $N_{\text{H}} = 1.79 \times 10^{21} \times A_V \text{ cm}^{-2}$). Moreover, spectral fits often indicates the presence of a partial covering absorber: a fraction of the photons is observed directly, the rest through an intervening absorber. This suggests that the size of the absorber is of the same order as the X-ray emission region, most likely indicating a location near the white dwarf, or at least somewhere within the binary itself.

Above 10 keV, Compton scattering, rather than photoelectric absorption, is the dominant form of interaction between X-rays and matter. Compton-scattering optical depth reaches 1 for $N_{\text{H}} \sim 1.5 \times 10^{24} \text{ cm}^{-2}$. While only a small fraction of intrinsic absorbers observed in AWDs have a column density high enough for Compton scattering not to be negligible, the white dwarf itself is always, and the accretion disk is sometimes, Compton thick. So, when the X-rays strike the white dwarf surface, soft and medium energy X-rays are largely absorbed and reprocessed, while hard X-rays are “reflected” ([Rothschild et al. 1981](#)). At the same time, X-rays above 7 keV have a high probability of interacting with K-shell electrons in iron atoms. A vacancy in the K-shell of a neutral (or mildly ionized) iron atom often leads to the emission of fluorescent line at 6.4 keV.

It is customary to measure the X-ray flux of AWDs, and also estimate the “unabsorbed” flux, by setting all the absorbers to zero after spectral fitting. One then calculates the X-ray luminosity by multiplying the unabsorbed flux by $4\pi d^2$, where d is the estimated distance to the source. However, there is some ambiguity in the definition of X-ray luminosity: how to account for the X-rays that are reprocessed by the white dwarf surface, or those that are absorbed and reprocessed by intrinsic absorbers. There probably is no single solution that is applicable to all AWDs for all situations. For now, the best option may be to stick with the simple procedure described above, while paying attention to its implications in individual situations.

3. OBSERVATIONS AND ANALYSIS METHODS

3.1. X-ray Surveys

AWDs are discovered using a variety of methods, including optical variability, optical colors and emission lines, and X-ray surveys. Over the last several decades, X-ray surveys have been instrumental in establishing magnetic CVs as an important class, and in providing valuable samples with which to study the space densities of various types of AWDs.

Several all-sky surveys in the medium energy X-rays were conducted during the 1970s, including those with *Uhuru* and *Ariel V*, all with non-imaging instrument. *HEAO-1* (1977-1979) was the last to carry out such an all-sky survey, which also localized point source positions using a scanning modulation collimator ([Gursky et al. 1978](#)). Of the 660 sources with modulation collimator positions, [Silber \(1992\)](#) considered 43 to be CVs, although some of these proposed identifications have not been confirmed using imaging X-ray observations. [Silber \(1992\)](#) further concluded that roughly half the *HEAO-1* sample of CVs were magnetic, including both IPs and polars. Subsequent studies of individual magnetic CVs established most IPs and some polars as luminous, hard X-ray sources (see, e.g., [Ishida 1991](#)). To illustrate the differences among various subclasses of CVs in terms of the importance of the X-ray band, I show a sample of objects in the 2–10 keV X-ray flux vs. V-band optical magnitude plane in [Figure 3](#).

The *ROSAT* mission carried an imaging soft X-ray telescope and was operated in a scanning mode during the first 6 months of the mission to conduct an all-sky survey. In addition, even during the rest of the mission when it was operated in a pointed mode, its wide filed-of-view led to the serendipitous discovery of many additional sources. The most significant impact of *ROSAT* mission on AWDs is the large increase in the number of known polars ([Beuermann 1999](#)).

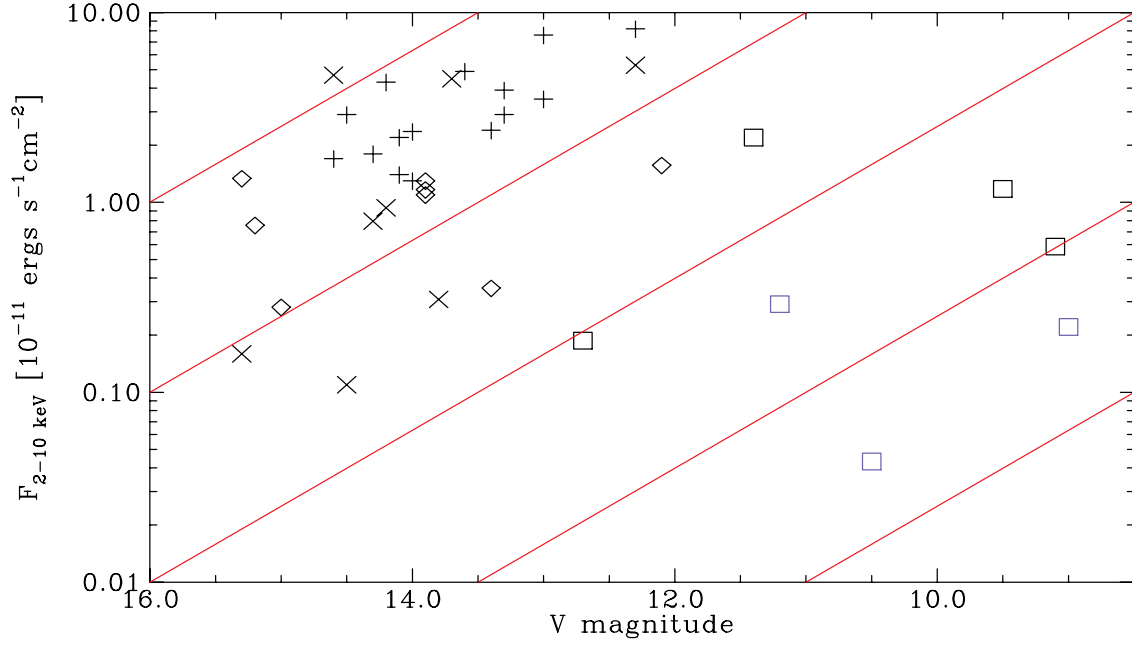


Figure 3. Selected CVs of various subtypes in the F_X/F_{opt} plane. Pluses are IPs, crosses are polars, diamonds are dwarf novae in quiescence, and open squares are non-magnetic nova-like systems (black) and dwarf novae in outburst (blue). The diagonal red lines are for equal F_X/F_{opt} ratios, separated by factors of 10.

Table 1. AWDs in the BAT 70 month catalog

No. ^a	BAT designation	Common Name	Type ^b	flux ^c	22 mo. ^d
1010	Swift J1855.0–3110	V1223 Sgr	IP	117.71	97.1
782	Swift J1548.0–4529	NY Lup	IP	91.75	101.4
625	Swift J1234.7–6433	RT Cru	S	81.41	71.9
181	Swift J0331.1+4355	GK Per	IP	77.52	48.3
15	Swift J0028.9+5917	V709 Cas	IP	74.72	89.1
887	Swift J1730.4–0558	V2731 Oph	IP	69.46	67.8
790	Swift J1559.6+2554	T CrB	S,RN	63.88	64.0
281	Swift J0529.2–3247	TV Col	IP	59.99	51.1
1123	Swift J2142.7+4337	SS Cyg	DN	54.45	45.7
1115	Swift J2133.6+5105	1RXS J213344.1+510725	IP	52.64	52.3
1147	Swift J2217.5–0812	FO Aqr	IP	52.40	58.5
873	Swift J1712.7–2412	V2400 Oph	IP	50.28	52.7
1044	Swift J1940.3–1028	V1432 Aql	AP	49.28	54.0
877	Swift J1719.6–4102	IGR J17195–4100	IP	40.36	35.9
158	Swift J0256.2+1925	XY Ari	IP	36.45	31.2
962	Swift J1816.1+4951	AM Her	P	36.17	
312	Swift J0558.0+5352	V405 Aur	IP	34.93	31.7

Table 1 continued on next page

Table 1 (*continued*)

No. ^a	BAT designation	Common Name	Type ^b	flux ^c	22 mo. ^d
1175	Swift J2255.4–0309	AO Psc	IP	31.72	29.2
393	Swift J0750.9+1439	PQ Gem	IP	31.32	30.3
299	Swift J0542.6+6051	BY Cam	AP	29.95	29.1
422	Swift J0838.0+4839	EI UMa	IP	29.23	32.1
375	Swift J0732.5–1331	V667 Pup	IP	27.48	29.7
758	Swift J1509.4–6649	IGR J15094–6649	IP	25.81	
835	Swift J1649.9–3307	IGR J16500–3307	IP	25.65	
253	Swift J0502.4+2446	V1062 Tau	IP	25.27	
642	Swift J1252.3–2916	EX Hya	LLIP	24.34	25.4
845	Swift J1654.7–1917	IGR J16547–1916	IP	23.48	
248	Swift J0457.1+4528	IGR J04571+4527	IP	23.07	
374	Swift J0731.5+0957	BG CMi	IP	22.82	21.5
491	Swift J1010.1–5747	V648 Car	S	22.18	22.5
40	Swift J0055.4+4612	V515 And	IP	20.62	19.7
798	Swift J1617.5–4958	IGR J16167–4957		20.56	20.8
890	Swift J1731.9–1915	V2487 Oph	RN	20.03	
278	Swift J0525.6+2416	1RXS J052523.2+241331	IP	19.43	
1071	Swift J2015.9+3715	RX J2015.6+3711 ^e	P?	19.23	
563	Swift J1142.7+7149	YY (DO) Dra	LLIP	18.65	17.4
1107	Swift J2123.5+4217	V2069 Cyg	IP	17.64	12.1
749	Swift J1453.4–5524	IGR J14536–5522	P	17.07	22.8
424	Swift J0838.8–4832	IGR J08390–4833	IP	16.83	
332	Swift J0625.1+7336	MU Cam	IP	16.58	
853	Swift J1701.3–4304	IGR J17014–4306		16.15	
1055	Swift J1958.3+3233	V2306 Cyg	IP	15.61	
288	Swift J0535.1–5801	TW Pic		15.56	
300	Swift J0543.2–4104	TX Col	IP	15.54	18.0
386	Swift J0746.3–1608	1RXS J074616.8–161127		15.49	
963	Swift J1817.4–2510	IGR J18173–2509	LLIP:	14.46	
943	Swift J1800.5+0808	V2301 Oph	P	14.45	
415	Swift J0820.6–2805	1RXS J082033.6–280457	IP:	12.86	
951	Swift J1807.9+0549	V426 Oph	DN	12.83	
341	Swift J0636.6+3536	V647 Aur	IP	12.38	
598	Swift J1212.3–5806	IGR J12123–5802		12.31	
1035	Swift J1924.5+5014	CH Cyg	S	11.85	22.6
1022	Swift J1907.3–2050	V1082 Sgr		11.69	27.5
1144	Swift J2214.0+1243	RU Peg	DN	11.34	
724	Swift J1424.8–6122	IGR J14257–6117		11.32	

Table 1 continued on next page

Table 1 (*continued*)

No. ^a	BAT designation	Common Name	Type ^b	flux ^c	22 mo. ^d
324	Swift J0614.0+1709		IP	11.04	
355	Swift J0704.4+2625	V418 Gem	IP	10.94	
356	Swift J0706.8+0325		P	10.14	
1190	Swift J2319.4+2619		P	9.86	2.8
462	Swift J0927.7–6945		IP	9.76	
479	Swift J0958.0–4208	1RXS J095750.4–420801	IP	9.16	
331	Swift J0623.9–0939			9.11	
1103	Swift J2116.0–5840	CD Ind	AP	9.04	
627	Swift J1238.1–3842	V1025 Cen	LLIP	8.99	
275	Swift J0524.9+4246	Paloma	LLIP	8.97	
1109	Swift J2124.6+0500			8.93	
1004	Swift J1848.4+0040	V603 Aql	N	8.74	
322	Swift J0610.6–8151	AH Men		8.59	
11	Swift J0023.2+6142	V1033 Cas	IP	8.43	
1101	Swift J2113.5+5422	1RXS J211336.1+542226		8.40	
709	Swift J1409.2–4515	V834 Cen	P	8.31	
255	Swift J0503.7–2819	1WGA J0503.8–2823	IP	8.23	
393	Swift J0749.7–3218			8.10	
365	Swift J0717.8–2156	1RXS J071748.9–215306		7.86	
708	Swift J1408.2–6113	IGR J14091–6108	IP:	7.82	
417	Swift J0826.2–7033	1RXS J082623.5–703142		7.72	20.8
508	Swift J11039.8–0509	YY Sex	P	7.56	
1148	Swift J2218.4+1925	1RXS J221832.8+192527	P	7.40	
1201	Swift J2341.0+7645	1RXS J234015.8+64207	P:	7.19	
219	Swift J0426.1–1945	IW Eri	P	6.69	
469	Swift J0939.7–3224	1RXS J093949.2–322620	IP:	5.97	

^aEntry number in the BAT 70 month catalog (Baumgartner et al. 2013)

^bAbbreviated types: IP for intermediate polars, LLIP for low luminosity IPs, P for polars, AP for asynchronous polars, N for (old) novae, RN for recurrent novae, DN for dwarf novae, and S for symbiotic stars. A blank in this column indicates objects of unknown subtype, while a colon indicates proposed but unconfirmed type. For references of IP nature, see <http://asd.gsfc.nasa.gov/Koji.Mukai/iphome/iphome.html>.

^cThe BAT-band flux in the 70 month catalog.

^dThe BAT-band flux in the 22 month catalog (Tueller et al. 2010), for those objects that were also detected.

^eThis object is one of possible counterparts of the BAT source.

The *INTEGRAL* mission has detected a large number of previously unknown hard X-ray sources, as a by-product of pointed observations using its wide-angle, coded-aperture mask instruments. Barlow et al. (2006) was the first to carry out a systematic search for CVs among *INTEGRAL* sources. Of the 15 CVs thus identified, the majority were confirmed or candidate IPs. Since many *INTEGRAL* observations are aimed at studies of Galactic sources, the *INTEGRAL* survey is particularly deep along the Galactic plane, and this has led to the discoveries of many CVs. This is both an advantage and a disadvantage. Here I focus instead on the hard X-ray survey with *Swift* BAT, particularly

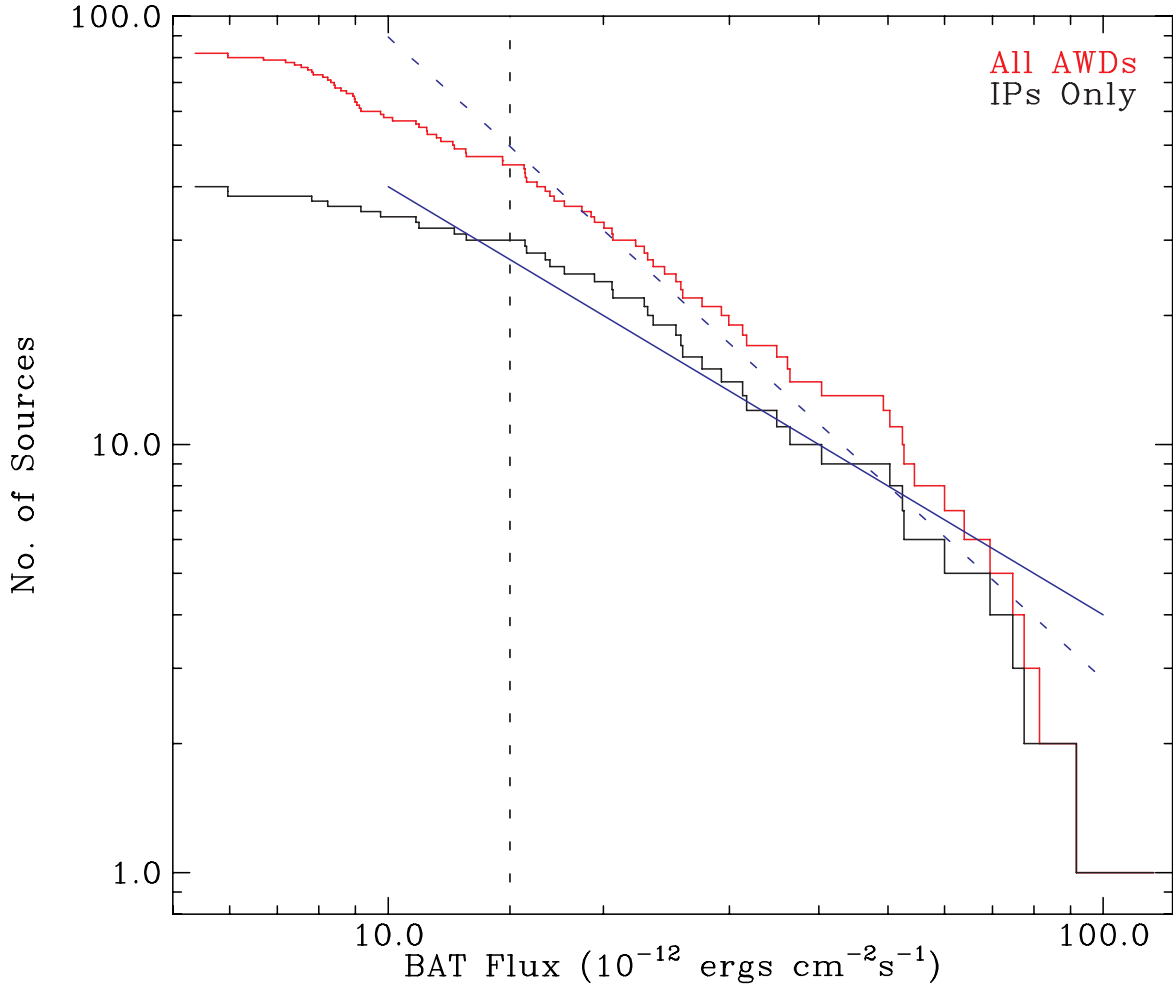


Figure 4. $\log N$ - $\log S$ diagram for BAT detected AWDs. The red histogram shows the cumulative number of all AWDs in Table 1 above given flux, while black histogram is for confirmed IPs only. The dashed vertical line is the approximate completeness limit of the BAT 70 month survey. Blue solid line is the expected slope for objects with a 2-dimensional spatial distribution, while dashed line is for those with a 3-dimensional distribution.

the 70-month catalog (Baumgartner et al. 2013), whose sky coverage is relatively uniform (see their Figure 1) because *Swift* is primarily a gamma-ray burst mission. In Table 1, I list 81 AWDs in the literature as of 2016, with confirmed, probable, or proposed classification, sorted by the BAT-band flux. Roughly half are confirmed or proposed to be IPs. This fraction is sufficiently high that it makes sense to search for IP signatures in all newly discovered hard X-ray emitting CVs; it is not so high that all such systems should be assumed to be IPs. The remaining objects include polars, non-magnetic CVs, and four symbiotic stars (Kennea et al. 2009). I show a $\log N - \log S$ plot of all BAT detected AWDs, as well as that of a subset of them that have been confirmed as IPs, in Figure 4. In the BAT 22-month catalog (Tueller et al. 2010), 35³ out of 479 sources are AWDs; in the BAT 77-month catalog (Baumgartner et al. 2013), the corresponding numbers 81 out of 1210, subject to some uncertainties in the source classification.

There are also deeper surveys concentrating on smaller areas of the sky. For example, Pretorius et al (2007) took advantage of the fact that the *ROSAT* all-sky survey was deeper near the north ecliptic pole to infer the space density of CVs. Another example is the survey of the Galactic center region: Munro et al. (2009) cataloged 9017 X-ray sources in the *Chandra* observations of a $2^\circ \times 0.8^\circ$ field, of which 6760 have high absorption consistent with sources lying at or beyond the Galactic center distance, and argued that a large fraction of the latter were probably magnetic CVs. Such

³ Of these, 34 are listed in Table 1; V2491 Cyg was also listed in the 22-month catalog, although the association of the BAT source with this nova is not 100% certain (Ibarra et al. 2009), and it does not appear in any subsequent versions of the BAT source catalog.

focused surveys, while useful, must deal with either small number statistics (if the field is at a high Galactic latitude, and a survey of local population) or faint counterparts (if detectable at all) in crowded regions of the sky (Galactic plane and center).

Finally, many stellar clusters have been the subject of X-ray surveys, mainly to probe dynamical formation of close binaries. For example, [Gosnell et al. \(2012\)](#) discovered a candidate cataclysmic variable in their survey of the intermediate-age rich open cluster, NGC 6819, using *XMM-Newton*. Globular clusters have been more frequent targets of X-ray surveys, usually with *Chandra*; for example, of the X-ray sources in 47 Tuc ([Grindlay et al. 2001](#)), about 30 are considered likely CVs ([Edmonds et al. 2003a,b](#)).

3.2. Imaging Analysis

The X-ray emission region on a white dwarf is far too small to be resolved by direct imaging for the foreseeable future. However, nova ejecta, after several years, can become large enough to be resolved with current technology. First such detection was made by [Balman & Ögelman \(1999\)](#) in their *ROSAT* observation of GK Per (Nova Persei 1901). This is by far the best observed X-ray shell around a nova, likely due to the unusual circum-binary environment ([Bode et al. 1987](#)). Most recently, [Takei et al. \(2015\)](#) compared the *Chandra* images taken in 2000 and 2013 and detected the expansion of the X-ray nebulosity at a rate of $0''.14 \text{ yr}^{-1}$. The remnant has also significantly faded in X-rays by 30–40% during these 13 years, which they interpret as due to adiabatic expansion, since radiative cooling time is far too long to account for this.

In the case of GK Per, extended X-ray emission is obvious to the eye in the *Chandra* data without sophisticated analysis. Even so, a careful analysis is needed to quantify the spatial extension: the central source, the binary GK Per itself, is a bright enough source that one must worry about readout streak, and the source is piled up at the center. For all other AWDs, the spatial extent of the detectable X-ray nebulosity is of order $1''$, only slightly larger than the point-spread function (PSF) of *Chandra*, so specialized processing and analysis are essential. This involves sub-pixel event repositioning, ray-tracing simulation to model the PSF appropriate for the spectral shape and detector position of the central source, and maximum likelihood de-convolution (as was done for RS Oph: [Luna et al. 2009](#)). The resulting X-ray images, in conjunction with images taken in other wavelengths, have the potential to provide valuable insights into the energetics and spatial distribution of the nova ejecta as well as the circum-binary environment.

In addition, extended X-ray emissions have been detected in a few symbiotic stars, and are interpreted as due to thermal emission from non-relativistic jets (see, e.g., [Nichols et al. 2007](#); [Karovska et al. 2010](#)). In the case of Mira AB system, there is a faint X-ray source linking the two stars ([Karovska et al. 2005](#)). However, such analysis is technically challenging and positive detection of extended X-ray emission is rare.

3.3. Timing Analysis

The X-ray emission from AWDs is variable on a variety of time scales, from seconds to >centuries. Periodic signals can be seen on the orbital and the spin periods, ; quasi-periodic oscillations (QPOs) have been detected in some cases; and aperiodic variability also contain some valuable information, at least in principle.

3.3.1. Sampling

Pointed observations with observatories in high Earth orbits (*Chandra* and *XMM-Newton*, as well as *EXOSAT*, which operated during 1983–1986: [Taylor et al. 1981](#)) can observe a target continuously for up to several days. More often, X-ray observatories are placed in low Earth orbits, with spacecraft orbital periods near 95 min. Some of these observatories minimize the number of slews by pointing towards a single target for hours to days. In such cases, good on-source data are interrupted by Earth occultations, and passage of the satellite through high particle background regions such as the South Atlantic Anomaly (SAA). Some low Earth orbit observatories (e.g., *ROSAT*, *RXTE*, and *Swift*) achieve high overall observing efficiencies by interleaving observations of multiple targets during each spacecraft orbit. Data taken with such missions have even longer gaps and span a longer calendar time to achieve the same good on-source exposure time.

The presence of frequent data gaps of significant durations (comparable to the periods of interest) makes the use of the fast Fourier transform (FFT) algorithm rather problematic. Discrete Fourier transform (DFT) is far more suitable, has well understood statistical properties ([Scargle 1982](#)), and there is an implementation that is computationally fast enough to tackle large data sets ([Press & Rybicki 1989](#)).

Regardless of how the light curves are analyzed, one unfortunate fact remains: whenever one uses data taken with low Earth orbit satellites, one encounters difficulties when searching for periods near ~ 95 min, ~ 190 min, ~ 285 min

etc., where quite a few CVs are found. This situation is analogous to the problem of 1-day aliases and the difficulties detecting period near 1 day that plague ground-based observations.

3.3.2. Background Subtraction

The need for background subtraction is obvious in non-imaging observations. For example, in the *RXTE* PCA observation of the IP, V709 Cas, reported by de Martino et al. (2001), the raw count rate averaged 110 ct s^{-1} in all five proportional counter units of the PCA. After background subtraction, the net rate was 35 ct s^{-1} . Note that V709 Cas is among the X-ray brightest CVs on the sky. Useful results have been obtained for AWDs more than an order of magnitude fainter than V709 Cas using *RXTE*. While the accuracy background subtraction (rather than the counting statistics of the source photons) is the limiting factor in the resulting light curves in such cases, there is a clear recommendation from the instrument team on how to do this, and the PCA background model has proved to be sufficiently accurate for most purposes.

During a *Suzaku* observation reported by Yuasa et al. (2010), the count rate for V709 Cas with one of the units of XIS was $\sim 1.8 \text{ ct s}^{-1}$, of which $\sim 0.14 \text{ ct s}^{-1}$ is likely to be due to background⁴. In this case, some timing analysis can be performed without any background subtraction, but that is far from ideal. Background subtraction is clearly essential for fainter AWDs.

Both for non-imaging and imaging instruments, the background is a mixture of X-ray and particle events. The former includes contributions of faint, unresolved, background AGN and hot gas in our Galaxy. The particle event rate is strongly variable as a function of the location of the satellite in the geomagnetic field, hence of time. To account for both in data taken with imaging X-ray telescopes, one generally extracts the background from a source-free region on the same detector during the same observation. An ideal background region must be large enough to introduce little additional statistical errors, close enough to the source extraction region so that it can be considered to have the same X-ray and particle background levels as the source extraction region, yet far enough from the object of interest so that it contains no source photons.

In practice, one often assumes both X-ray and particle background to be flat near the center of the FOV, so that a single scaling factor (the ratio of detector areas covered by the background and the source extraction regions) can be used. Since this is the default for spectral analysis when using *xspec*, spectral and timing analyses can serve as a useful cross-check. If the light curve is modulated on the spacecraft orbital period, this may indicate a background subtraction problem. If the net spectrum shows features known to be present in the background spectrum (such as instrumental lines), there probably is a problem with background subtraction. When neither the light curve nor the spectrum shows suspicious features, it is a likely indication that any systematic errors due to background subtraction are smaller than statistical errors.

The other ideals of background regions are difficult to realize for missions with large PSFs, particularly those with large extended wings in the PSFs, such as *ASCA* and *Suzaku*. Some compromises are inevitable; one should always keep the potential consequences of those compromises in mind. Also, background light curves can be averaged over multiple time bins to smooth out statistical fluctuations, as long as they add up to an interval much smaller than the spacecraft orbit. However, if the background region also contains a fraction of the source count due to the wings of the PSF (true for *ASCA* and *Suzaku*), and if the source varies suddenly (e.g., during a total eclipse), this procedure can introduce artifacts in the net light curve.

3.3.3. Warner's Warning

CVs are variable across many time scales. As Warner (1989) warned in the context of optical observations, random processes can lead to the impression of a periodic signal where only aperiodic variability exists, when a short segment of a light curve is inspected. This is also true of periodograms: there is always a highest peak in any periodogram, so finding a peak is not the same thing as establishing the presence of a periodic signal. If the underlying aperiodic variability is frequency independent (“white noise”), then DFT as modified by Scargle (1982) provides a statistical test, in the form of “false alarm probability.” However, the variability of AWDs is often frequency dependent. Ideally, more sophisticated methods should be used for AWDs, such as the autoregressive technique of Hakala et al. (2004).

Another simple, yet highly effective, check is to see if the same period is detected in multiple data sets. This also allows to test the coherence of the signal. On the other hand, if a period is detected with apparently high statistical

⁴ Note that Table 1 of Yuasa et al. (2010) reported the net XIS rate in the 3–12 keV range; the numbers above are for the entire XIS bandpass.

significance but not seen in another data set of comparable or higher quality, it is quite possible that the assumption behind the statistical test did not match the reality of the object.

3.3.4. Eclipse Analysis

The procedure to analyze eclipse light curves of CVs is well established for optical data (see, e.g., [Patterson 1981b](#)) and can also be used for X-ray light curves if a total eclipse is observed. First one measures the times of the four contacts (the beginning and the end of ingress and the beginning and the end of egress in order). One then measures the eclipse duration, defined as the length between the mid-ingress to the mid-egress, as well as the ingress/egress durations (the two should be the same). This procedure differs from that used for high mass X-ray binaries (HMXBs; see, e.g., [Coley, Corbet & Krimm 2015](#)), for which the eclipse duration is defined as the time interval between the second and the third contacts.

In both cases, the eclipse duration reflects the size of the part of the mass donor that passes in front of the X-ray emission region divided by the relative velocity of the two stars in the plane of the sky. In HMXBs, the X-ray emission region has the size of the same order as that of the neutron star, and is negligible, so the duration of totality can be used. For CVs, the diameter of the white dwarf (of order 15,000 km) is a significant fraction of the size of the secondary, and therefore one must use the eclipse duration defined as mid-ingress to mid-egress: these are when the edge of the secondary passes through the center of the eclipsed object. The size of the eclipsed object can be inferred from the ingress/egress durations in AWDs, because the edge of the secondary is sharp. This is not the case for HMXBs, in which the ingress and egress durations are often seen to be variable, due to the variable absorption by the stellar wind.

Note also that the ratio of the projected size of the secondary to the diameter of the white dwarf is of order 10 for CVs below the period gap. Therefore, it is inevitable that a fraction (of order 1/10th) of CVs in which the white dwarf is eclipsed should show a partial, rather than a total, eclipse of the white dwarf. Prominent examples are the low luminosity IP EX Hya ([Rosen et al. 1991](#)) and the dwarf nova V893 Sco ([Mukai, Zietsman & Still 2009](#)).

3.4. Spectral Analysis

Once source and background spectra are extracted, and the response file(s) downloaded or generated, one can proceed to spectral fitting. Here, I provide some guidance on the usage of some common models available in the X-ray fitting package, `xspec`.

3.4.1. Optically Thin Emission

When the nature of the object is unclear, it is often customary to fit the the medium energy X-ray spectrum with simple analytical models, such as a blackbody, a power law, and a Bremsstrahlung. Of the three, we do not expect a blackbody fit to be successful for AWDs above 1 keV, and if it is, it should indicate an unphysically high temperature (see the Eddington limit argument in §2). Medium energy X-rays from AWDs most likely originate from optically thin, thermal plasma, and the Bremsstrahlung model is likely to provide a good description of the continuum. However, power law can also often provide an adequate description, regardless of the underlying emission mechanism, within a limited energy range. Moreover, an optically thin thermal component seen through a complex absorber can give the appearance of being flatter than a Bremsstrahlung continuum (see §5.4 below).

The first discrete spectral feature to be noticed in the X-ray spectrum of AWDs is the Fe K complex near 6.6 keV, initially fit as a single Gaussian. An early example includes the spectrum of SS Cyg ([Yoshida, Inoue & Osaki 1992](#)) who derived a Bremsstrahlung temperature of 17.5 keV and a line centered at 6.7 keV. The line energy suggests that the line is dominated by the He-like Fe, confirming the thin thermal nature of the emission. At this point, it makes sense to fit X-ray spectra of CVs using modern models of thermal emission from collisionally excited thermal plasma, including both the Bremsstrahlung continuum and discrete lines⁵.

However, in a pure $kT=17.5$ keV plasma, Fe should be completely ionized. Therefore, [Yoshida, Inoue & Osaki \(1992\)](#) inferred that the emission was multi-temperature in nature, one of the first observational demonstration of this fact in any non-magnetic CVs. High S/N observations with CCD detectors can resolve the Fe complex into H-like (6.97 keV), He-like, and fluorescent (6.4 keV) components, and the presence of K-shell lines from medium-Z elements clearly demonstrate the multi-temperature, optically-thin, thermal nature of the emission (see, e.g., the *Suzaku* observation of SS Cyg; Figure 3 of [Ishida et al. 2009](#)).

⁵ See the home pages of the two major efforts currently active in this field, ATOMDB (<http://atomdb.org/>) and SPEX (<http://www.sron.nl/spex>). In addition to ever increasing, but still imperfect, knowledge of atomic physics, the parameter regime occupied by AWDs is often outside the main focus of both these groups, sometimes resulting in the lack of suitable models (e.g., for plasma of sufficiently high temperatures).

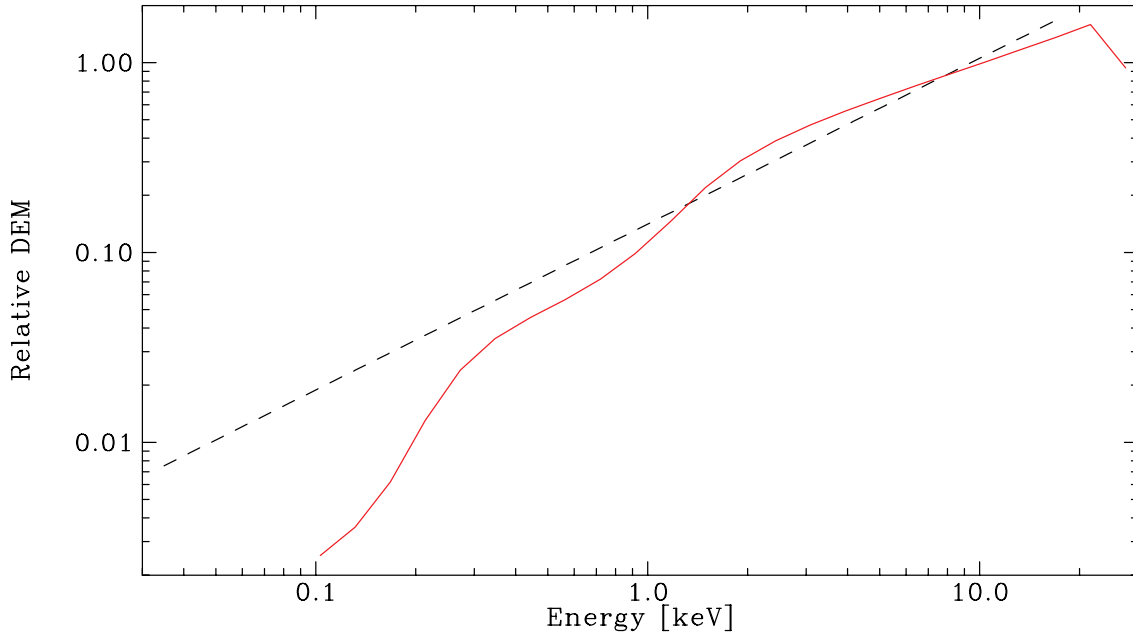


Figure 5. A comparison of a power-law DEM distribution with power law index 1.0, appropriate for pure Bremsstrahlung cooling with no additional energy source or cooling term, and that of the cooling flow model, `mkcflow`.

Finally, the plasma pressure is nearly constant in an accretion column. Therefore, the isobaric cooling flow model (`mkcflow` in XSPEC; Mushotzky & Szymkowiak 1988) provides a good approximation for many AWDs. Note that, when using the `mkcflow` model in XSPEC, a small but non-zero redshift (z) must be specified. This parameter is used to redshift the model and, in combination with the cosmological parameters, as a proxy for distance. One can reset the Hubble constant to $50 \text{ km s}^{-1} \text{ Mpc}^{-1}$ and the cosmological constant to 0.0 for ease of conversion between z and distance (e.g., $z = 5 \times 10^{-8}$ corresponds to a distance of 300 pc using these cosmological parameters). One important advantage of this model is that the cumulative contribution of line cooling is properly taken into account in calculating the cooling time at each temperature, which is often not the case for models specifically created for CVs (including the original Aizu model). The expected emission measure distribution (DEM) is a pure power law with index of 1.0 for Bremsstrahlung cooling, while the DEM for a cooling flow is more complex (Figure 5). Note that, if one calculates the temperature and density structure assuming that only Bremsstrahlung cooling operates, and then integrates the appropriate plasma (continuum+line) emission based on that profile, the strength of low-temperature lines will be overestimated. On the other hand, an important limitation of `mkcflow` model is that it does not account for the pressure increase toward the bottom of the accretion column. This is a small but real effect in magnetic CVs, as the post-shock plasma near the top has a non-negligible ram pressure, and retain 1/16th of the kinetic energy of the pre-shock flow.

3.4.2. *Optically Thick Emission*

The first model to be applied to the soft components in AWDs is the blackbody. Although this is an idealized model and one expects that real astrophysical objects do not radiate as a perfect blackbody, it provides a useful first approximation. Since the total luminosity is proportional to the emitting area and effective temperature (T_{eff}) to the fourth power ($L \propto A \times T_{eff}^4$), it can be used to estimate the emitting area A (§5.2). However, one must be cautious because we often do not observe the peak of the blackbody curve. This can lead to the best-fit kT and N_H values to be strongly anti-correlated, and hence a large uncertainty in inferred luminosity and area, even within the blackbody approximation.

The problem is even more severe if one considers a more physically realistic model: stellar atmosphere. As I already discussed in §2, the physical structure of the emission region is an active research topic and there are a large number of free parameters in the case of novae. I discuss the case of the soft component in magnetic CVs in depth in §5.6.

3.4.3. *Absorption Models*

Table 2. Typical X-ray Characteristics of CVs and symbiotic stars

Energy Source	Energy Range	Size ^a	Time Scale ^b	Luminosity (ergs s ⁻¹)	Temperature (keV)
Accretion	Hard	WD	Short	10 ²⁹ –10 ³³	5–50 keV
	Soft	WD	Short	10 ³¹ –10 ³⁴	20–50 eV
Nuclear Burning	Hard	Large	Days	10 ³³ –10 ³⁵	1–30 keV
	Soft	WD	Short	10 ³⁵ –10 ³⁸	30–80 eV
Colliding Winds	Medium	Binary	Days?	10 ³² ?	1 keV

^aX-ray emission region size, compared to the white dwarf, the binary, or larger. Only the hard X-rays from novae (under “nuclear burning”) can be spatially resolved using the current and near-future technology.

^bShortest variability time scale, which can be as short as <10 s.

Currently, the best model of X-ray absorption by the ISM is `tbabs` and its successor, `tbnew` (Wilms, Allen & McCray 2000), which accounts for the fact that a significant fraction of ISM exists in the form of molecules and dusts. However, intrinsic absorbers within CVs and symbiotic stars probably exist largely as atoms. In modeling them, it is in fact a drawback that `tbabs` and `tbnew` account for the presence of molecules and dusts. The older absorption model, `phabs`, may well be the best option, in combination with the XSPEC convolution model `partcov` which creates a partial covering absorber model based on any absorber model. Note that `pcfabs` is a partial covering model that is hard-wired to use the even older absorption model, `wabs`, and so no longer recommended. Instead of molecules and dusts, one effect that should be considered is the partial ionization of intrinsic absorber, a topic we will return to in §5.4.

4. IDENTIFYING AWDs AND DETERMINATION OF MAGNETIC NATURE

As this review makes clear, AWDs display a wide range of characteristics and so there is no hard and fast rules that can be applied mechanically to identify all of them when an unknown X-ray source is examined. For non-experts’ convenience, I list typical properties of X-ray emissions from AWDs in Table 2. These properties, along with information obtained through optical observations, including the X-ray to optical flux ratios (Figure 3), provide a useful guide to identify likely AWDs among poorly studied X-ray sources.

Objects showing a distinct soft component can be considered candidate polars, since many polars are known to be soft X-ray bright (King & Watson 1987). See, however, Haberl & Motch (1995) for IPs with a soft component. In the X-rays, polars exhibit a strong modulation on a single period ($P_s = P_o$) or two similar periods (if asynchronous). However, true verification of the polar nature requires optical observation, such as detection of circular polarization or cyclotron humps.

The presence of the HeII $\lambda 4686$ is often used to judge if a CV is magnetic or not. While this is a useful diagnostic, the mere presence of this line is far from conclusive. Polars generally have a soft component with strong ionizing continuum shortward of the HeII 228Å edge, and IPs probably have a similar soft component. Note, however, that the hot white dwarf photosphere of a recent nova, or the optically thick boundary layer of non-magnetic CVs, are also capable of ionizing HeII. Another important factor is the accretion column or curtain of magnetic CVs, which produce strong emission lines but little continuum in the optical. In polars, there is no accretion disk to dilute the stream emission; in IPs, the truncated disk provides some dilution. This explains the empirical rule-of-thumb proposed by Silber (1992): if the equivalent width of the H β line is greater than 20Å, and the HeII $\lambda 4686$ /H β ratio is greater than 0.4, then the object is likely to be a magnetic CV. In CVs studied by Silber (1992), however, many IPs have weaker H β lines and cannot easily be from non-magnetic systems using this diagnostic.

A large fraction of AWDs detected in hard X-ray surveys are IPs. Most IPs have a flat X-ray continuum that cannot be explained as due to simply absorbed thermal emission; these same systems have strong 6.4 keV fluorescent lines (see, e.g., Ezuka & Ishida 1999). Non-magnetic CVs, on the other hand, tend to be less absorbed and have weaker 6.4 keV lines. However, there are exceptions to both these trends, so they cannot be used for a definitive classification. A stronger statement can only be made if the X-ray light curve shows a coherent and persistent period, and if this is not the orbital period: it likely the detection of the spin period. In many well-known IPs, there is an obvious

and dominant peak in the power spectrum at the spin period, with amplitudes in the 10s of percent range (see, e.g., Norton & Watson 1989), and the exact details of how the data are analyzed do not matter.

However, there are also IPs with relatively weak spin modulations, and there are objects which are presumed non-magnetic even though they share some characteristics with magnetic objects. In searching for periodicities, one can emphasize sensitivity and accept certain number of false positives, or one can emphasize reliability and accept a lower sensitivity (see §3.3 above). Note, however, that most studies estimate false alarm possibility assuming a white (i.e., frequency independent) using, e.g., the Lomb-Scargle periodogram Scargle (1982). In reality, many AWDs exhibit a red noise, so a more sophisticated methodology (see, e.g., Ramsay et al. 2008) is required to assess the significance of an apparent peak in the periodogram. Ramsay et al. (2008) considered three objects to be candidate IPs based on the complex absorber in their X-ray spectra. Of the three, one (EI Uma) was later recognized as an IP (Reimer et al. 2008) while the other two (V426 Oph and LS Peg) still lack a definite spin signature. They may well be non-magnetic systems with some resemblance to IPs, or they may be IPs whose spin signature is almost perfectly hidden.

The true hallmark of the white dwarf spin period is the stability of the clock (Patterson 1981a), so it is a good idea to treat any proposed spin period as merely a candidate until the same period is detected in another observation, to within the expected limits of white dwarf spin up/down. This also presupposes that the spin period is often, if not always, detectable given observations of a comparable quality.

Another useful check is the energy dependence of the spin modulation. In IPs, the spin modulation is generally more prominent at lower energies, although not as strongly as would be expected if the spin modulation was purely due to a single photoelectric absorber (Norton & Watson 1989). However, this is not generally the case for polars, or for some IPs.

When a late type giant is found to be the likely optical candidate for an unknown X-ray source, it may be a symbiotic star with a white dwarf accretor. While they exhibit a wide variety of X-ray spectra (see §6.5), all are thermal emissions⁶. This should be checked by searching for emission lines (see, e.g., Luna & Costa 2005) or additional blue and variable continuum, as per the original definition of symbiotic stars. Note, however, that the optical emission lines in some X-ray bright symbiotic stars are relatively weak. For example, the recurrent nova and BAT source, T CrB, can become very weak at times (Munari, Dallaporta & Cherini 2016). Recently, Mukai et al. (2016) identified a newly discovered BAT source with a poorly studied red giant, SU Lyn, whose emission lines are undetectable in low resolution optical spectroscopy (they are clearly present in high resolution spectra). Thus, if a candidate optical counterpart of a X-ray source is a red giant without obvious emission lines in low resolution data, it should not be immediately discounted without first taking high resolution optical spectra or UV data.

In a comprehensive study of X-ray sources in M31 and M33 detected with *ROSAT*, *XMM-Newton*, and *Chandra*, Pietsch et al. (2005) found that a large fraction of SSSs in M31 are novae. This demonstrate that X-ray observations are capable of discovering novae in their supersoft phase out to local group galaxies and beyond, even though M31 itself is well monitored optically for novae so few are likely to be discovered through their X-ray emissions first. Such independent discoveries are harder in the Galaxy, because of the larger solid angle involved and due to the ISM on the Galactic plane. For example, assuming an average density of 0.1 cm^{-3} , the column density is $2.0 \times 10^{21} \text{ cm}^{-2}$ at 6.5 kpc. This is high enough to significantly reduce the count rate of any supersoft component. Nevertheless, one object, V1375 Cen (=XMMU J115113.3–623730), originally discovered in the *XMM-Newton* slew survey as a soft source, is thought to have been a nova, based on post X-ray discovery follow-up observations (Greiner et al. 2010).

The hard X-rays from shocked nova ejecta are less well observed, but they appear to be widespread and have peak luminosities in the 10^{33} – $10^{35} \text{ ergs s}^{-1}$ range (Mukai, Orio & Della Valle 2008). They predicted that some faint X-ray transients in the Galactic Center region may turn out to be associated with novae, which may have been confirmed by the pre-discovery *Chandra* detection of the IR-discovered nova, VV-NOV-13 (Orio, Mukai & Della Valle 2016).

5. X-RAY EMISSION FROM MAGNETIC CVs

Next, I highlight selected results on accretion onto magnetic white dwarfs. Because Z And is the only confirmed magnetic symbiotic system (Sokoloski & Bildsten 1999), and there are no high quality X-ray data on this object (the *XMM-Newton* and *Chandra* observations obtained during an outburst are of low statistical quality, and probably tell us more about the outburst than about the accretion processes; Sokoloski et al. 2006a), this section will entirely focus on magnetic CVs. However, the apparent lack of magnetic symbiotic stars may simply reflect the difficulty in

⁶ A late type giant associated with a non-thermal X-ray source probably is a symbiotic X-ray binary with a neutron star accretor (see, e.g., Corbet et al. 2008).

identifying magnetic systems while shell burning is in progress. When more symbiotic stars driven purely by accretion are discovered, a fraction may well turn out to contain a magnetic white dwarf.

There are relatively few in-depth observations of polars with *Chandra* and *XMM-Newton*. One reason for this is that polars are frequently found in low state (16 of 37 in an *XMM-Newton* survey of polars; Ramsay et al. 2004). This makes observations risky: proposals for regularly scheduled observations of polars are often rejected because the success is not guaranteed, and proposals for target-of-opportunity (TOO), or triggered, proposals are often rejected because competition for such constrained time is stronger. Regardless of the reasons, there is no option but to rely heavily on older X-ray observations for several key aspects of polars.

For magnetic CVs, timing and spectral analyses must be considered together to establish a coherent picture. Not only can such studies reveal the detailed physics of the X-ray emission regions, but also allow us to estimate the white dwarf mass (M_{wd}) and gain some insight into how the magnetic field interacts with the accretion stream.

5.1. X-ray Modulation of Polars

In discussing magnetic CVs, it is useful to establish a terminology to distinguish the two poles of a magnetic dipole. In this review, I will call the pole closer to Earth (i.e., on the same side of the orbital plane as Earth) the “upper pole,” and the other the “lower pole.” I will largely avoid the terms “1-pole” and “2-pole” due to possible confusion, as these can refer to the number of poles that are visible from the Earth, or the number of poles that are accreting.

Polars accrete without an intervening accretion disk. The matter lost from the inner Lagrangian (L_1) point of the secondary first follow a ballistic trajectory, and subsequently captured by the magnetic field and follow the field lines to the white dwarf surface. The locations of the interaction region, and hence the accretion footprint, are determined by the complex interaction between the accretion flow and the magnetic field. To first order, the interaction region is where the ram pressure of the ballistic stream and the magnetic pressure are equal. If the accretion is predominantly to the upper pole, then the magnetic stream should also be curved above the orbital plane; lower pole, below.

Some polars, such as ST LMi (=CW 1103+254) and VV Pup, exhibit simple X-ray light curves consisting of a faint phase, during which they are hardly detected, and a bright phase (see Fig. 2 of Mason 1985). The faint phase is indicative of self occultation: the accretion region being hidden by the solid body of the white dwarf. In these systems, the faint phase lasts for over half a cycle; one therefore infers that accretion occurs predominantly onto the lower pole⁷. Since the hard X-rays are emitted above the surface in optically thin region, the hard X-ray light curves are shaped predominantly by self occultation. On the other hand, the soft X-rays are emitted from the surface that is optically thick; projection and limb-darkening effects are also important. The hard and soft X-ray light curves of ST LMi are qualitatively consistent with such simple expectations, with perhaps a modest spatial extension of the emission region.

The prototype polar, AM Her typically show a faint phase lasting ~ 0.2 cycle (see, e.g., Matt et al. 2000), suggesting that accretion mainly occurs on the upper pole that suffers a short self occultation. However, using archival *SAS-3* data, Friedhorsky, Marshall & Hearn (1987) reported the disappearance of the faint phase in 1976 November in both soft and hard X-rays. In contrast, during the 1998 August high state, modulation was absent in soft X-rays but persisted in hard X-rays. More puzzlingly, 1983 *EXOSAT* observation caught it in a so-called reverse soft X-ray mode, during which the hard X-ray light curve was similar to that during normal mode, but soft X-rays were brighter for \sim half a cycle centered on what is normally the faint phase (Heise et al. 1985).

The soft X-ray light curves of EF Eri, AN UMa, V834 Cen (=E1405–451), and QQ Vul (=E2003+225) are even more complex (Fig. 1 of Mason 1985). The hard X-ray light curve of EF Eri can be described as sinusoidal, and that of V834 Cen may be considered similar. The lack of faint phase indicates either that the active pole is always visible (so it must be the upper pole) or that both poles accrete. One particular feature is a dip lasting about 0.1 cycle, which is thought to be due to occultation by the magnetic stream toward the upper pole (King & Williams 1985). There is a narrower dip ~ 0.1 cycle later in AN UMa and V834 Cen (Mason 1985), which these papers do not explain. Neither is there a full explanation for the general complex shape of the soft X-ray curves of these polars.

One potential scheme to interpret such complex light curves is treat each peak as representing a distinctive emission region, possibly invoking a complex magnetic field geometry beyond a simple dipole. However, it is worth emphasizing that a presence of multiple emission regions, even if confirmed, does not necessarily imply a complex magnetic field geometry. The presence of other factor is obvious because both QQ Vul and V834 Cen, seen to have complex soft X-ray light curves in their first *EXOSAT* observations (Mason 1985), were seen to have drastically different light curves in

⁷ Therefore, ST LMi is an example of a “1-pole” system in terms of physical amount of accretion, which is, at the same time, a “2-pole” system if one counts the number of observable poles.

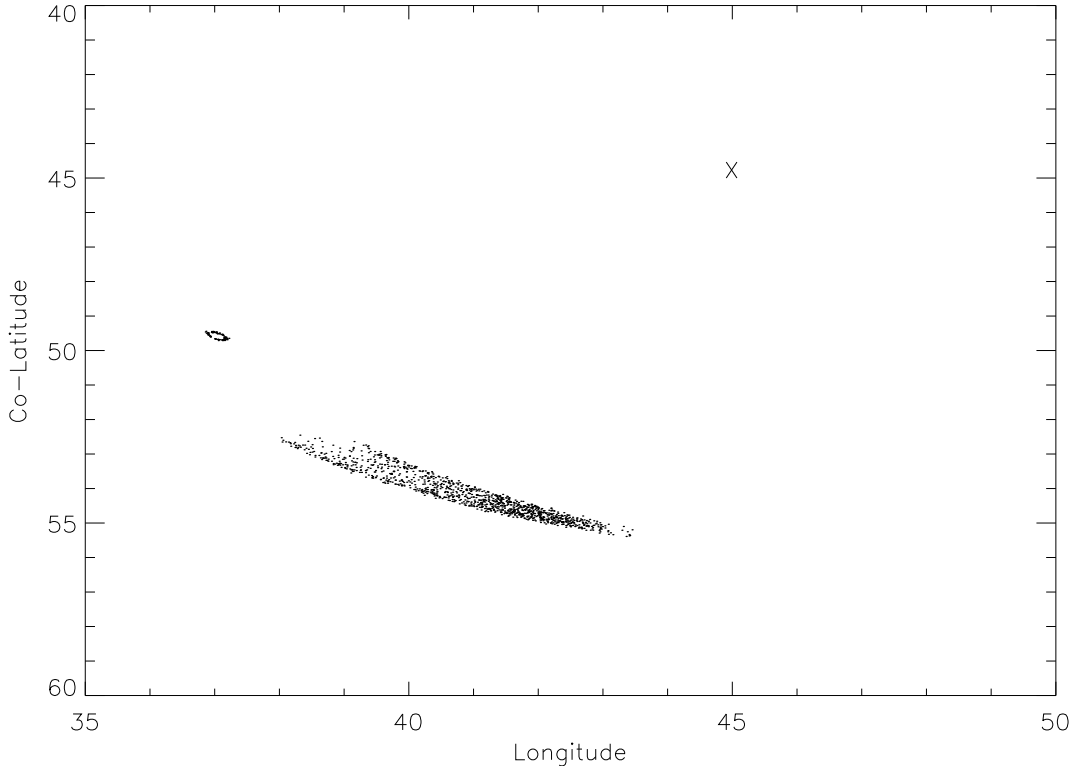


Figure 6. An example of the elongated spot shape expected in polars, in the simplest magnetic field geometry of a centered dipole. See text for details. This is Figure 4.16 of Cash (2002), reproduced with permission.

later observations (Osborne et al. 1987; Sambruna et al. 1994). In the first two *EXOSAT* observations of QQ Vul, there was a broad peak at phase 0.8–1.0, and a much narrower peak at 0.45–0.55. During the third observation, there were two roughly equal peaks at phases 0.25 and 0.65. Since the magnetic field configuration cannot conceivably change within a few years, the changes, hence an important part of the reason for complex light curves, must lie in factors that can change from epoch to epoch.

The interaction of the magnetic field and the ballistic stream almost certainly leads to an elongated accretion spot, or spots, even if the white dwarf has a simple, centered, dipole field (Mukai 1988; Cash 2002). The key ingredients of these studies are (1) a realistic density profile (higher density core and lower density halo) of the stream that leaves the L_1 point (Lubow & Shu 1975); and (2) the assumption that each element of the stream is captured by the magnetic field according to the local balance of ram and magnetic pressures. Thus, different parts of the stream couple to magnetic fields at different locations along the ballistic trajectory. A sample map of accretion region from Cash (2002) is reproduced in Figure 6, in which a cross marks the location of the magnetic pole. As can be seen, the main accretion region is significantly offset from the magnetic pole. Moreover, there is an additional spot (upper left of the figure), which result from low density stream coupling directly to the magnetic field at or very near the L_1 point, where the stream velocity and hence the ram pressure is very low.

Such double spot structure, with an elongated main spot, has the potential to generate complex soft X-ray light curves, which is yet to be fully studied. Moreover, by changing the mass transfer rate, the spot geometry and the light curve morphology will change. Finally, the double stream implied by the double spot structure may explain the double dips seen in AN UMa and V834 Cen.

5.2. Size of the Accretion Region(s)

In magnetic CVs, the accretion rate per unite area (\dot{m}), also called the specific accretion rate, is more important in determining the physical characteristics of the outgoing X-rays than the total accretion rate (\dot{M}). In recent years, therefore, X-ray emission models are usually provided as a function of \dot{m} , typically expressed in the units of $\text{g s}^{-1} \text{cm}^{-2}$.

In the early literature, however, it this was more often expressed as \dot{M}/f , where f is the size of the accretion region expressed as the fraction of the white dwarf surface, allowing a direct comparison with models of spherically symmetric, radial accretion onto non-magnetic white dwarfs (see, e.g., Lamb & Masers 1979). Note that, for a wide range of M_{wd} , \dot{m} of $1 \text{ g s}^{-1} \text{ cm}^{-2}$ corresponds to L/f of $8.0\text{--}9.5 \times 10^{35} \text{ ergs s}^{-1}$, because the larger surface area of the lower mass white dwarf compensates for the smaller amount of potential energy released per unit mass.

The soft X-ray spectrum contains information about the emitting area, modulo the distance to the system. However, there are practical difficulties. First, one does not know the true spectral shape, and a blackbody fit may not be reliable. Second, in blackbody fits, there often are correlated errors on kT and N_H , resulting in large uncertainties in the emitting area and the luminosity determined from X-ray spectral analysis (see, e.g., Fig. 10 of Patterson et al. 1984). Note also that the precise meaning of the accretion spot size, whether expressed as area or as f , can be murky, particularly when blobby (inhomogeneous) accretion is considered (King 2000).

The most robust method to estimate f is via the measurement of eclipse light curves. In the X-ray eclipsing polar, HU Aqr, Schwope et al. (2001) found that ingress is compromised because of the stream dips of the kind discussed above. However, the egress is clean and lasts 1.3 s (or 4° or 450 km). Such rapid transitions can be measured only with the highest quality X-ray light curves. For example, Pandel et al. (2002) could not resolve the egress duration for DP Leo or WW Hor. Note also that eclipse light curves provides a measurement in one dimension (in longitude), and hence provides incomplete, if important, information when the accretion region has a complex shape.

Multiple emission regions have the potential to complicate eclipse analysis further. In the hard X-ray bright eclipsing polar, V2301 Oph, Ramsay & Cropper (2007) found that the ingress consisted of two steps of rapid (<5 s) decline separated by a ‘standstill’ lasting 26 ± 4 s. The egress lasted 23 ± 4 s in a single step, without a standstill.

Among IPs, only XY Ari is X-ray bright and deeply eclipsing, and hence the only object for which emission region size has been estimated using the eclipse method. There is an obvious complication, however: the location of the emission region, relative to the secondary, changes as a function of the spin phase. Nonetheless, Hellier (1997) found that, by aligning the individual eclipses, the composite egress (their Fig. 8) showed 2/3rd of the flux emerging in <2 s, with the rest emerging over a ~ 20 s period. However, the timing changes not strictly as a function of spin phase but has jitters (their Figure 6). Therefore, it appears that, at any moment, the majority of the flux is emitted in a small ($f < 0.002$) area, but the accretion foot points wanders around on a larger ($f < 0.01$) area on the white dwarf.

While these measurements can inform our understanding of the X-ray light curves and spectra, they are not precise enough to lead to definite, quantitative conclusions. For example, while the L/f values, or \dot{m} , of HU Aqr and XY Ari are constrained, it does not pinpoint the vertical location of these systems in the magnetic field – L/f diagram in which X-ray dominated and cyclotron dominated shocks can be separated (see, e.g., Figure 2 of Lamb & Masers 1979).

5.3. X-ray Spin Modulation of IPs

As mentioned previously, the amplitude of X-ray spin modulation of IPs is usually a function of the photon energy, in that the amplitude is larger at lower energies. However, Norton & Watson (1989) found that the energy dependence of spin modulation seen in the EXOSAT data was not as strong as expected if it was caused by a single photoelectric absorber: I show an example in Figure 7. A simple absorber with a column density high enough to modulate the 4–10 keV count rate ($N_H \sim 10^{23} \text{ cm}^{-2}$) should completely absorb all photons below 2 keV, yet roughly one half of soft photons are unabsorbed. Norton & Watson (1989) therefore introduced the concept of partial-covering absorber to IPs, which improved the spectral fit for both the phase-averaged and phase-resolved spectra. Changes in the column density and/or the covering fraction of the partial covering absorber can reproduce the energy dependence of spin modulation observed. Since then, it has become routine for spectral fit to IPs to use partial covering absorbers (`pcfabs` or any absorber model convolved with `partcov` in `xspec`), sometimes more than one depending on the data quality.

The partial covering nature of the spin modulation of IPs is in clear contrast to the stream dips in polars, which is caused by a distant part of the stream. The logical candidate location for the absorber is the immediate pre-shock flow: since the emission region (the post-shock region) and the absorption region are of similar size and are adjacent, it is hard for the absorption to be anything but partial in this case. In fact, a deeper examination of the geometry leads to the conclusion that the traditional partial covering models are not complex enough (Done & Magdziarz 1998). As the lines of sights to different parts of the X-ray emission region go through differing amounts of matter (Figure 8), the absorption cannot be modeled as an absorber with a unique N_H or as partial covering absorbers with several discrete values of N_H , each covering a fraction of the X-ray source. The geometry of absorption by the pre-shock flow requires

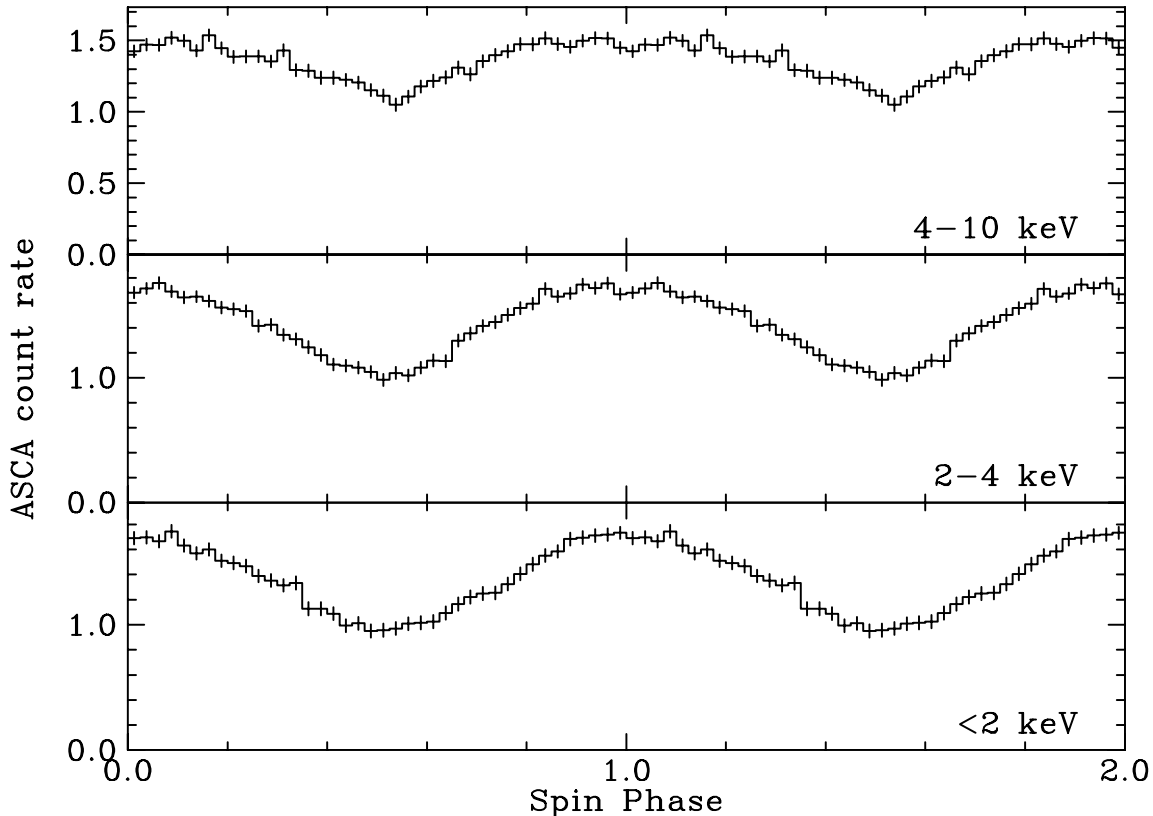


Figure 7. An example of energy-dependent X-ray spin modulation of IPs, V1223 Sgr observed with ASCA.

a distribution of covering fraction as a function of N_{H} , which Done & Magdziarz (1998) approximated as a power law, and implemented in `xspec` as `pwab`. While a simple photometric absorber results in an exponential cut-off at low energies, this complex absorber has an approximately power-law dependence on photon energy (Figure 9). In the context of this model, the spin modulation of IPs can be explained as changes in the parameters of such a complex absorber, most likely the maximum N_{H} .

However, this model may not be applicable to all IPs. In EX Hya, there is little evidence for absorption (simple or complex) either in the phase-averaged spectrum (see next section) or in the energy-resolved spin light curves. Allan et al. (1998) therefore advocated the possibility that the spin modulation in this unusual IP is due to self-occultation (i.e., by the body of the white dwarf). Mukai (1999) introduced the concept of “horizon angle,” the angle between the line connecting the emission region to the white dwarf and the line of sight. An emission region infinitesimally above the surface will disappear behind the limb of the white dwarf when the horizon angle is 90 degrees. However, for a realistic range of \dot{m} , the shock height can easily be a few percent of the white dwarf radius (see their Figure 1), so it would not be surprising if the horizon angles in some IPs were in the 100–120° range. This means that, assuming these IPs accrete at both poles of a centered dipole, there is a wide range of viewing angles at which emissions from both poles are simultaneously observable. This is the kind of effect envisioned by Allan et al. (1998). The same model may also apply to HT Cam, another IP with little evidence of absorption and energy-independent spin amplitude (de Martino et al. 2005). Note that both EX Hya and HT Cam are short period IPs below the period gap, and hence expected to have low accretion rates. This naturally results in low \dot{m} and hence tall shocks, which makes pre-shock absorption geometrically less important, likely making the visibility of two tall post-shock regions the main mechanism for spin modulation. Such low luminosity IPs (LLIPs) will be discussed again in §8.

5.4. Hard X-ray Spectra of Magnetic CVs

Mukai et al. (2003) presented early HETG spectra of 7 CVs then available in the *Chandra* archive, and showed that they can be divided into two types, “cooling-flow” and “photoionized.” Non-magnetic CVs SS Cyg, U Gem, and V603

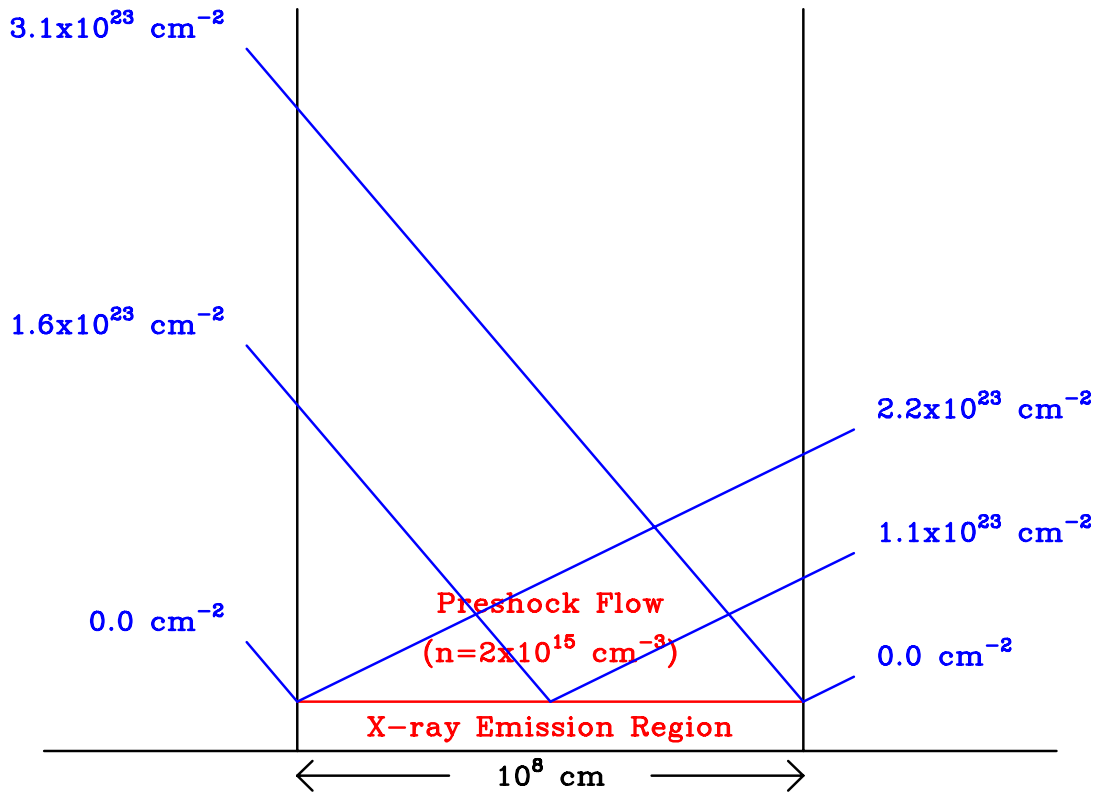


Figure 8. A schematic diagram illustrating the pre-shock flow acting as a complex absorber.

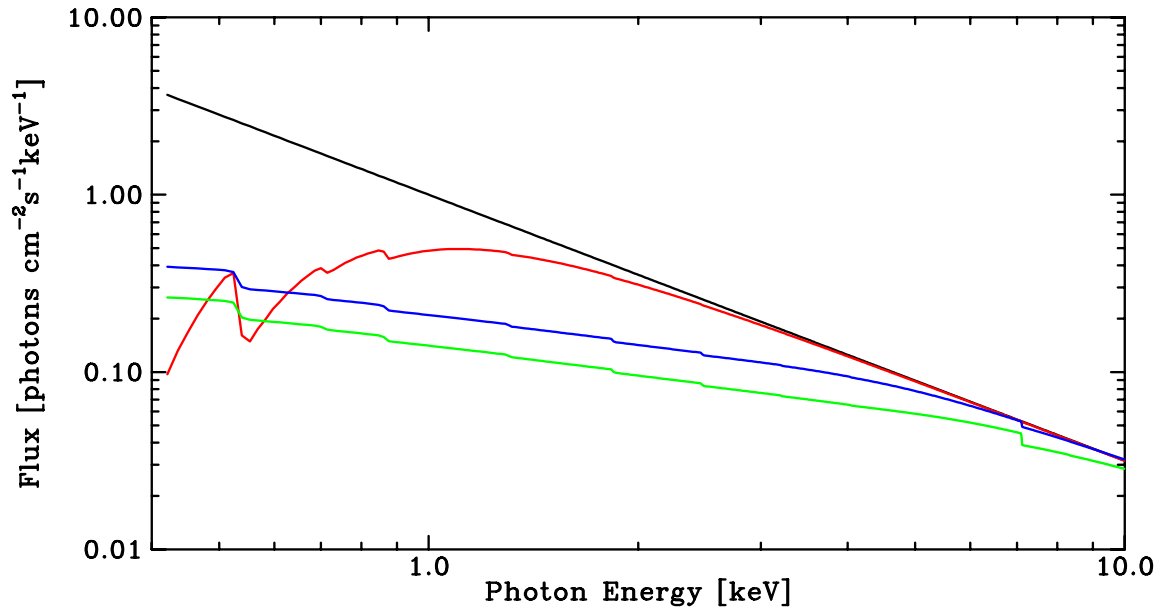


Figure 9. The energy dependence of the complex absorber as encoded in the `pwab` model. Unlike a simple photoelectric absorber, which results in an exponential cutoff at low energies (red curve), this absorber is power-law like (blue and green lines, shown for different maximum values of N_{H}).

Aql, as well as the LLIP, EX Hya, belong to the first type. The second group is the photoionized type, comprised of 3 IPs, V1223 Sgr, AO Psc, and GK Per. Their X-ray spectra are characterized by a hard, power law-like continuum

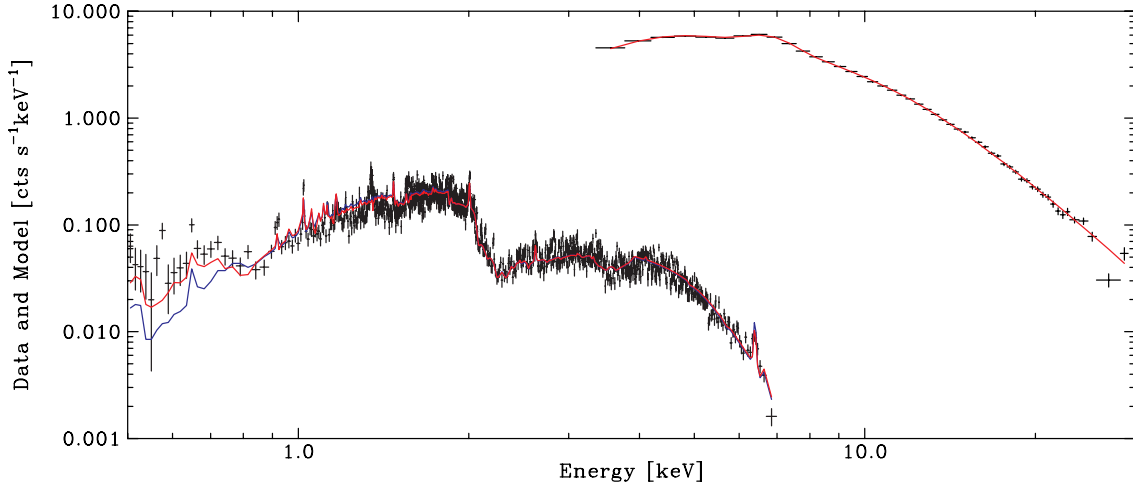


Figure 10. Preliminary joint spectral fit to simultaneous *RXTE* PCA and *Chandra* HETG observations of V1223 Sgr. A single model (but allowing for a cross normalization factor between *RXTE* and *Chandra* data) was fit to MEG, HEG, and PCA data (HEG spectrum is omitted from the figure for simplicity). The blue model is the `mkcflow` cooling flow model modified by the complex absorber model, `pwab`; in the red model, `pwab` was replaced with an ionized absorber version of `pwab` currently in development.

in the 0.5–8 keV range that is too flat to be reproduced by the cooling flow model modified by simple absorber. Also, their emission line ratios do not follow the prediction of the cooling flow model. Mukai et al. (2003) therefore fitted the *Chandra* HETG-band spectra of these systems using an *ad hoc* power law with a model of photoionized emission. However, such a model is clearly unphysical: the strong shock is the primary energy source in IPs, and their X-ray spectra above 10 keV are well fit by cooling-flow type models. The solution is likely to lie in the effect of the complex absorber: Mukai et al. (2015) showed that the joint *NuSTAR-XMM-Newton* spectra of IPs above 1–2 keV can be fit well with an `mkcflow` model modified by `pwab`. In Figure 10, I show an example of fitting simultaneous *Chandra* HETG and *RXTE* PCA spectra of V1223 Sgr, again showing that this model can reproduce the gross features of the X-ray spectra of IPs.

As already discussed in §2, reflection plays an important role in the observed X-ray spectra of CVs and symbiotic stars, and one can borrow from the studies of reflection off the accretion disk in active galactic nuclei (AGN) and in X-ray binaries (George & Fabian 1991). In magnetic CVs, the 6.4 keV line is usually present often with equivalent widths of order 150 eV. Although this line is also expected from the intrinsic absorber, statistical analysis of the *ASCA* sample led Ezuka & Ishida (1999) to conclude that some of the 6.4 keV line is indeed from reflection off the white dwarf surface. The Compton reflection hump was first detected in AM Her by Rothschild et al. (1981), and a few other reports followed sporadically (see, e.g., Beardmore et al. 1995; Done, Osborne & Beardmore 1995). Recently, the analysis of joint *XMM-Newton* spectra of V709 Cas, NY Lup and V1223 Sgr by Mukai et al. (2015) led to a direct and robust detection of the Compton hump in these systems.

Not only did Mukai et al. (2015) securely detect reflection, they measured the reflection amplitude. The amplitude is defined as 1.0 when the reflector subtends 2π steradian of sky as seen from the X-ray emitter. If the emission region is just above the white dwarf surface in magnetic CVs, we expect a reflection amplitude close to 1.0. However, at least in V709 Cas, the reflection amplitude was estimated to be significantly lower (<0.60 in the cooling flow fit to the joint *NuSTAR-XMM-Newton* data). This can be accommodated within the standard framework if the shock height is not negligible. For example, an X-ray emission region $0.2 R_{wd}$ above the surface would result in a reflection amplitude of 0.45. Such an emission region will also have a horizon angle of 123.5° , so both poles should remain visible for a substantial fraction of the spin period. Indeed, spin modulation above 10 keV was already seen in V709 Cas by de Martino et al. (2001) and even more clearly in the *NuSTAR* data by Mukai et al. (2015). This is the most likely mechanism for hard (>10 keV) X-ray spin modulation of IPs, where the photoelectric absorption is negligible, although viewing geometry dependence of reflection hump and Compton scattering in the accretion flow (Rosen 1992) also needs to be considered.

Additional complication is the warm absorber edge reported in the *Chandra* HETG spectrum of V1223 Sgr (Mukai et al. 2001) and the *XMM-Newton* RGS spectrum of V2731 Oph (de Martino et al. 2008). Mukai et al. (in preparation) have begun experimenting with an ionized version of the `pwab` model, with at least qualitative success (Figure 10). This is to be expected, since the immediate pre-shock flow in IPs, the site of the complex absorber, is situated adjacent to the post-shock region emitting X-rays at a rate of several times 10^{33} ergs s $^{-1}$. One expects warm absorber features when directly viewing the post-shock region through the pre-shock flow, and photoionized emission features from parts of the pre-shock flow not in front of the post-shock region, consistent with the findings of Mukai et al. (2003).

5.5. The White Dwarf Mass

The potential utility of X-ray spectra of magnetic CVs for estimating M_{wd} has been known since at least Rothschild et al. (1981). Several groups have applied this basic idea using a variety of X-ray data and several different spectral models.

Cropper, Ramsay & Wu (1998) applied their post-shock region model to the 2–20 keV spectra of 14 magnetic CVs (polars and IPs) and often found high values for the M_{wd} . However, when Ramsay et al. (1998) compared M_{wd} estimates for XY Ari derived from X-ray spectra (using *ASCA*, and *RXTE* data) using the same model, against that derived from X-ray eclipse timings, the former were found to be systematically too high. One plausible interpretation is that the continuum shape below 20 keV is too heavily influenced by complex absorbers and the reflection hump to allow a reliable estimate of M_{wd} .

Ezuka & Ishida (1999) took a different approach, instead focusing on the intensity ratio of He-like and H-like Fe K lines. In an isothermal plasma, the ratio can be interpreted as ionization temperature; in a multi-temperature plasma, it is the emission measure weighted average of the ionization temperature within the post-shock region, which can be related to the shock temperature, hence M_{wd} . Although this method is potentially subject to systematic uncertainties of its own due to the accuracy of continuum fit (particularly the depth of the Fe K edge) and detailed physics of the lines (see §9.5), it does provide a useful check of the broadband fitting method.

Suleimanov, Revnivtsev & Ritter (2005) applied their own structured post-shock region model to *RXTE* PCA and HEXTE data of magnetic CVs, covering the 3–100 keV range, and obtained lower M_{wd} estimates than those previously obtained from X-ray spectral fitting. The key is the use of the broadband data: this approach has the advantage that the data include the energy range where the exponential cut-off of the multi-temperature Bremsstrahlung continuum is expected. Although their spectral model does not include line emission, and the Fe K triplet is modeled as a single Gaussian, this is not an issue as long as the high energy continuum shape is well constrained by the data. The same basic approach was followed by Yuasa et al. (2010) using *Suzaku* XIS and HXD data and their own model of the post-shock region, which does include the lines. The disadvantage of this approach is the relatively poor quality of the HEXTE and HXD data for most objects, which, combined with the additional complication of reflection, might introduce systematic errors. For the *Suzaku* work, an additional weakness is that these IPs are near the faint limit for HXD, where the systematics of background subtraction is an issue, coupled with the uncertainties in the XIS-HXD cross calibration. Nevertheless, these methods have potential to make routine determination of M_{wd} possible given X-ray data of sufficient quality.

5.6. The Soft Component of Magnetic CVs

In the simplest picture, one might expect that the hard and the soft luminosities of magnetic CVs are roughly equal (Lamb & Masers 1979). In contrast, observations through the early 1990s indicated a soft X-ray excess in polars and a lack of detectable soft components in IPs. Before going into more recent observations that modified these views, it is important to consider the reason why polars can have soft excess: at low \dot{m} and high magnetic field, cyclotron cooling of the post-shock region becomes important. Furthermore, it may enter the non-hydrodynamic regime (Lamb & Masers 1979) and a stream of fast ions may directly heat the white dwarf atmosphere (“cyclotron-dominated low- \dot{m} bombardment solution”; Fischer & Beuermann 2001 and references therein). In addition, the shock height is lowered compared to the Aizu values for the same M_{wd} and \dot{m} , and the electron temperature is lower than in corresponding Aizu case.

The differences in the physics of post-shock region will also impact the spectrum of the soft component. As discussed in Section 2, stellar atmosphere models are necessary to describe the outgoing radiation of a white dwarf whose energy source is deep inside the atmosphere, while irradiation from above alters the temperature gradient and the outgoing

spectrum is closer to a blackbody (Williams, King & Brooker 1987). This was studied by Mauche (1999) using *EUVE* grating spectra of polars, who found the blackbody to provide superior fits to the data compared to pure-H or solar abundance stellar atmosphere models suggesting that irradiation from above plays a significant role. However, there are departures from the blackbody, so what is needed is an irradiated stellar atmosphere model. Note also that the effective temperatures derived from the blackbody fits are in the 15–25 eV range for the 9 polars, lower than typically found using lower resolution X-ray data. Also note that the bolometric fluxes inferred from the fits depend strongly on the choice of models. Any inferences we can currently draw from X-ray data should be treated with caution, until a full set of irradiated stellar atmosphere models are developed and high quality data that can test them are obtained.

Two further complications exist in fitting the soft component. First, it is likely that the heated area of the white dwarf cannot be characterized using a single temperature (Beuermann, Burwitz & Reinsch 2012). This might result from intrinsic density gradients in the accretion flow from the L_1 point (Lubow & Shu 1975) that survives beyond the interaction region (Cash 2002). Even a uniform density stream can lead to a distribution of temperatures, if the soft component is primarily due to irradiation and the shock is well above the white dwarf surface. Only the center of the accretion foot point is fully illuminated and reaches the highest temperature, which is surrounded by a halo of partially illuminated region with lower temperatures, the outer parts of which may primarily emit in the UV (Gänsicke et al. 1998).

The other complication is whether the soft component can escape going through the same complex absorbers that hard X-rays do. Traditional view is that the soft component is unaffected. In general, the soft X-ray component of polars appears unabsorbed, except by the ISM. Moreover, there are no obvious spectral changes as a function of spin phase, even as intensity changes by a significant factor (see, e.g., the *EXOSAT* grating observation of QQ Vul; Osborne et al. 1986). These arguments do exclude the model in which the soft component is affected by a simple absorber or a partial covering absorber. However, as noted above, complex absorbers of the *pwab* type do not manifest themselves as exponential cut-off of low energy photons (Figure 9), so the possibility of a *pwab*-type absorber is not ruled out by the data. Geometrically speaking, while the outer halo may effectively escape the shadow of the pre-shock flow, the soft X-rays are likely to be from the smaller core and is probably subject to absorption in the pre-shock flow.

Ramsay & Cropper (2004) published the most up-to-date summary of the soft excess to date, using a snapshot survey of polars using *XMM-Newton*. They find large soft excesses (more than a factor of 5) in only 13% of their sample, significantly down from earlier studies based on *ROSAT* data (58% according to Ramsay et al. 1994, but 24% in the re-analysis using updated calibrations by Ramsay & Cropper 2004). They also found several polars without a detectable soft component. The *XMM-Newton* data are far better suited for the accurate characterization of the hard component, and Ramsay & Cropper (2004) used their multi-temperature shock emission model with complex absorbers, as necessary. However, they used a blackbody model with simple absorber for the soft component, which clearly is a limitation of this study, or rather, that of our current understanding of the soft component. Moreover, the blackbody temperatures determined using the *EUVE* grating data (Mauche 1999) are systematically lower than those determined from *ROSAT* data (Ramsay et al. 1994) — unfortunately, Ramsay & Cropper (2004) did not tabulate their best-fit temperatures — possibly indicating that both may have been influenced by the choice of an imperfect spectral model. Also, these recent paper concentrated solely on the luminosity ratios, and not the actual luminosity values. A direct comparison of hard component luminosity against evolutionary expectations (King & Watson 1987) would have provided an additional check of the soft excess.

On the IP side, PQ Gem and V405 Aur were discovered to have a distinct soft component, by Haberl & Motch (1995), and were called soft IPs. Evans & Hellier (2007) analyzed the *XMM-Newton* data on 12 IPs and found that the fit improved with the addition of a blackbody component for 8 of them. Note, however, that this is not necessarily the same as proving the existence of a soft component. In some cases, the conclusion that there is a separate soft component appears inescapable, because the data are plainly above any reasonable extrapolation of models that fit above 2 keV. In other cases, however, the blackbody may be fitting the residuals created by the fact that the spectral model for the hard component is imperfect (emission model with incorrect DEM, the use of double partial covering absorber model etc.). Discoveries of additional IPs with apparent soft components have continued since then (see, e.g., Anzolin et al. 2008). Taken at face value, these fits indicate that the soft component in IPs tend to be hotter (many above 50 eV and as high as 120 eV; Figure 11 of Anzolin et al. 2008) than in polars, arise from smaller spots, and represent smaller fractions of the total luminosity of these systems. The inferred temperature are close to the Eddington limit of very high mass white dwarfs, and are higher than the atmosphere limit for (Williams, King & Brooker 1987), however.

5.7. *The Magnetospheric Boundary of IPs*

Theories of interaction between a partial accretion disk and the magnetic field of a compact object start with the simplest geometry, that of an aligned rotator (magnetic pole=rotational pole), and often stop there. In an aligned rotator with a centered dipole, there is azimuthal symmetry. The accretion flow must make a 90° change in direction of motion at the magnetospheric boundary. The inner radius of the disk is determined by the balance between the kinetic energy density of the disk and the magnetic energy density. The equilibrium spin period of the white dwarf is determined by the balance between the material torque and the magnetic torque. In equilibrium, the inner disk radius is near the co-rotation radius (Ghosh & Lamb 1979), although the exact location (their fastness parameter) is subject of debate. Other things being equal, a weaker magnetic field leads to a smaller inner disk radius, hence a faster equilibrium spin period. Long-term campaign of optical photometry can reveal spin period changes over several years, and this can be used to infer the magnetic moment and other properties of the IPs (Patterson 1994). Finally, if the inner edge of the disk is sufficiently close to the white dwarf surface, then one of the basic assumptions of Aizu (1973) breaks down: the flow velocity is determined by the free-fall condition starting from the magnetospheric boundary, and not the free-fall velocity from infinity.

If the magnetospheric radius is inside the co-rotation radius, the Keplerian flow must first decelerate; outside, the flow must accelerate to match the motion, if it is able to accrete at all. However, IPs by definition are oblique rotators, or spin modulations will not be observable. There is no well-developed theory of how accretion disk matter couples to the magnetic field lines in this situation. Observers sometimes vaguely describe two accretion curtains, each 180° wide, centered on the sub-polar point of the inner edge of the disk. How wide are the curtains, and what is the azimuthal dependence of accretion rate?

X-ray observations of two IPs may provide a clue (Hellier 2014). Both FO Aqr and PQ Gem show sharp absorption notches in the spin profiles in addition to the general, smoother, spin modulation. The latter is due to the complex absorption by the immediate pre-shock flow, while the former is thought to be the equivalent of the stream dips in polars, and similarly thought to be caused by the distant part of the accretion curtain. Based on the relative phasing of the two, accretion in FO Aqr appears to occur predominantly from points behind the poles (Evans et al. 2004) while that in PQ Gem is predominantly ahead (Evans, Hellier & Ramsay 2006). Since the white dwarf in PQ Gem is spinning down (Evans, Hellier & Ramsay 2006), it is reasonable to assume that the inner edge of the disk is outside the co-rotation radius. The X-ray data can then be explained if the more rapidly moving field lines sweeps up the disk material from behind in regions where they are sufficiently tilted and only small-angle deflections are necessary. Similarly, in FO Aqr, which has been spinning up in recent years (Williams 2003), disk material experiences a small-angle deflection to start following the tilted field line which is moving more slowly than the local Keplerian velocity.

5.8. *The Partial Disk and Related Phenomena*

Observers often take it for granted that most IPs have a partial accretion disk, but this issue needs a careful examination. King & Lasota (1991) reviewed the conditions for the existence and the formation of partial accretion disks. When accretion initially starts, the stream from the L_1 point follows a ballistic trajectory. If the minimum distance that this ballistic trajectory takes, R_{\min} , is less than R_{wd} , no disk can form. Similarly, if the magnetospheric radius R_{mag} is greater than R_{\min} , then no disk can form, and the accretion proceeds directly to the magnetic pole(s): such a system should be a polar. Once a partial disk is well established, the accretion stream can be absorbed into the disk at its outer radius, but the conservation of angular momentum dictates that the inner and outer radii of the disk (R_{in} and R_{out}) must encompass R_{circ} , the circularization radius where the specific angular momentum of the Keplerian motion equals that of matter at L_1 point. If one further assumes spin equilibrium, then the spin period is a proxy for $R_{\text{in}}=R_{\text{mag}}$. King & Lasota (1991) noted that IPs with $P_s=0.1 \times P_o$ (see Figure 11 for an updated plot) were near the limit of where partial disks could exist, depending on the mass ratio.

There are now multiple examples of IPs below the period gap in which P_s significantly exceeds $0.1 \times P_o$, including EX Hya. They may be accreting via a standard, partial, accretion disk, with $R_{\text{mag}} < R_{\text{in}}$, in which case they are severely out of spin equilibrium and one expects them to be spinning up much faster than those with $P_s=0.1 \times P_o$. On the other hand, if they are at or near spin equilibrium, their accretion flow is unlike the standard accretion disk in non-magnetic CVs (Norton et al. 2008). If the X-ray spectrum of EX Hya indeed indicates that R_{in} is small (Luna et al. 2015), this strongly favors the first interpretation.

Although most IPs with $P_s < 0.1 \times P_o$ are believed to accrete via a partial accretion disk, V2400 Oph (=RX J1712.6–2414) is an exception. Its X-rays are modulated at the 1003 s period, not the 927 s period seen

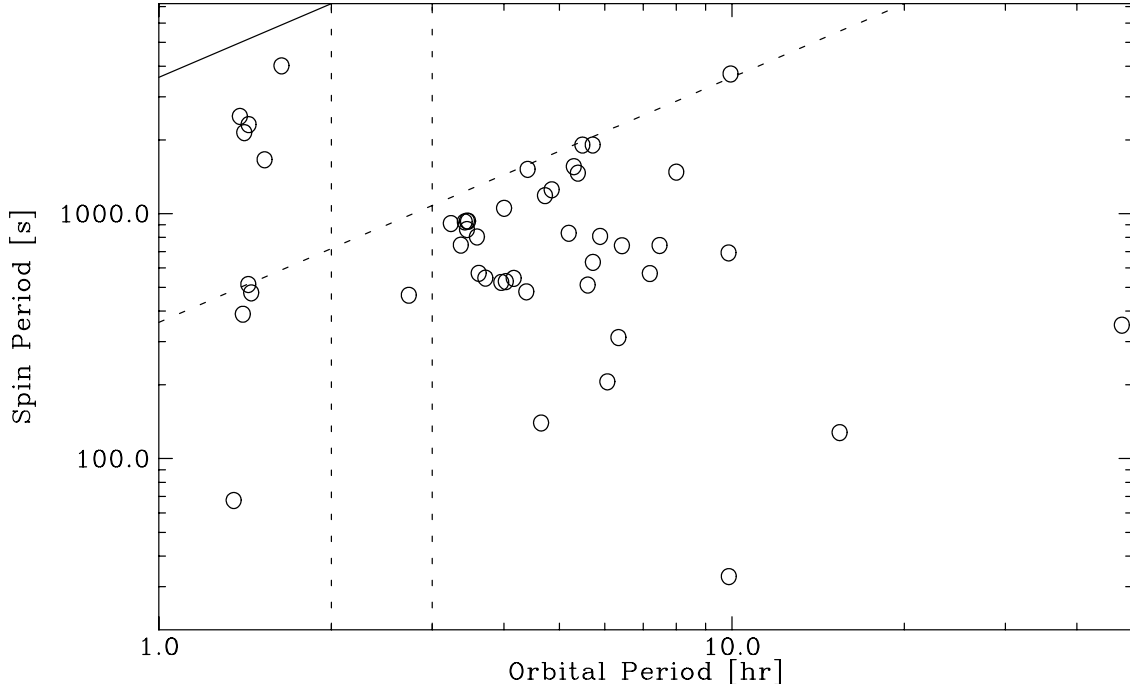


Figure 11. Locations of 47 confirmed IPs with well-established orbital and spin periods. Vertical dashed lines show the approximate location of the CV period gap (2-3 hrs), while the diagonal lines are shown for $P_s=P_o$ (solid; i.e., polars) and for $P_s=0.1 \times P_o$.

in optical polarimetry (Buckley et al. 1997), which is almost certainly the true spin period. The X-ray modulation is at the beat (or synodic) period: $P_b = (P_s^{-1} - P_o^{-1})^{-1}$. This is the expected behavior for a diskless IP seen at a low inclination angle (Wynn & King 1992) due to pole-switching. That is, one pole is favored to capture the majority of the matter in the accretion stream from the secondary during \sim half the beat cycle. While beat period modulation in the optical is often seen and is likely due to reprocessing of X-rays in structures fixed in the binary frame (the secondary and/or the bright spot region of the disk), any X-ray beat modulation almost certainly requires pole-switching.

While the X-ray modulation in FO Aqr is spin-dominated, some modulation is also observed at the beat period. To explain this, Hellier (1993) proposed disk overflow accretion as the model: at the outer edge, some of the accretion stream from the secondary is incorporated into the disk, but the rest continues on the ballistic trajectory above the orbital plane, and can accrete directly onto the magnetic poles. The relative importance of disk and overflow accretion appears to change from epoch to epoch in FO Aqr (Beardmore et al. 1998) and in TX Col (Norton et al. 1999).

For disk overflow accretion to take place, the magnetic field of the white dwarf must reach the ballistic overflow. Since a well-developed disk can in principle shield its outer region from the field, it is likely that the ballistic stream needs to reach or approach the inner edge of the accretion disk. Both FO Aqr and TX Col has P_s close to $0.1 \times P_o$, so this condition is likely to be satisfied. In addition, Hellier et al. (2000) discovered an X-ray beat modulation in EX Hya during the 1998 outburst (itself a likely sign of partial accretion disk; Angelini & Verbunt 1989), suggesting disk overflow accretion. If so, $R_{in} \sim R_{circ}$ in EX Hya even in outburst, and R_{in} is expected to decrease during outburst (cf. the case of XY Ari: Hellier, Mukai & Beardmore 1997), contrary to the inference from X-ray spectroscopy mentioned above. Thus, the true nature of accretion flow in EX Hya remains a mystery.

5.9. AE Aqr: a Probable Propeller

AE Aqr is a highly unusual IP with a rapidly rotating ($P_s=33$ s) white dwarf. Optical spectroscopy failed to show the signatures of an accretion disk, with the H α line likely originating in matter being ejected by a propeller mechanism (Welsh, Horne & Gomer 1998). At the same time, AE Aqr is a well-known X-ray source, if atypically soft for IPs (Ezuka & Ishida 1999). If it is a propeller, what is the origin of these soft X-ray emission? Itoh et al. (2006) analyzed the XMM-Newton RGS data, and found that the intensity ratios of N and O helium-like triplets implied a modest plasma density of $\sim 10^{11}$ cm $^{-3}$. This, combined with the emission measure, led them to conclude that the emission

region is much larger than the white dwarf. [Mauche \(2009\)](#) analyzed the *Chandra* HETG data, and found that Ne, Mg and Si lines favored progressively higher densities (or else subject to higher degree of photoexcitation). Considering this and also the velocity information, [Mauche \(2009\)](#) proposed that the X-rays may be produced by accretion onto the white dwarf in the bombardment regime. [Kitaguchi et al. \(2014\)](#) observed AE Aqr with *NuSTAR* and detected pulsed thermal emission up to ~ 20 keV. They also considered it likely that they originated in accretion onto the white dwarf surface, although their interpretation differed from that of [Mauche \(2009\)](#) in details. That is, despite the propeller effect well established through optical spectroscopy, some of the matter appears to accrete onto the white dwarf successfully.

The origin of X-rays in AE Aqr can be questioned because the white dwarf is spinning down, with sufficient spin-down power to explain the luminosity in the X-rays and at other wavelengths in principle ([Mauche 2006](#)). In this respect, AE Aqr remained unique among all magnetic CVs, until it was realized that an previously obscure object, AR Sco, was an M star-white dwarf binary that was also spin-down powered ([Marsh et al. 2016](#)). The actual emission mechanisms in AR Sco appear completely different from those in AE Aqr, however.

6. X-RAY EMISSION FROM NON-MAGNETIC CVs AND SYMBIOTIC STARS

In non-magnetic CVs and symbiotic stars, the starting point for interpretation is the boundary layer model, in which the Keplerian accretion disk extends all the way down to the white dwarf surface. The disk converts half the potential energy to kinetic energy and the rest is radiated away in the IR, optical, and UV. The boundary layer, in which the Keplerian disk connects with the white dwarf surface, should emit equal luminosity as the disk, if the white dwarf is a slow rotator. At high accretion rates, the boundary layer should become optically thick and emit in the soft X-ray/EUV range, yet optically thin, medium energy X-ray component is usually observed ([Patterson & Raymond 1985b](#)). At low accretion rates, the boundary layer should be optically thin and emit hard X-rays ([Patterson & Raymond 1985a](#)); however, one should note that models in which the accretion disk develops a central hole have also been proposed.

6.1. Observational Overview

Although X-rays from non-magnetic CVs had been detected using non-imaging instruments, it was the imaging capability of *Einstein* that established them as a class of X-ray sources (see [Córdova & Mason 1984](#) and references therein). More recent compilation papers include those of *ASCA* data by [Baskill, Wheatley & Osborne \(2005\)](#), and *XMM-Newton* data by [Pandel et al. \(2005\)](#). These and other works firmly established non-magnetic CVs in general, and quiescent dwarf novae in particular, as an important class of medium-energy X-ray sources, at luminosities in the $10^{30} - 10^{32}$ ergs s⁻¹ range. They also established that their X-rays originated in an optically thin, multi-temperature region. Furthermore, [Mukai et al. \(2003\)](#) showed that the cooling flow model provided a reasonable description of their X-ray spectrum. At high accretion rates, a few nearby dwarf novae in outburst have also been detected as soft X-ray/EUV sources. While the soft component is almost certainly from the optically thick boundary layer, the optically thin emission never completely disappear, as was already noted by [Patterson & Raymond \(1985b\)](#).

The presence of exhibit X-rays from the accretion disk boundary layer is now well established. For example, [Luna et al. \(2013\)](#) conducted a *Swift* XRT snapshot survey of known symbiotic stars, and found a number of them to emit optically thin, thermal X-rays in the medium energy band, which they named the δ -type X-ray emission. Some δ -type emissions are hard enough and luminous enough for five symbiotic stars to have been detected in the *Swift* BAT survey ([Kennea et al. 2009](#); [Mukai et al. 2016](#)). The δ component is often heavily absorbed. Some symbiotic stars show a $kT \sim 1$ keV, optically thin, thermal (β -type; [Mürset, Wolff & Jordan 1997](#)) component, which is likely due to colliding winds. Several systems show a combination of a relatively unabsorbed β component and a heavily absorbed δ component ([Ezuka, Ishida & Makino 1998](#)). Shell-burning symbiotic stars, on the other hand, have been detected as supersoft (α -type; [Mürset, Wolff & Jordan 1997](#)) X-ray sources, in the few cases where absorption is relatively low⁸. These, as well as the spatially extended, optically thin, thermal X-rays (see §3.2) are discussed further in §6.5.

6.2. Quiescent Dwarf Novae

The outburst behavior of dwarf novae is widely interpreted in the framework of the disk instability model (DIM; see [Lasota 2001](#) and references therein)⁹. According to DIM, quiescence is when the disk is in a low temperature, low

⁸ [Mürset, Wolff & Jordan \(1997\)](#) used the term, γ -type, to describe the spectrum of the symbiotic X-ray binary, GX 1+4, which has a neutron star accretor.

⁹ Note, however, this is not a universally accepted model for all dwarf novae (see, e.g., [Baptista, Borges & Oliveira 2016](#)).

surface density state that is incapable of transporting all the incoming matter onto the white dwarf surface; the disk mass increases gradually, until a critical value is reached and the disk transitions to a hot state, allowing a large amount of matter to accrete onto the white dwarf in a relatively short span of time. DIM has been successful in reproducing the observed properties of dwarf nova outbursts (see, e.g., Cannizzo et al. 2012), less so those of quiescence (see below). Regardless of the details, the accretion rate onto the white dwarf (\dot{M}_{acc}) in quiescence must always be smaller than the average mass transfer rate from the secondary (\dot{M}_{tr} , usually taken to be constant) for DIM to work. The latter can be estimated by integrating the luminosity of a dwarf novae through outburst cycles, while X-ray observations in quiescence offers a simple and plausible method for estimating the former.

The X-rays from quiescent dwarf novae are optically thin, thermal emissions from multi-temperature plasma. While such models are required to achieve a good fit to high quality data (spectral resolution of a CCD detector combined with good signal-to-noise ratio), current data are insufficient to derive DEM distribution purely from data. Thus, Baskill, Wheatley & Osborne (2005) used a purely phenomenological power-law DEM distribution in their analysis of ASCA data, while Mukai et al. (2003) used the cooling flow model (see Figure 5) in the analysis of *Chandra* HETG data. A hybrid approach was adopted by Pandel et al. (2005) in their analysis of *XMM-Newton* data: they used their own, modified version of `mkcflow` model which allowed the DEM to be tilted relative to that of the standard cooling flow by multiplying with a power law (see their equation 2). They often found statistically significant deviation of this power law index from 0.0, which should be investigated further in the future, even though they remark that the isobaric cooling flow model provides a good description of the X-ray spectra.

An important parameter of such fits is the maximum temperature of the plasma. Pandel et al. (2005) started their comparison with the Virial temperature (kT_{vir}) and concluded that the maximum temperature is $\sim 0.6kT_{vir}$. This is close to the temperature expected of a strong shock for Keplerian flow ($9/16 kT_{vir}=0.5625kT_{vir}$) that Byckling et al. (2010) compared their data to (see also Figure 1). Note that both these papers took the white dwarf mass estimates from the literature, with varying precision and accuracy. In particular, unless the system is eclipsing, the inclination angle is often uncertain, which to a large uncertainty in the mass estimate. Having said that, currently available data are consistent with the idea that the X-ray emission from quiescent dwarf novae are powered by a strong shock in the boundary layer between the white dwarf surface and the Keplerian disk that extends all the way down to it.

This picture is consistent with the fact that the X-ray emission region in quiescent dwarf novae is compact, as shown by sharp transitions in the X-ray light curves of deeply eclipsing dwarf novae HT Cas, OY Car, and Z Cha (Mukai et al. 1997; Ramsay et al. 2001; Nucita et al. 2009, 2011). For OY Car, Wheatley & West (2003) found that the eclipse duration (mid-ingress to mid-egress) and the ingress/egress durations (see §3.3.4) were both shorter in X-rays than in the optical, but in such a way that the second and the third contacts were aligned in these two different wavelength regimes to within measurement errors. This implied an effective vertical displacement of X-ray emission region. Wheatley & West (2003) interpreted as implying that X-rays were emitted at the polar regions, but the lower pole was occulted, presumably by the accretion disk. The absorption (and hence the apparent displacement) is less prominent for X-rays above 2 keV than those below 2 keV in Z Cha, the latter dominating the total *XMM-Newton* EPIC light curve (Hickman et al. 2009).

Absorption in the disk had already been invoked by van Teeseling, Beuermann & Verbunt (1996) to explain the inclination dependence of the soft X-ray fluxes among non-magnetic CVs studied with *ROSAT*. The *XMM-Newton* spectrum of the deeply eclipsing system, HT Cas had a measured absorbing column of $1.6 \times 10^{21} \text{ cm}^{-2}$, far in excess of what would be expected from the ISM for an object at a distance of 130 pc (Thorstensen, Lépine & Shara 2008). The *Suzaku* spectrum of the partially eclipsing system, V893 Sco required a partial covering absorber with $\sim 50\%$ covering fraction at $N_H \sim 2 \times 10^{22} \text{ cm}^{-2}$ (Mukai, Zietsman & Still 2009), again suggestive of absorption by the inner disk. However, if it is a disk, it is quantitatively very different from the standard optically thick, geometrically thin, steady state disk, which predict a surface density of order 1 g cm^{-2} near the inner edge of the disk (see, e.g., Hameury et al. 1998), hence should result in a much higher N_H .

Once the modest absorption (N_H of order 10^{21} to 10^{22} cm^{-2}) in the disk plane is considered, the eclipse results on OY Car (Wheatley & West 2003) does not necessarily imply the displacement of the emission region. It only proves that a large fraction of photons detected with *XMM-Newton* EPIC instruments are from above the orbital plane, which is still qualitatively consistent with a boundary layer emission.

These and other observational results pose a severe challenge to the basic version of DIM. It predicts that matter simply accumulates in the outer disk with very low accretion rate onto the white dwarf during quiescence. Byckling et al.

(2010) used a sample with parallax based distances¹⁰, and derived a luminosity in the 10^{30} – 10^{32} ergs s⁻¹ range, which requires an accretion rate that is many times higher than can be achieved through a cold disk (Lasota 2001). DIM also predicts that the accretion rate should increase during quiescence from the end of one outburst to the beginning of the next, as the surface density of the disk increases. This has never been observed at any wavelengths: In particular, in X-rays, dwarf novae appear to remain constant or decline slowly in luminosity during the inter-outburst intervals (e.g., McGowan, Priedhorsky & Trudolyubov 2004; Collins & Wheatley 2010; Fertig et al. 2011). Moreover, the WZ Sge type stars, i.e., dwarf novae with extremely long quiescent intervals, cannot be explained with DIM with $\alpha \sim 0.01$ that works for shorter recurrence period dwarf novae. Finally, Britt et al. (2015) discovered a correlation between the quiescent X-ray luminosity and the duty cycle of dwarf novae. While this does not immediately contradict DIM, there does not appear to be a ready explanation for it, either.

For the unexpectedly high quiescent X-ray luminosity, relative to the basic version of DIM, an often cited fix is the truncated disk, perhaps via the coronal siphon flow (Meyer & Meyer-Hofmeister 1994). For the exceptionally long inter-outburst of WZ Sge, a proposed solution is also a truncated disk (Lasota, Kuulkers & Charles 1999). It is implausible for the truncated disk to be the solution for both problems, however: If quiescent dwarf novae with normal inter-outburst intervals (weeks to a few months) needs a truncated disk, WZ Sge with 30-year inter-outburst interval would need an even bigger hole, leaving little room for a disk to exist. A possible alternative is the evaporative instability of the accretion disk (Shaviv & Wehrse 1986) combined with the irradiation from the boundary layer (de Kool & Wickramasinghe 1999). Unfortunately, none of these models have provided, to date, an explanation of how quiescent dwarf novae maintain a constant or slowly declining X-ray luminosity during quiescence¹¹.

The question of the possible central hole has been explored by several groups by studying the aperiodic variability of X-rays in quiescent dwarf novae. They concluded that these disks are truncated (Balman & Revnitvsev 2012; Dobrotka, Mineshige & Ness 2014), by interpreting the data in the framework of propagating fluctuation model. However, this is a model-dependent statement, and these studies did not explain how this model applies to a cold disk in which little matter is transported (as required for DIM to work at all). A quantitative study is necessary to assess if a cold disk can nevertheless propagate fluctuations sufficiently effectively for this interpretation to hold. In addition, proponents of central holes must also explain the lack of obvious central holes in the eclipse maps of quiescent dwarf novae such as V4140 Sgr, both in total optical emission and its fluctuations (Baptista, Borges & Oliveira 2016).

While observers have used cooling flow and other analytical models, there are theoretical efforts to model the X-ray emission from quiescent dwarf novae from first principles (see, e.g., Liu et al. 2008 and references therein). Several such studies have started with the assumption that the optically thin boundary layer is radiatively inefficient, hence spatially extended, and advection plays an important role, based on a study by Narayan & Popham (1993). However, it is puzzling that this paper claimed the optically thin boundary layer to be radiatively inefficient, considering that the Bremsstrahlung cooling time for a 10^8 K, 10^{-9} g cm⁻³ (appropriate for the $10^{-10.5}$ M_⊙ yr⁻¹ case; their Figure 2) plasma is ~ 2 s (0.2 s for the $10^{-9.5}$ M_⊙ yr⁻¹ case). Note that Narayan & Popham (1993) based their calculations on the accretion disk structure of Hubeny (1990), in which disk is represented by a set of mutually non-interacting annuli. As Hubeny (1994) noted, this approach is inapplicable at both the inner and the outer boundaries of the disk. A study of the boundary layer structure that fully incorporates the interaction among annuli is therefore highly desirable.

6.3. *The Optically Thick, Soft X-ray/EUV Component*

At high accretion rates (dwarf novae in outburst and non-magnetic nova-like systems), the boundary layer is expected to become optically thick (Patterson & Raymond 1985b; Popham & Narayan 1995). Indeed, luminous soft X-ray/EUV emission has been seen in some nearby dwarf novae in outburst (Wheatley, Mauche & Mattei 2003). At the same time, the optically thin emission never disappears. However, before the X-ray data can be used to infer the properties of the boundary layer, it is necessary to investigate if the observed X-rays are indeed from the boundary layer.

It is clear that there is a soft X-ray component that is not from the boundary layer. This was first demonstrated by Naylor et al. (1988), who reported that the soft X-ray emission observed with EXOSAT in OY Car during its 1985 May superoutburst was never eclipsed (their Figure 13). Note that OY Car is a well known high inclination system

¹⁰ Even so, the distance to SS Cyg has since been revised (Miller-Jones et al. 2013).

¹¹ This is in contrast to the situation for the constant optical/UV luminosity, where an increasing disk luminosity can in principle be hidden by a decreasing luminosity of a cooling white dwarf.

in which both the white dwarf photosphere (in optical/UV) and the optically thin X-ray component are eclipsed in quiescence (Wheatley & West 2003). Thus, the soft X-rays observed during the superoutburst had an extended origin. Using an *EUVE* observation of OY Car during its 1997 March superoutburst, Mauche & Raymond (2000) confirmed the lack of eclipse, and showed that its EUV spectrum consisted of prominent emission lines on a weak continuum. However, this should not be taken as the evidence for a lack of the expected optically thick boundary layer emission: In fact, Mauche & Raymond (2000) successfully modeled the observed emission as due to a warm accretion disk wind photoionized by a $T \sim 90,000\text{--}130,000$ K boundary layer emission.

Pratt et al. (2004) observed the deeply eclipsing nova-like system, UX UMa, with *XMM-Newton*, and discovered that there were two X-ray components. The component that dominates in the 3–10 keV range is heavily absorbed ($N_{\text{H}} \sim 8 \times 10^{22} \text{ cm}^{-2}$) and is deeply eclipsed. The component that dominates below 2 keV is also optically thin, does not suffer the heavy absorption (observed $N_{\text{H}} \sim 8 \times 10^{19} \text{ cm}^{-2}$), and is UN-eclipsed. This is an intermediate-temperature component whose origin remains unclear (for the photoionized wind explanation for the softer component in OY Car to apply here, the temperature and the luminosity of the boundary layer component need to be much higher). The fact that we do not detect the expected soft, blackbody-like component from the optically thick boundary layer cannot be taken as evidence for the lack of such a component, given the hard component goes through a column sufficiently high to hide it from our view. In fact, all eclipsing, high accretion rate CVs may have sufficiently high column density to hide the soft component from the optically thick boundary layer.

The soft component is best studied systems such as SS Cyg, which is nearby ($d=114$ pc: Miller-Jones et al. 2013) and seen at a low inclination angle ($i \sim 50^\circ$: Bitner, Robinson & Behr 2007). The best data to date have been obtained with *Chandra* LETG and show a strong, blackbody-like continuum with a host of absorption features (Mauche 2004). In fact, the theory of optically thick boundary layer was developed to explain an earlier detection of this component in SS Cyg (Pringle 1977). However, this soft X-ray component as predicted by Pringle (1977) is rarely detected, leading to the idea of the missing boundary layer (Ferland et al. 1982). In a compilation of *EUVE* spectra of dwarf novae in outburst (SS Cyg, U Gem, VW Hyi and OY Car), Mauche (2002) found that, with the exception of SS Cyg, they did not have any significant flux shortward of $\lambda \sim 80 \text{ \AA}$ ($E > 0.15$ keV), with estimated blackbody temperatures of order $kT \sim 10$ eV, much less than theoretically expected, presumably because the boundary layer occupies a much larger area than the theory assumed¹². This makes it impossible to detect this component unless the interstellar N_{H} was exceptionally low. That is, the missing boundary layer “problem” is really a mismatch between the expected and observed properties of the optically thick boundary layer.

Nevertheless, the optically thick boundary layer of SS Cyg appears less luminous than the disk ($L_{\text{bl}}/L_{\text{disk}} \sim 0.06_{-0.03}^{+0.18}$), according to the blackbody fits (Mauche 2004). So a version of the “missing boundary layer problem” may still be present, if the blackbody fit results are reliable. For OY Car, on the other hand, for which the properties of boundary layer emission are inferred indirectly through the observation of photoionized wind, Mauche & Raymond (2000) found a plausible solution in which $L_{\text{bl}}/L_{\text{disk}} \sim 1.0$. Interestingly, Mauche (2004) inferred a small fractional area of the boundary layer for SS Cyg (best fit value of 5.6×10^{-3} and an upper limit of 6.6×10^{-2} , both for $d=160$ pc) while Mauche & Raymond (2000) inferred a much larger (>0.1) value for OY Car. Perhaps the most alarming aspect of the boundary layer emission of SS Cyg is its homologous spectral evolution as the luminosity changed by two orders of magnitude (Mauche et al. 1995), implying that its temperature remained roughly constant. In contrast, if the fractional area remained constant, the temperature should have changed by a factor of ~ 3 , which is well within our capability to detect. This suggests caution in proceeding further with our interpretation of the spectra of the optically thick boundary layer.

Dwarf nova oscillations (DNOs), the short period (<1 min) oscillations in the optical light of high accretion rate, non-magnetic CVs with high coherence ($Q \sim 10^4\text{--}10^6$), are also seen in their soft X-ray/EUV component. Mauche & Robinson (2001) discovered that EUV and optical DNOs of SS Cyg had the same period and phase, and also observed a frequency doubling from $P=6.59$ s to 2.91 s. If the period is associated with the Keplerian motion around the white dwarf, then the minimum period of 5.6 s (observed as 2.8 s oscillations after period doubling) requires a white dwarf mass of at least $1.1 M_{\odot}$. This is also consistent with the maximum temperature inferred for the cooling flow of $kT \sim 42$ keV (Byckling et al. 2010), which implies a $1.15 M_{\odot}$ white dwarf¹³.

¹² That is, the specific accretion rate, \dot{m} , is lower than assumed, using the terminology frequently used for magnetic CVs; see §5.2

¹³ While the most recent optical determination of the white dwarf mass in SS Cyg is $0.81 \pm 0.19 M_{\odot}$ (Bitner, Robinson & Behr 2007), this is based on the inclination angle they infer ($45^\circ < i < 56^\circ$). This, in turn, was determined using an unstated assumption that the fractional contribution of the accretion disk light remained the same between two epochs, one at which they measured the average flux from the secondary, and the other when they measured the amplitude of the ellipsoidal variation.

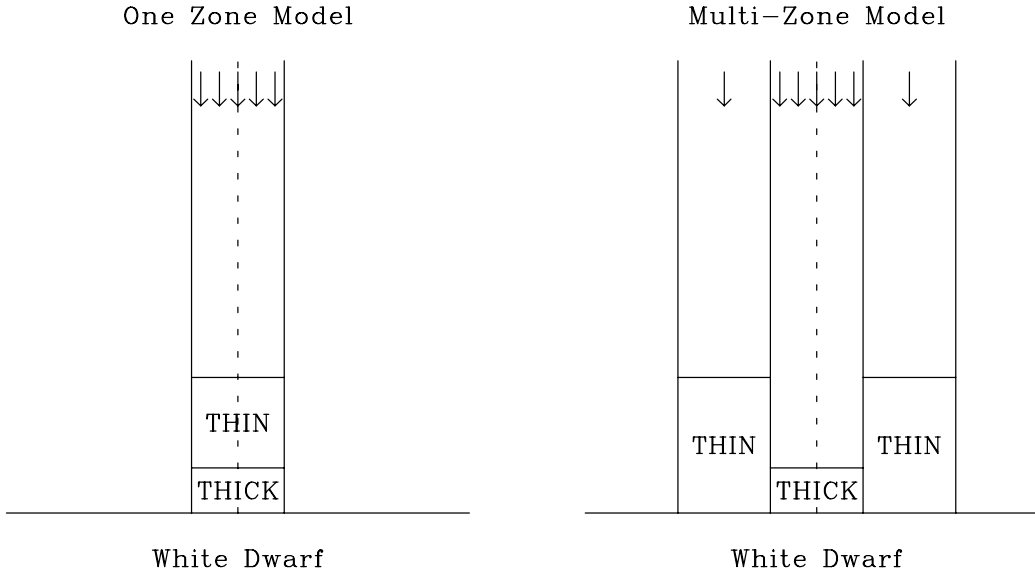


Figure 12. These schematics show two extremes of how optically thick and thin regions might co-exist in the boundary layer. In both, the white dwarf surface is shown as a horizontal line, and the orbital plane is indicated by dashed vertical line. (Left) In a one-zone scheme, the boundary layer may consist of an optically thick layer near the stellar surface and an optically thin layer on top. (Right) In a multi-zone scheme, of which this shows a simplest version, there could be an optically thick region near the orbital plane where the accretion rate is high; since the density in the disk falls off exponentially with height above the mid-plane, this may well be sandwiched between optically thin regions.

6.4. *The Residual Hard X-rays*

One would not expect any optically thin, hard X-ray emission from the boundary layer if it is completely optically thick. However, nova-likes and dwarf novae in outbursts do emit optically thin X-rays in the 0.5–10 keV range (see, e.g., Wada et al. 2017 and references therein).

When a single dwarf has been observed both in quiescence and in outburst, preferably using identical set of instruments, it is often the case that the hard X-ray component is more luminous and harder in quiescence (see, e.g., SS Cyg: Ishida et al. 2009). Known exceptions to this general rule are GW Lib, which is so X-ray faint in quiescence that this may not be surprising (Byckling et al. 2009), and U Gem, whose outburst X-ray spectrum is too complex to allow a straightforward measurement of the temperature change (Güver et al. 2006). The picture of Patterson & Raymond (1985b), in which an optically thin region exists in the outskirts of an optically thick boundary would not provide a prediction for the luminosity. In principle, the optically thick and thin regions could co-exist in different configurations (Figure 12). In either geometry, one might expect the maximum temperature to be set by the gravitational potential of the white dwarf, and therefore remain constant. This is often taken as a severe difficulty of the “optically thin skin” interpretation for the residual hard X-ray emission.

It is clear that there is an intermediate temperature (~ 1 keV), optically thin component that is not from the boundary layer in at least a subset of high state objects. I have already noted the case of UX UMA in §6.3. The UN-eclipsed X-ray component seen in OY Car in superoutburst with the *ROSAT* HRI (Pratt et al. 1999), which was assumed to be a component distinct from that seen with EUVE (Mauche & Raymond 2000), may be the same. Wada et al. (2017) found it necessary to add an optically thin component of similar temperatures to obtain satisfactory fits to their *Suzaku* data on dwarf novae in outburst. The evidence may favor a non-boundary layer origin of this intermediate temperature, optically thin component, but this is a separate question from the origin of the residual X-rays seen in the medium energy band.

One possibility is that these residual, medium-energy X-rays are not from the boundary layer. This is the option preferred by Wheatley, Mauche & Mattei (2003), citing the observed temperature drop compared to the quiescence as key evidence. Ishida et al. (2009) proposed a corona above the accretion disk to be the origin of the residual

X-rays¹⁴. They based this model partly on the reflection fraction they measured in quiescence and during outburst using *Suzaku* XIS and HXD. Since the HXD signal in outburst was weak, this is subject to considerable systematic uncertainty due to our limited ability to model the HXD background, so this needs to be confirmed with higher quality data with *NuSTAR*. They also argued that the line broadening observed in SS Cyg in outburst was consistent with an accretion disk corona. While undoubtedly true, there may well be other explanations for the increased line width. Additional consideration should be given to the smooth recovery of the hard component temperature during outburst decay of SS Cyg (Figure 5 of McGowan, Priedhorsky & Trudolyubov 2004) which might be easier to interpret if the hard X-rays in quiescence and in outburst shared a single origin¹⁵.

The other possible explanation for the lower temperature is that the residual X-rays are indeed from the optically thin part of the largely optically thick boundary layer, but there is a second cooling mechanism that competes with hard X-ray emission. In particular, Fertig et al. (2011) proposed that the optically thick part could provide sufficient number of seed photons to Compton-cool the optically thin part of the boundary layer. The same model was used to explain the relatively faint, very soft emission from RS Oph observed in 2007 and 2008, 537 and 744 days since its 2006 nova eruption (Nelson et al. 2011). In this case, the still hot photosphere of the white dwarf contributes a significant number of UV photons that can serve as seed photons. Finally, this scenario also explains the lack of detection of optically thin emission in SSSs, even though accretion is necessary to fuel the continued nuclear burning. The weakness of this scenario that it is feasible if and only if the density of the plasma in the optically thin part of the boundary layer is relatively low, which has not been established yet.

Another possibility is suggested by the UV detection of a rapidly spinning accretion belt in several dwarf novae (Sion et al. 1996; Cheng et al. 1997). It is possible that the temperature drops in outburst because the boundary layer is between the Keplerian disk and the accretion belt, and the kinetic energy of the belt is radiated later.

If the quiescent X-rays are from the boundary layer, which transitions to an optically thick state when the accretion rate exceeds a critical value, one would expect a hard X-ray brightening at the onset of a dwarf nova outburst, before the sudden appearance of the soft component, and the reverse is expected during decline (Schreiber, Hameury & Lasota 2003). This is indeed seen in SS Cyg (Wheatley, Mauche & Mattei 2003) and has been taken by many as the paradigm applicable to all dwarf novae. However, as Fertig et al. (2011) pointed out, such behavior has only ever been seen in SS Cyg; in other dwarf novae, the optically thin X-rays simply increase during outburst (U Gem, GW Lib) or is suppressed during outburst without a temporary increase. There is no published explanation for why the SS Cyg like behavior is atypical. Moreover, Fertig et al. (2011) attempted to derive the critical accretion rate empirically, and found values that are much lower than the theoretical values (Popham & Narayan 1995).

Nova-like systems are thought to be systems in which the mass transfer rate is high enough to maintain the disk in the high (dwarf nova outburst-like) state. If so, the boundary layer properties of nova-like systems should be similar to those of dwarf novae in outburst, perhaps with a lower temperature, lower luminosity (than in quiescent dwarf novae) optically thin component and an optically thick, blackbody-like, soft X-ray component. Unfortunately, the number of high quality X-ray observations of such systems is limited, and the results are often confusing. In particular, Zemko et al. (2014) studied VY Scl type systems in high and low states, likely caused by variations in the mass transfer rate, and found no clear pattern of correlated or anti-correlated changes of optical and X-ray brightness.

It is quite possible that the residual hard X-rays in dwarf novae in outburst has the same origin as the hard X-ray component in UX UMa, almost certainly the boundary layer since it is deeply eclipsed (Pratt et al. 2004). On the other hand, the lack of a consistent pattern for nova-likes leaves open the possibility of multiple distinct origins.

6.5. X-ray Emission from Symbiotic Stars

Symbiotic stars can be powered by accretion, shell burning, or a combination of both. In principle, shell burning produces α type, supersoft, emission. However, the observability of this component depends on the combination of the effective temperature and absorption. For the latter, one must consider both the interstellar absorption and that due to the M giant wind, following a procedure similar to that provided by van den Berg et al. (2006)¹⁶.

¹⁴ Such models probably are motivated, in part, by analogy with the corona invoked for the power-law component in black hole X-ray binaries and in AGN. However, recent observations appear to favor compact “corona” of very limited spatial extent (Fabian et al. 2015), unlike that envisioned for SS Cyg by (Ishida et al. 2009).

¹⁵ The temperature does change suddenly during the rise.

¹⁶ However, one should not merely copy the specific N_{H} values they estimated. This is because the final N_{H} values depend both on the mass loss rate and the velocity of the M giant wind. In particular, van den Berg et al. (2006) assumed a 230 km s^{-1} wind for their specific case, which is much higher than typically seen in normal red giant. For wind velocities in the $10\text{--}20 \text{ km s}^{-1}$ range, wind can easily provide N_{H} of several times 10^{22} cm^{-2} , which is sufficient to hide a supersoft (α -type) emission.

Accretion-powered symbiotic stars are often detected as δ -type X-ray sources, indicating optically thin emission from the accretion disk boundary layer. This is the case with the four symbiotic stars detected in the BAT 22-month survey (Kennea et al. 2009). While one of them, CH Cyg, has a relatively soft spectrum for a BAT source, the other three are very hard, suggesting that they harbor massive white dwarfs. Their medium energy spectra require a partial-covering absorber, which is seen to be variable from epoch to epoch on time scales as short as several days. This suggests that the absorber is located close to the white dwarf. In contrast, the slow M giant wind, whose origin is located of order 1AU away, cannot change significantly over time scales of days.

While the BAT-detected symbiotic stars have high X-ray fluxes, high X-ray temperatures, and high absorbing column, other δ -type symbiotic stars are less extreme (Nuñez et al. 2016). Since both the β and δ -type emissions are optically thin thermal X-rays, it is not always trivial to assign an unambiguous classification. The β -type emission appears to peak around 1 keV, and is consistent with $kT \sim 1$ keV. This requires a shock velocity of order 1000 km s^{-1} , commonly seen in the optical and UV spectra of winds in symbiotic stars (see, e.g., Crowley, Espey & McCandliss 2008). Accretion can produce kT in excess of 10 keV, depending on the white dwarf mass. When the observed kT is 3 keV, for example, this probably indicates a δ -type origin, but other factors should be considered to make a definitive classification.

As with the optically thin X-rays observed in non-magnetic CVs, the δ type component of symbiotic stars can be fit successfully with `mkcflow` and minute time-scale X-ray variability is observed (e.g., RT Cru: Luna & Sokolowski 2007). Luna et al. (2013) found that the δ -type symbiotic stars exhibit significant UV flickering, which is absent in shell-burning systems. Although the distances to many symbiotic stars are poorly known, the X-ray luminosity appears to range from that similar to non-magnetic CVs to as high as $10^{34} \text{ ergs s}^{-1}$.

The β -type emission is interpreted as due to colliding winds. One is from the red giant, but what about the other? It is clear that shell burning can result in a fast wind from the white dwarf or its vicinity; this appears to be the case in, e.g., AG Peg (Ramsay et al. 2016). CH Cyg (Ezuka, Ishida & Makino 1998; Mukai et al. 2007) is the prototype of symbiotic stars that show composite β/δ type X-ray spectra (see also UV Aur, ZZ CMi, NQ Gem and V347 Nor: Luna et al. 2013). Such systems prove that the β -type emission can exist in purely accretion-powered symbiotic stars. These system may produce accretion disk winds that are strong enough to result in β -type emission.

As noted in §3.2, spatially resolved X-ray emission has been detected from several symbiotic stars including R Aqr (Nichols et al. 2007 and references therein) and CH Cyg (Galloway & Sokolowski 2004), and are interpreted as thermal emissions from a jet. Interestingly, jets, which are typically detected at radio wavelengths, are produced by symbiotic stars with a wide range of X-ray spectral types, e.g., AG Dra (α -type), Hen 3-1341 and V1329 Cyg (β type), CH Cyg (β/δ type), and Mira AB (δ type; Sokolowski & Bildsten 2010).

6.6. X-rays from AM CVn Systems

For the purposes of studying their X-ray emission, AM CVn systems can be divided into two classes: diskless systems HM Cnc and V407 Vul, and the rest (Solheim 2010). The former have extremely short periods (5.4 min and 9.5 min, respectively, for HM Cnc and V407 Vul). As a consequence, the ballistic trajectory from the L_1 point encounters the white dwarf photosphere before it can circularize to form a disk. In other words, they are direct impact accretors (Marsh & Steeghs 2002). They were originally discovered using *ROSAT* as soft X-ray sources, and their spectra can be approximated with a blackbody with emission features (HM Cnc: Strohmayer 2008) or with absorption component with non-solar abundances, in particular with enhanced with neon (V407 Vul: Ramsay 2008). Other than the possible emission lines in HM Cnc, no optically thin component has been detected. There does not appear to be a quantitative study of whether the lack of optically thin X-rays is to be expected in the direct impact shock regions, given the likely white dwarf mass and the specific accretion rate (Dolence, Wood & Silver 2008). The phasing of the optical and X-ray light curves, and the long-term period history derived from repeated X-ray observations (see, e.g., Ramsay et al. 2005) of HM Cnc and V407 Vul are consistent with the direct impact accretor model.

Longer orbital period AM CVn systems all appear to accrete via a disk, and their X-ray emission similar to normal hydrogen-rich CVs, including the dichotomy between the optically faint and X-ray bright state and the optically bright and X-ray faint state dichotomy (see Baskill, Wheatley & Osborne 2005, which included AM CVn stars GP Com and CR Boo along with normal CVs). The major difference is in elemental composition. While the abundances of H or He cannot be inferred from X-ray spectra, those of elements from O to Fe can be directly studied in the optically thin X-ray emission. Using the *XMM-Newton* RGS data, Strohmayer (2004) found overabundance of N and Ne in GP Com. Ramsay et al. (2006) also found N overabundance in V396 Hya and SDSS J124058.03–015919.2, although

one must caution that the fit was done using a plasma model with hydrogen abundance set to 0.0. Since these models usually assume that the bulk of electrons, responsible for the Bremsstrahlung continuum, are provided by hydrogen atoms, they may or may not work properly under these conditions. Different evolutionary scenarios for AM CVn systems predict different elemental abundances (Solheim 2010), which can be tested using future X-ray observations in principle.

7. X-RAY EMISSION FROM NOVAE

Two types of X-ray emission are commonly observed from novae in eruption. One is the optically thin emission from an extended region, and the other is the optically thick emission from the white dwarf surface.

7.1. Shock Emission

When nova eruptions happen in symbiotic stars, the ejecta are embedded in the dense M giant wind. In symbiotic recurrent novae, the ejecta velocities are high and the binary separations are often of order 1 AU ($P_o \sim 1$ yr). Since 3000 km s^{-1} ejecta can travel 1 AU in \sim half a day, strong shock and subsequent X-ray emission is expected almost immediately. This has indeed been found to be the case, most recently during the 2014 eruption of V745 Sco, which was strongly detected with *Swift* XRT 3.7 hr after the optical discovery (Page et al. 2015). During its 2006 eruption, RS Oph was an even brighter X-ray source as observed with *RXTE* PCA and *Swift* XRT, although the coverage was not quite as prompt or as densely sampled (Sokoloski et al. 2006b; Bode et al. 2006). Note, in particular, that it was luminous enough and hard enough during the first few days to have been detected above 10 keV using *RXTE* PCA and *Swift* BAT. Sokoloski et al. (2006b) found the flux and temperature evolution was consistent with a low-mass ejecta that swept up its own mass in red giant wind within the first few days. Bode et al. (2006) found the observed N_H evolution was consistent with that expected from the unshocked red giant wind ahead of the shock. Vaytet, O'Brien & Bode (2007) further compared the observations with a series of 1-dimensional hydrodynamic models and found that the shock was radiatively efficient. Moreover, the manner in which matter was ejected (e.g., the duration of strong mass loss) was found to have a strong influence on the evolution of the shocks. For example, the end of plateau in the shock velocity directly corresponds to the end of the fast wind in the context of their model.

Not all embedded novae immediately become X-ray luminous. In the case of V407 Cyg, a fast nova in a symbiotic system, there was only faint X-ray emission for the first ~ 20 days, whose origin remains unclear (Nelson et al. 2012). The X-ray luminosity rapidly increased thereafter. They interpreted this as the time it took for the blast wave to reach the immediate vicinity of the Mira type mass donor in a wide (20–25 AU separation) binary. In the *Suzaku* XIS spectrum of V407 Cyg 30 days since optical discovery, Nelson et al. (2012) found strong He-like lines of Si and S, inconsistent with the measured electron temperature of 2.8 keV if the emission was from a single temperature plasma in collisional ionization equilibrium (CIE). They interpreted this as due to some of the X-rays being from non-CIE plasma, which is understandable since some ejecta are running into low density wind away from the M giant.

Shock X-ray emission is a common, if not universal, feature of novae, whether embedded or not (Mukai, Orio & Della Valle 2008). The very presence of such X-rays proves that mass ejection in novae is a complex process. Presumably a fraction of mass is ejected at low velocity first, and a faster system catches up to it. One of the best-observed cases is that of V382 Vel (Mukai & Ishida 2001). It was undetected at first, then detected as an intrinsically hard and highly absorbed source, becoming softer and less absorbed in subsequent observations. Mukai & Ishida (2001) interpreted these features as due to a collision of massive, slow shell that was ejected first, and a fast wind inside it. The slow expansion of outer shell provides the required N_H decline, without invoking a significant amount of ionization (that is, it is consistent with being so massive as to remain largely unshocked). In the peculiar recurrent nova, T Pyx, the combined X-ray and radio data suggest that the initial ejecta was far less massive than the later, faster system (Nelson et al. 2014; Chomiuk et al. 2014), but it may well be an exception in this regard.

One of the most exciting recent findings in the field of nova research is that classical novae produce GeV γ -rays (Abdo et al. 2010; Ackermann et al. 2011). The detection of X-ray emission from shocks contemporaneous with radio synchrotron emission (Krauss et al. 2011; Weston et al. 2016a,b) suggests that X-rays could play a vital role in diagnosing the shocks that accelerate particles and produce γ -rays.

7.2. Supersoft Emission

TOO observations with *Chandra* and *XMM-Newton* gratings have provided a number of high quality, high spectral resolution spectra of the supersoft emission from novae (see, e.g., Ness et al. 2003; Nelson et al. 2008; Ness et al.

2011). In addition, the flexible observing capability of the *Swift* mission has enabled monitoring observations of a large number of novae (Schwarz et al. 2011), and has become a pre-requisite for triggering *Chandra* or *XMM-Newton* TOOs. Currently, the data are far ahead of our ability to model them, which must consider non-LTE effects, non-stationary effects, and non-solar abundances. One potential use of the supersoft emission is to measure the effective temperature and convert it to white dwarf mass by assuming, e.g., the Eddington limit (Williams, King & Brooker 1987). Even if the absolute values are not trustworthy, novae can certainly be placed in mass order when comparable data are available.

Combined X-ray and optical monitoring of novae in M31 has resulted in a large sample of novae with known distances. This allowed Henze and co-workers to derive correlation between the blackbody temperature, turn-on times, and turn-off times of the supersoft emission against each other, and against expansion velocities measured through optical spectroscopy (Henze et al. 2014). The supersoft emission is powered by continued shell burning, and the turn-off time is believed to indicate when the residual nuclear fuel is exhausted and shell burning turns off. The turn-on time, on the other hand, is purely observational: shell burning is thought to continue from the time of the thermonuclear runaway, but the supersoft emission hidden by the ejected shell. Thus, the turn-on time is set by the combination of the total ejecta mass and its velocity. The standard understanding of the white dwarf mass as the key parameter is confirmed by this study: more massive white dwarf requires smaller mass for nova eruption, eject matter more violently, and its supersoft emission reaches a higher temperature.

Variability has emerged as a major feature of supersoft emission in novae. The *Chandra* LETG data on V4743 Sgr showed a ~ 22 min oscillation followed by a sudden drop in count rate (Ness et al. 2003). High amplitude variabilities on hours to days timescales (oscillations seen from one *Swift* pointing to the next, or state changes during a single *Chandra* or *XMM-Newton* observation) have been discovered in RS Oph (Osborne et al. 2011) and several other novae. In addition, QPOs on 30–70 s time scale have been detected in 4 novae as well as persistent supersoft source, CAL 83 (Ness et al. 2015). A possible explanation is that it is a non-radial oscillation that is excited by the nuclear burning.

While the spectra of supersoft emission are blackbody-like when observed at CCD resolution, grating spectroscopy has revealed the presence of absorption or emission lines. Ness et al. (2013) conducted a systematic study of this and compared the properties of those with emission lines and those with absorption lines. The former appear to be less luminous than the latter, and appear to be found predominantly in high inclination systems (again, with the exception of the atypical recurrent nova, T Pyx). Among them are several eclipsing systems in which the smooth orbital modulation of the supersoft emission is seen, including the persistent supersoft source, CAL 87. For this object, Ebisawa et al. (2001a) argued that the central source was permanently hidden from our view and only scattered emission is seen, which is essentially the same explanation as was applied to the boundary layer emission of OY Car in superoutburst (Mauche & Raymond 2000). Among the novae, the same explanation clearly holds for U Sco (Orio et al. 2013) and V959 Mon (Page et al. 2013). The degree of orbital modulation allows us to infer the size of the scattering to be the same order as the secondary in these systems. This suggest that the accretion disk was present in these novae during the supersoft phase to hide the direct emission. As to the absorption lines in the low inclination systems, two possible origins had been considered: they may be intrinsic feature of the white dwarf atmosphere, or caused by discrete shells ejected by the novae (Pinto et al. 2012). In addition, it may be worth exploring the scenario in which a single scattering region is seen in emission in high inclination systems and in absorption in low inclination systems.

8. COLLECTIVE PROPERTIES

8.1. Population and Luminosity Function

CVs are discovered through X-ray surveys (§3.1) and through optical surveys. Because the discovery efficiency varies greatly for different method–subclass combinations, the aggregate catalog of all known CVs is highly heterogeneous. It is therefore meaningless simply to list the fraction of magnetic CVs, for example, in published catalogs: the results are as likely to tell us about the selection effects as about the underlying populations.

It is far more meaningful to derive the space densities of various subclasses. For this purpose, volume-limited samples would be ideal, but this is impractical for the time being. Flux-limited samples are therefore the method of choice, assuming that one can estimate the distances to individual objects to the required degree of accuracy. An early, perhaps the first, application of this method to X-ray discovered CVs was that by Hertz et al. (1990). While they derived a local space density of CVs of at least a few $\times 10^{-5}$ pc $^{-3}$, there are reasons to be wary of this number. One is

the perennial difficulties in estimating distances to CVs; the other, specific to this work, is that they did not consider a realistic Galactic distribution of CVs.

The most up-to-date work on this subject is the series of papers by Pretorius and collaborators using *ROSAT* and *Swift* BAT flux-limited samples (Pretorius & Knigge 2012; Pretorius, Knigge & Schwobe 2013; Pretorius & Mukai 2014). Summarizing the highlights of these papers: the local space density of non-magnetic CVs detected with *ROSAT* is $4_{-2}^{+6} \times 10^{-6} \text{ pc}^{-3}$, but this number may double when the X-ray faint population ($L_x < 5 \times 10^{29} \text{ ergs}^{-1}$) is also considered. Polars, if their duty cycle is 0.5, have a total space density of $9.8_{-3.1}^{+5.4} \times 10^{-7} \text{ pc}^{-3}$, of which roughly three quarters are below the period gap. Long-period IPs have an estimated space density of $1.0_{-0.5}^{+1.0} \times 10^{-7} \text{ pc}^{-3}$. These are systems with BAT band luminosities in the 10^{32} – $10^{34} \text{ ergs}^{-1}$ range; there appears to be a separate population of LLIPs (see also §5.3), with a few systems around $L_{BAT} \sim 10^{31} \text{ ergs}^{-1}$, and they could be more numerous than the normal, X-ray luminous, IPs.

Pretorius and colleagues found the intrinsic fraction of magnetic CVs (polars and IPs) to be $\sim 16\%$ to within a factor of 2. This value is smaller than, but consistent within errors with, the fraction of magnetic CVs found in catalogs. This value is also consistent with the figure of $\sim 10\%$ for the fraction of magnetic white dwarfs among non-interacting samples (Liebert, Bergeron & Holberg 2003). Note, however, even among field white dwarfs, the incident of magnetism is an active research area (see, e.g., Valyavin et al. 2014).

Several caveats should be kept in mind. Current studies rely on our ability to measure distances to a sample of CVs using indirect methods. In addition, the scale height of Galactic distribution of CVs is an additional source of uncertainty. Pretorius adopted a scale height of 120 pc for long-period (and hence relatively young) CVs, and 260 pc for short-period (old) ones. While these are reasonable assumptions, these space density numbers should be reviewed once *Gaia* distances become available for a large number of CVs.

In these studies, X-ray luminosity function (XLF) and space density are strongly linked. Both luminous but extremely rare type of objects and numerous but faint class can be missed in a flux-limited survey. This is the reason for the uncertainty in the true population of LLIPs. Similarly, there are reasons to believe that the current X-ray surveys are missing the bulk of non-magnetic CVs. Early X-ray studies of non-magnetic CVs focused on well-known objects already detected in X-rays, many of which had X-ray luminosities above $10^{31} \text{ ergs}^{-1}$ (Mukai & Shiokawa 1993). Byckling et al. (2010) studied optically selected sample, those with parallax-based distance measurements, and found that their XLF peaked in the 10^{30} – $10^{31} \text{ ergs}^{-1}$ range. However, even this sample is biased towards optically bright CVs. Non-magnetic CV population probably is dominated by the very faint population discovered with Sloan Digital Sky Survey (SDSS), which are thought mostly to be WZ Sge type dwarf novae with extremely long recurrence types (Gänsicke et al. 2009). Reis et al. (2013) observed 20 optically faint non-magnetic CVs (16 of which were discovered in SDSS) with *Swift*, and found all of them to have 0.5–10 keV luminosity less than $\sim 2 \times 10^{30} \text{ ergs}^{-1}$ (and the majority less than $\sim 1 \times 10^{30}$).

As noted earlier, Britt et al. (2015) found a correlation between the X-ray luminosity and the duty cycle of local dwarf novae. They applied this relationship to the optical variability study of *Chandra* Galactic bulge survey sources, and derived the space density of dwarf novae, which was consistent with those derived for local, long period dwarf novae (Pretorius & Knigge 2012). The Britt et al. (2015) measurement is based on the distant CV population, it is consistent with the local sample of Pretorius & Knigge (2012) only when the Galactic distribution of dwarf novae is taken into account.

Finally, the space density of symbiotic stars is highly uncertain, as discussed by Mukai et al. (2016). They considered it likely that there up to several dozen symbiotic stars within 1 kpc, which implies a lower space density than for CVs.

8.2. X-rays from the Galactic Ridge, Bulge, and Center Regions

There is an apparently diffuse X-ray emission throughout the Galaxy, around the Galactic Center, in the Galactic Bulge, and in the disk (the last is usually referred to as the Galactic ridge X-ray emission, or GRXE; see, e.g., Warwick et al. 1985). Considerations of fluctuations and the lack of *Einstein* point source led Warwick et al. (1985) to conclude that, if the GRXE was made up of discrete sources, those with luminosities in the $10^{33.5}$ to $10^{36} \text{ ergs}^{-1}$ were not major contributors. Mukai & Shiokawa (1993) proposed dwarf novae as a potential major contributor to the GRXE, based on the best understanding of the space density and the XLF of dwarf novae available at the time. More importantly, they recognized that this was only plausible when the realistic Galactic distribution of CVs were considered. This was later shown to be essential, since Revnivtsev et al. (2006) showed that the GRXE intensity traces the Galactic stellar mass distribution.

Ebisawa et al. (2001b) performed a deep *Chandra* observation of a Galactic plane field and concluded that resolved sources with fluxes above 3×10^{-15} ergs cm $^{-2}$ s $^{-1}$, corresponding to 4×10^{31} ergs s $^{-1}$ at 10 kpc, made up about 10% of the total GRXE flux in this field. They also suggested that CVs were not major contributors to the GRXE, but this is true only when neglecting the Galactic distribution of CVs. A later, deeper *Chandra* observation of a Galactic bulge field resolved the majority (up to $88 \pm 12\%$ in the 6.5–7.1 keV band) of the GRXE into point sources (Revnivtsev et al. 2009). It is now thought likely that faint, point sources including CVs contribute the majority of apparently diffuse X-rays from the ridge, the bulge, and the Galactic center regions (see, e.g., Yamauchi et al. 2016).

However, the specific types of CVs that significantly contribute to these emission is an open question. For example, Munro et al. (2003) detected 2357 sources in the $17' \times 17'$ field around Sgr A*, and found more than half of the sources brighter than 4×10^{-15} ergs cm $^{-2}$ s $^{-1}$ (2–8 keV; $3 \sim 10^{31}$ ergs s $^{-1}$ at 8 kpc) to be hard, perhaps indicating them to be magnetic CVs. Yuasa et al. (2012) studied the spectral properties of the ridge and bulge emissions and found them to be consistent with those of IPs with an average white dwarf mass of $0.66^{+0.09}_{-0.07} M_{\odot}$. This is lower than those of IPs in the solar neighborhood (Yuasa et al. 2010). Moreover, for this population to explain the apparently diffuse emission, the XLF of IPs must extend smoothly down to $\sim 10^{30}$ ergs s $^{-1}$ to explain the bulk of the observed X-rays, in contradiction with the observed XLF (Pretorius & Mukai 2014). In contrast, Xu, Wang & Li (2016) studied the Fe K lines of CVs and the GRXE, and found the properties of the latter to be consistent with those of dwarf novae. Hailey et al. (2016), on the other hand, found that the Galactic center diffuse X-rays to have spectral characteristics similar to those of field IPs, but again required IP XLF to extend to lower luminosities than found in the solar neighborhood.

9. CURRENT ISSUES AND FUTURE PROSPECTS

In this section, I discuss major unresolved questions and topics that are under active investigation.

9.1. Extreme Objects

It is perhaps unavoidable that our knowledge of the faintest CVs is incomplete. In the context of X-ray emissions, X-ray dim WZ Sge type dwarf novae must exist in large numbers (Reis et al. 2013) and there may well be numerous LLIPs (Pretorius & Mukai 2014). The discovery that SU Lyn was a previously unrecognized symbiotic star prompted Mukai et al. (2016) to speculate that there probably are a large number of similar systems.

On the other end, our knowledge of most X-ray luminous CVs is also incomplete, because they are rare. The recurrent nova V2487 Oph (Hernanz & Sala 2002) is a luminous X-ray source in quiescence which is detected also with *INTEGRAL* and with *Swift* BAT (Barlow et al. 2006 and Table 1) with an estimated luminosity of $\sim 10^{35}$ ergs s $^{-1}$. Despite multiple X-ray observations, no sign of spin modulation has ever been found (cf. §4), although it has complex absorber that Hernanz and co-workers considered to be the signature of an IP. V2491 Cyg is another nova with quiescent X-ray luminosity above 10^{34} ergs s $^{-1}$ (Zemko, Mukai & Orio 2015). In this case, an X-ray modulation on a time scale of ~ 38 min has been seen, but it may not be strictly periodic. Clearly, one issue for future study is how X-ray luminous accreting white dwarfs can be, both in magnetic and non-magnetic cases, as highest luminosity systems should have non-negligible optical depths. Another is the evolutionary status of these extremely luminous CVs. There are indications that both V2487 Oph (Darnley et al. 2013) and V2491 Cyg (Darnley et al. 2011) harbor evolved mass donors.

The other issue is the birth rate (BR) of such objects, which is of interest in addition to the space density (SD). The two are connected by the relation $SD = BR \times LT$, where LT is the life time of the binary as that subclass. LT is limited by the mass of the donor divided by the mass transfer rate. Thus, two subclasses of CVs with an identical BR can have two different present-day SD because the differences in LT — one luminous and short-lived, one dimmer and longer lasting. Currently available data allow the possibility that the very luminous CVs have a birth rate similar to those of more familiar cousins. This is of particular interest in the context of single degenerate channel of the progenitors of SNIa. This leads to the open question of whether these high luminosity white dwarf binaries harbor especially massive white dwarfs.

In addition, there may be a population of white dwarfs accreting from early-type stars. There have long been speculations about Be-white dwarf binaries, including γ Cas and γ Cas-like objects (Lopes de Oliveira et al. 2006). There are apparent UV counterparts to SSSs in M31 that may indicate shell-burning white dwarfs in orbit around early type stars (Orio et al. 2010). There is CI Cam, unusual X-ray transient whose nature has been disputed. Ishida, Morio & Ueda (2004) proposed a nova interpretation, which is now favored given the *Gaia* distance of $1.4^{+0.7}_{-0.4}$ kpc (Wijngaarden et al. 2016). Finally, there is MAXI J0158–744, a transient supersoft source in the SMC that has been interpreted as a Be-white dwarf binary (Li et al. 2012).

9.2. *Asynchronous Polars*

Of the roughly 100 polars known to date, four are definitely asynchronous, with small ($<1\%$) but significant differences between their spin and orbital periods. In the case of the prototype, V1500 Cyg, it was almost certainly the 1975 nova eruption that desynchronized it, and it was seen to be synchronizing on a timescale of ~ 150 yrs (Schmidt & Stockman 1991). For the other three, no evidence for recent nova eruptions have been found so far (see, e.g., Pagnotta & Zurek 2016), although the failure to do so does not disprove the nova origin of asynchronism. More troublingly, Warner (2002) noted that a mean synchronization time of ~ 300 yrs implied a nova recurrence time of all polars needed to be of order 5000 yrs to explain the presence of four asynchronous systems among 68 polars known at the time. Such a short recurrence time would be very surprising, suggesting that either asynchronous polars are over-represented in our current sample, or some are asynchronous for reasons unrelated to nova eruptions.

X-ray properties may provide a clue. Of the ~ 100 known or suspected polars, 14 have been detected in the *Swift* BAT survey (Table 1). These 14 include three of the four known asynchronous polars (BY Cam, V1432 Aql, and CD Ind). What physical properties distinguish the BAT-detected polars from the rest? Does asynchronism make polars X-ray bright, or do the underlying properties that make them X-ray bright also make them more prone to asynchronism? Are all asynchronous polars the results of recent nova eruptions, or is there another path to asynchronism? These are all interesting questions without no definitive answers so far.

9.3. *The Accretion Disk and X-ray Orbital Modulations*

X-ray emissions from non-magnetic CVs and symbiotic stars arise very close to the white dwarf, where the accretion disk ought to be axisymmetric. It appears likely that X-ray orbital modulation is limited to high inclination systems, via eclipses or dips. We have already discussed X-ray eclipses, and inferences that we can derive from them.

Dips are often seen in low-mass X-ray binaries (LMXBs), and are caused by azimuthal structures in the outer accretion disks, probably associated with the impact region where the ballistic stream from the secondary hits the outer disk rim (see, for example, Parmar et al. 1986). In the dipping LMXBs, while the average behavior is often predictable, individual dips are not repeatable from cycle to cycle.

Among CVs, dips have been observed in U Gem (Szkody et al. 1996) and in WZ Sge (Patterson et al. 1998) in quiescence. Both are high inclination systems in which the bright spot, but not the white dwarf, is eclipsed by the secondary. Naylor & la Dous (1997) studied the UV and X-ray data on U Gem in outburst and concluded that the column density along the line of sight, some 25° above the orbital plane, varied from $< 10^{19}$ to $\sim 10^{22}$ cm^{-2} in this case. Another example is IX Vel, a nova-like system, which appears to show X-ray and EUV orbital modulations (van Teeseling et al. 1995). The inclination is now thought to be $\sim 57^\circ$ (Linnell et al. 2007), which may define the current low inclination limit for systems in which X-ray orbital modulation is observed. The only exception is the mysterious recurrent nova, T Pyx, which exhibit X-ray orbital modulation in quiescence (Balman 2014) even though it is thought to be a low inclination system ($\sim 10^\circ$ according to Uthas, Knigge & Steeghs 2010).

Many IPs also exhibit X-ray orbital modulation: Parker, Norton & Mukai (2005) found statistically significant modulation in seven of sixteen systems they studied. Because the depth of orbital modulation is deeper at lower energies, the likely origin is absorption by azimuthal structures in the outer accretion disk. From the fraction of systems exhibiting modulations, they estimated that such structures existed up to $\sim 30^\circ$ above the orbital plane. Moreover, they found such structures come and go from epoch to epoch for individual systems.

It might seem surprising that the outer disk has sufficient matter 30° above the orbital plane to be able to cause X-ray orbital modulation, compared to the theoretical models of accretion disk: after all, these are supposed to be optically thick, geometrically thin disks. However, note that the theory uses exponential scale heights, and we do expect the presence of lower density matter several scale heights above the mid-plane. Moreover, soft X-ray dips require modest (up to $\sim 10^{22}$ cm^{-2} for U Gem in outburst) column densities along lines of sight that are almost parallel to the disk surface, much less than that required to reach electron scattering optical depth of ~ 1 ($\sim 10^{24}$ cm^{-2}) which presumably defines the disk surface. Therefore, it is not immediately obvious if there is a conflict between theory and observation, except in the case of T Pyx. On the other hand, it is possible that the disks are geometrically thicker than commonly thought. While the luminosity of CV disks are well below the Eddington limit, they are never fully ionized, so the potential effect of radiation pressure on the disk structure should be investigated. After all, radiation-driven accretion disk wind is a common phenomenon among dwarf novae in outburst and nova-like CVs (Drew & Proga 2000).

The nature of the intrinsic absorber in symbiotic stars (Kennea et al. 2009) remains an unsettled issue. If systems like V426 Oph (Ramsay et al. 2008) and V2487 Oph (Hernanz & Sala 2002) are indeed non-magnetic, their absorbers

require an explanation, too. Mukai, Zietsman & Still (2009) argued that the inner accretion disk, just outside the boundary layer, can provide partial covering absorbers if the system is highly inclined. Another attractive possibility is the accretion disk wind (Drew & Proga 2000). Quantitative studies are needed to evaluate if the observed intrinsic absorbers can be explained as due to accretion disk wind.

9.4. The Constant Temperature Problem

The soft, blackbody-like component from the optically thick boundary layer is rarely observed, which was considered to be the ‘missing boundary layer’ problem (Ferland et al. 1982). This appears to be largely due to theories overestimating the boundary layer temperature. A different problem that emerged is the apparent constancy in the boundary layer temperature (Mauche et al. 1995).

An analogous problem has been found in a completely different context. During the supersoft phase of the nova V2491 Cyg, Page et al. (2010) found the supersoft component to stabilize at about ~ 70 eV after an initial rise. Around day 160, the inferred luminosity of the supersoft component drooped by over an order of magnitude, but the temperature remained the same (see their Figure 6). Moreover, Zemko, Mukai & Orio (2015) found a blackbody-like component with a similar temperature but at a luminosity that was several orders of magnitude lower still in their quiescent *Suzaku* observation. Perhaps the temperature was pegged by either the Eddington or the atmosphere limit (Williams, King & Brooker 1987).

9.5. Advanced X-ray Diagnostics

As mentioned in §6.6, X-ray spectra allow us to measure relative elemental abundances, most commonly that of Fe. It is often found to be sub-solar (see, e.g., Byckling et al. 2010). In contrast, Mukai & Orio (2005) measured an apparent overabundance of Ne in the old nova, V603 Aql. It is not yet clear what the true astrophysical implications are of these findings, but it is essential to keep this possibility in mind when fitting high quality data that are potentially sensitive to elemental abundances.

The ratios of forbidden to intercombination lines of He-like triplets can be used to constrain the density of emitting plasma in principle. However, as is well known in the case of X-rays from early type stars (Leutenegger et al. 2006), photoexcitation by UV photons can also change these ratios. Ratios of certain pairs of Fe L lines can also be used to constrain density (Mauche, Liedahl & Fournier 2001, 2003), and the latter (ratio of intensities of Fe XXII 11.92Å and 11.77Å lines) in particular are less sensitive to photoexcitation. Unfortunately, suitable data with high spectral resolution and high signal-to-noise currently exist only for EX Hya. The story is similar for the He-like triplets: most existing grating data are not of sufficient quality to be useful in this regard (Schlegel et al. 2014). In addition, resonant scattering may play a significant role in shaping the line spectra of some magnetic CVs (Terada et al. 2001, 2004).

Dynamical studies of X-ray emitting plasma have the potential to advance our knowledge of CVs and symbiotic stars significantly. X-ray radial velocity study has so far successfully been performed only for EX Hya (Hoogerwerf, Brickhouse & Mauche 2004) and perhaps marginally for AM Her (Girish, Rana & Singh 2007). The 500 ks HETG observation of EX Hya allowed Luna et al. (2010) to identify a narrow and a broad component in some emission lines. They interpreted the broad component as due to photoionization of the pre-shock flow. The emission lines in SS Cyg and U Gem are found to become broader during outburst (Mauche et al. 2005). In contrast, the lines are narrow in the old nova V603 Aql (Mukai & Orio 2005) and the nova-like system TT Ari (Zemko et al. 2014). Some of this may be due to inclination effect, since V603 Aql is supposed to be a low inclination angle system. However, those of TT Ari and SS Cyg are not very different. This implies that, perhaps, there is a difference between nova like systems and dwarf novae in outbursts, despite the common perception that they are both non-magnetic CVs with high accretion rates.

With the advent of *NuSTAR*, reflection has now securely been detected in magnetic CVs (Mukai et al. 2015). There are efforts under way to study reflection in non-magnetic CVs and in symbiotic stars. These observations should securely measure the reflection amplitudes in the target objects, and allow us to infer if an optically thick disk extends down to the white dwarf surface and/or where the X-ray emission region is located. While such a study was pioneered for SS Cyg by Ishida et al. (2009) using *Suzaku* HXD data, it is worth checking their conclusions with the imaging *NuSTAR* data that are not subject to the systematic uncertainty in the background level of the non-imaging HXD data. Moreover, observations of magnetic CVs may allow us to study the inclination angle dependence of reflection off the white dwarf surface.

Luna et al. (2015) performed a comprehensive spectral analysis of the long *Chandra* HETG observation of EX Hya. Seen in detail, they found the cooling flow model to be lacking in several respects. In particular, while the model can

reproduce the gross features of the spectrum, H-like to He-like line ratios in particular deviated from model predictions. It is clear that we do not yet have a full understanding of the post-shock plasma in magnetic CVs.

Finally, all X-ray emissions convincingly detected from accreting white dwarf binaries so far are thermal emissions, whether they are optically thick or thin. However, non-thermal processes do operate in CVs and symbiotic stars. Radio emissions have been detected from magnetic (Mason & Gray 2007) and non-magnetic (Coppejans et al. 2016) CVs. γ -rays from novae during eruption with *Fermi* (Abdo et al. 2010; Ackermann et al. 2011) are strong evidence of particle acceleration in shocks in novae. However, Kitaguchi et al. (2014) did not confirm the earlier report of non-thermal X-rays in AE Aqr made using non-imaging detectors. One nova, V2491 Cyg that erupted before the launch of *Fermi*, was probably detected above 15 keV using *Suzaku* HXD, and, if confirmed, the origin is likely to be non-thermal (Takei et al. 2009). There was also a transient source in the vicinity of V382 Vel (Nova Velorum 1999) in the *Compton* Gamma Ray Observatory data in the 50–300 keV range (Cheung et al. 2016) that is now suggested to have been the non-thermal emission from this nova. A secure detection of non-thermal X-ray emission would likely allow us to constrain the particle acceleration processes in novae.

10. SUMMARY AND FUTURE PROSPECTS

In this review, I have presented the large body of X-ray observations of accreting white dwarfs, along with introductory materials. The number of objects and subtypes is large to the point of being bewildering to newcomers to the field. The body literature is large, and it is easy for newcomers to miss important papers of the past. I hope this review serves as a useful guide.

I hope to have convinced the readers that the X-ray studies of CVs and symbiotic stars have a lot to teach us about the physics of accretion, including that of accretion disks and the interaction between accretion flow and magnetic field; that they are an important part of the study of the Galaxy we live in, including its collective X-ray emission; that they allow us valuable insight into the evolution of close binaries. Although existing observations have already taught us a lot, there are obviously a lot more to learn. Upcoming releases of *Gaia* distances may also force us to revise our old conclusions.

Existing X-ray missions are still extremely useful, including the flagship missions *Chandra* and *XMM-Newton*; they allow us to reach low flux levels on the one hand and high resolution spectroscopy of the bright sources on the other. *Swift* continues to provide an essential service using its flexible observing capability for CVs and symbiotic stars, particularly novae. We have only scratched the surface of what *NuSTAR* can do, and have not heard any results on accreting white dwarfs using *Astrosat* yet.

The number of known accreting white dwarf binaries will continue to increase. Some will come from X-ray surveys, including the continued use of *INTEGRAL* and *Swift* BAT hard X-ray surveys. Since some of them are highly variable, time-resolved hard X-ray surveys need to be utilized (see, e.g., the case of SU Lyn: Mukai et al. 2016). The forthcoming *eROSITA* mission should discover many new CVs in the soft and medium energy X-rays. The serendipitous source catalogs from *XMM-Newton* (Rosen et al. 2016) and *Swift* (Evans et al. 2014) contain a large number of sources, which have not been fully utilized by the community yet. It might require new approaches such as machine learning focused on variable X-ray sources to select CVs and symbiotic stars for more in-depth studies (see, e.g., Lo et al. 2014). One could perform short, pointed X-ray observations of objects that may turn out to be accreting white dwarf binaries. For example, Sahai et al. (2015) observed asymptotic giant branch stars with far UV excess and detected six, which implies they are previously unrecognized symbiotic stars. Any projects in the area of time-domain astronomy are guaranteed to discover CVs and symbiotic stars; here, again, the problem may well be how to manage and exploit the huge volume of data.

Finally, there will be future X-ray missions with unprecedented capabilities. It is highly likely that there will be an X-ray polarimetry mission in the near future: The *IXPE* mission has been approved in the US, and the *XIPE* mission is being considered in Europe. A sensitive X-ray polarimetry mission has the potential to provide unique insights into the accretion columns of magnetic CVs (Matt 2004). In terms of X-ray spectroscopy, the Japanese and US groups hope to re-fly the ill-fated *Hitomi* mission with an X-ray microcalorimeter, an instrument that provides ~ 5 eV spectral resolution in the Fe K band. This mission will enable dynamical studies and density diagnostics using atomic lines above 2 keV for accreting white dwarfs. Further in the future, *Athena* will bring the era of even higher resolution X-ray spectroscopy as a routine tool for the study of CVs and symbiotic stars.

ACKNOWLEDGMENTS

I thank my frequent collaborators Drs. Jennifer Sokoloski, Thomas Nelson, and Juan Luna, with whom I have had many fruitful discussions. Many others researchers helped me over the years through their own research papers and through more informal discussion. Such colleagues are too numerous to list, but I would like to single out Dr. Christopher Mauche, whose thoughtful papers still have a lot to teach. Specific comments on the earlier versions of this manuscript by Drs. Sokoloski and Luna, as well as by Dr. John Cannizzo on matters related to disk instability have hopefully improved it, although any remaining inaccuracy are my responsibility. In addition to these professional astronomers, I thank the countless volunteer astronomers, many of whom are anything but amateurish, who have contributed to the studies summarized here through the data and the alerts provided through American Association of Variable Star Observers (AAVSO), Center for Backyard Astrophysics (CBA) and other worthy organizations. I acknowledge the financial support NASA under Astrophysics Data Analysis Program grant NNX13AJ13G during the writing of this review.

REFERENCES

- Abdo, A.A., Ackermann, M., Ajello, M., et al. 2010, *Science*, 329, 817
- Ackermann, M., Ajello, M., Albert, A., et al. 2014, *Science*, 345, 554
- Aizu, K. 1973, *Prog. Theoret. Phys.*, 49, 1184
- Allan, A., Hellier, C. & Beardmore, A. 1998, *MNRAS*, 295, 167
- Angelini, L. & Verbunt, F. 1989, *MNRAS*, 238, 697
- Anzolin, G., de Martino, D., Bonnet-Bidaud, J.-M., Mouchet, M., Gänsicke, B.T., Matt, G. & Mukai, K. 2008, *A&A*, 489, 1243
- Balman, S. & Ögelman, H.B. 1999, *ApJ*, 518, L111
- Balman, S. & Revnivtsev, M. 2014, *A&A*, 546, A112
- Balman, S. 2014, *A&A*, 572, A114
- Baptista, R., Borges, B.W. & Oliveira, A.S. 2016, *MNRAS*, 463, 3799
- Barlow, E.J., Knigge, C., Bird, A.J., Dean, A.J., Clark, D.J., Hill, A.B., Molina, M. & Sguera, V. 2006, *MNRAS*, 372, 224
- Baskill, D.S., Wheatley, P.J. & Osborne, J.P. 2005, *MNRAS*, 357, 626
- Baumgartner, W.H., Tueller, J., Markwardt, C.B., Skinner, G.K., Barthelmy, S., Mushotzky, R.F., Evans, P.A. & Gehrels, N. 2013, *ApJS*, 207, A19
- Beardmore, A.P., Done, C., Osborne, J.P. & Ishida, M. 1995, *MNRAS*, 272, 749
- Beardmore, A.P., Mukai, K., Norton, A.J., Osborne, J.P. & Hellier, C. 1998, *MNRAS*, 297, 337
- Beuermann, K. 1999, *Proc. "Highlights in X-ray Astronomy,"* eds. B. Aschenbach & M.J. Freyberg, 1999, MPE Report 272, 410
- Beuermann, K., Burwitz, V. & Reinsch, K. 2012, *A&A*, 543, A41
- Bitner, M.A., Robinson, E.L. & Behr, B.B. 2007, *ApJ*, 662, 564
- Bode, M.F., Seaquist, E.R., Frail, D.A., Roberts, J.A., Whittet, D.C.B., Evans, A. & Albinson, J.S. 1987, *Nature*, 329, 519
- Bode, M.F., O'Brien, T.J., Osborne, J.P., Page, K.L., Senziani, F., Skinner, G.K., Starrfield, S., Ness, J.-U., Drake, J.J., Schwarz, G., Beardmore, A.P., Darnley, M.J., Eyres, S.P.S., Evans, A., Gehrels, N., Goad, M.R., Jean, P., Krautter, J. & Novara, G. 2006, *ApJ*, 652, 629
- Bowyer, S. & Malina, R.F. 1991, *Extreme Ultraviolet Astronomy*, ed. R.F. Malina & S. Bowyer (New York: Pergamon), 391
- Britt, C.T., Maccarone, T., Pretorius, M.L., Hynes, R.I., Jonker, P.G., Torres, M.A.P., Knigge, C., Johnson, C.O., Heinke, C.B., Steeghs, D., Greiss, S. & Nelemans, G., 2015, *MNRAS*, 448, 3455
- Buckley, D.A.H., Haberl, F., Motch, C., Pollard, K., Schwarzenberg-Czerny, A. & Sekiguchi, K. 1997, *MNRAS*, 287, 117
- Byckling, K., Osborne, J.P., Wheatley, P.J., Wynn, G.A., Beardmore, A., Braitto, V., Mukai, K. & West, R., 2009, *MNRAS*, 399, 1576
- Byckling, K., Mukai, K., Thorstensen, J.R. & Osborne, J.P. 2010, *MNRAS*, 408, 2298
- Cannizzo, J.K., Smale, A.P., Wood, M.A., Still, M.D. & Howell, S.B. 2012, *ApJ*, 747, A117
- Cash, J.L. 2002, Ph.D Thesis, University of Wyoming
- Cheng, F.H., Sion, E.M., Horne, K., Hubeny, I., Huang, M. & Vrtilik, S.D. 1997, *AJ*, 114, 1165
- Cheung, C.C., Jean, P., Shore, S.N., Grove, J.E. & Leising, M. 2016, *The 34th International Cosmic Ray Conference*, 30 July–6 August 2015 (The Hague, The Netherlands), PoS(ICRC2015) 880
- Chomiuk, L., Nelson, T., Mukai, K., Sokoloski, J.L., Rupen, M.P., Page, K.L., Osborne, J.P., Kuulkers, E., Moduszewski, A.J., Roy, N., Weston, J. & Krauss, M.I. 2014, *ApJ*, 788, A130

- Coley, J.B., Corbet, R.H.D. & Krimm, H.A. 2015, *ApJ*, 808, A140
- Collins, D.J. & Wheatley, P.J. 2010, *MNRAS*, 402, 1816
- Coppejans, D.L., K rding, E.G., Miller-Jones, J.C.A., Rupen, M.P., Sivakoff, G.R., Knigge, C., Groot, P.J., Woudt, P.A., Waagen, E.A. & Templeton, M. 2016, *MNRAS*, 463, 2229
- Corbet, R.H.D., Sokoloski, J.L., Mukai, K., Markwardt, C.B. & Tueller, J. 2008, *ApJ*, 675, 1424
- C rdova, F.A. & Mason, K.O. 1984, *MNRAS*, 206, 879
- Cropper, M. 1990, *SSRv*, 54, 195
- Cropper, M., Ramsay, G. & Wu, K. 1998, *MNRAS*, 293, 222
- Crowley, C., Espey, B.R. & McCandliss, S.R. 2008, *ApJ*, 675, 711
- Darnley, M.J., Ribeiro, V.A.R.M., Bode, M.F. & Munari, U. 2011, *A&A*, 530, A70
- Darnley, M.J., Ribeiro, V.A.R.M., Bode, M.F., Hounsell, R.A. & Williams, R.P. 2013, *ApJ*, 746, A61
- de Kool, M. & Wickramasinghe, D. 1999, *MNRAS*, 307, 449
- de Martino, D., Matt, G., Mukai, K., Belloni, T., Bonnet-Bidaud, J.-M., Chiappetti, L., G nsicke, B.T., Haberl, F. & Mouchet, M. 2001, *A&A*, 377, 499
- de Martino, D., Matt, G., Mukai, K., Bonnet-Bidaud, J.-M., G nsicke, B.T., Gonzalez Perez, J.M., Haberl, F., Mouchet, M. & Solheim, J.-E. 2005, *A&A*, 437, 935
- de Martino, D., Matt, G., Mukai, K., Bonnet-Bidaud, J.-M., Falanga, M., G nsicke, B.T., Haberl, F., Marsh, T.R., Mouchet, M., Littlefair, S.P. & Dhillon, V. 2008, *A&A*, 481, 149
- Dobrotka, A., Mineshige, S. & Ness, J.-U. 2014, *MNRAS*, 438, 1714
- Dolence, J., Wood, M.A. & Silver, I. 2008, *ApJ*, 683, 375
- Done, C., Osborne, J. P. & Beardmore, A. P. 1995, *MNRAS*, 276, 483
- Done, C. & Magdziarz, P. 1998, *MNRAS*, 298, 737
- Drew, J.E. & Proga, D. 2000, *NewAR* 44, 21
- Ebisawa, K., Mukai, K., Kotani, T., Asai, K., Dotani, T., Nagase, F., Hartmann, H.W., Heise, J., Kahabka, P. & van Teeseling, A. 2001a, *ApJ*, 550, 1007
- Ebisawa, K., Maeda, Y., Kaneda, H. & Yamauchi, S. 2001b, *Science*, 293, 1633
- Edmonds, P.D., Gilliland, R.L., Heinke, C.O. & Grindlay, J.E. 2003a, *ApJ*, 596, 1177
- Edmonds, P.D., Gilliland, R.L., Heinke, C.O. & Grindlay, J.E. 2003b, *ApJ*, 596, 1197
- Evans, P.A., Hellier, C., Ramsay, G. & Cropper, M. 2004, *MNRAS*, 349, 715
- Evans, P.A., Hellier, C. & Ramsay, G. 2006, *MNRAS*, 369, 1229
- Evans, P.A. & Hellier, C. 2007, *ApJ*, 663, 1277
- Evans, P.A., Osborne, J.P., Beardmore, A.P., Page, K.L., Willingale, R., Mountford, C.J., Pagani, C., Burrows, D.N., Kennea, J.A., Perri, M., Tagliaferri, G. & Gehrels, N. 2014, *ApJS*, 210, A8
- Ezuka, H., Ishida, M. & Makino, F. 1998, *ApJ*, 499, 388
- Ezuka, H. & Ishida, M. 1999, *ApJS*, 120, 277
- Fabian, A.C., Lohfink, A., Kara, E., Parker, M.L., Vasudevan, R. & Reynolds, C.S. 2015, *MNRAS* 451, 4375
- Ferland, G.J., Langer, S.H., MacDonald, J., Pepper, G.H., Shaviv, G. & Truran, J.W. 1982, *ApJ*, 262, L53
- Fertig, D., Mukai, K., Nelson, T. & Cannizzo, J.K. 2011, *PASP*, 123, 1054
- Fischer, A. & Beuermann, K. 2001, *A&A*, 373, 211
- Galloway, D.K. & Sokoloski, J.L. 2004, *ApJ*, 613, L61
- G nsicke, B.T., Hoard, D.W., Beuermann, K., Sion, E.M. & Szkody, P. 1998, *A&A*, 338, 933
- G nsicke, B.T., Dillon, M., Southworth, J., Thorstensen, J.R., Rodr guez-Gil, P., Aungwerojwit, A., Marsh, T.R., Szkody, P., Barros, S.C.C., Casares, J., de Martino, D., Groot, P.J., Hakala, P., Kolb, U., Littlefair, S.P., Mart nez-Pais, I.G., Nelemans, G. & Schreiber, M.R. 2009, *MNRAS*, 397, 2170
- Gehrels, N. & Williams, E.D. 1993, *ApJ*, 418, L25
- Gehrels, N. et al. 2004, *ApJ*, 611, 1005
- George, I.M. & Fabian, A.C. 1991, *MNRAS*, 249, 352
- Ghosh, P. & Lamb, F.K. 1979, *ApJ*, 232, 259
- Giacconi, R., Branduardi, G., Briel, U., Epstein, A., Fabricant, D., Feigelson, E., Forman, W., Gorenstein, P., Grindlay, J., Gursky, H., Harnden, F.R., Henry, J.P., Jones, C., Kellogg, E., Koch, D., Murray, S., Schreier, E., Seward, F., Tananbaum, H., Topka, K., Van Speybroeck, L., Holt, S.S., Becker, R.H., Boldt, E.A., Serlemitsos, P.J., Clark, G., Canizares, C., Markert, T., Novick, R., Helfand, D. & Long, K. 1979, *ApJ*, 230, 540
- Girish, V., Rana, V.R. & Singh, K.P. 2007, *ApJ*, 658, 525
- Gosnell, N.M., Pooley, D., Geller, A.M., Kalirai, J., Mathieu, R.D., Frinchaboy, P. & Ramirez-Ruiz, E. 2012, *ApJ*, 745, A57
- Greiner, J., Kruehler, T., Schady, P., Rau, A. & Olivares, F. 2010, *ATel*, 2746
- Grindlay, J.E., Heinke, C., Edmonds, P.D. & Murray, S.S. 2001, *Sci.*, 292, 2290
- Gursky, H., Bradt, H., Doxsey, R., Schwartz, D., Schwarz, J., Dowder, R., Fabbiano, G., Griffiths, R.E., Johnston, M., Leach, R., Ramsey, A. & Spada, G. 1978, *ApJ*, 223, 973
- G ver, T., Ulu yazi, C.,  zkan, M.T. & G g s, E. 2006, *MNRAS*, 372, 450
- Haberl, F. & Motch, C. 1995, *A&A*, 297, L37

- Hailey, C.J., Mori, K., Perez, K., Canipe, A.M., Hong, J., Tomsick, J.A., Boggs, S.E., Christensen, F.E., Craig, W.W., Fornasini, F., Grindlay, J.E., Harrison, F.A., Nynka, M., Rahoui, F., Stern, D., Zhang, S. & Zhang, W.W. 2016, *ApJ*, 826, A160
- Hakala, P., Ramsay, G., Wheatley, P., Harlaftis, E.T. & Papadimitriou, C. 2004, *A&A*, 420, 273
- Hameury, J.-M., Menou, K., Dubus, G., Lasota, J.-P. & Huré, J.-M. 1998, *MNRAS*, 298, 1048
- Harrison, F.A., Craig, W.W., Christensen, F.E., et al. 2013, *ApJ*, A103
- Heise, J., Brinkman, A.C., Gronenschild, E., Watson, M., King, A.R., Stella, L. & Kieboom, K. 1987, *A&A* 148, L14
- Hellier, C. 1993, *MNRAS*, 265 L35
- Hellier, C. 1997, *MNRAS*, 291, 71
- Hellier, C., Mukai, K. & Beardmore, A.P. 1997, *MNRAS*, 292, 397
- Hellier, C., Kemp, J., Naylor, T. Bateson, F.M., Jones, A., Overbeek, D., Stubbings, R. & Mukai, K. 2000, *MNRAS*, 313, 703
- Hellier, C. 2014, *EJP Web of Conferences*, 64, id.07001
- Henze, M., Pietsch, W., Haberl, F., Della Valle, M., Sala, G., Hatzidimitriou, D., Hofmann, F., Hernanz, M., Hartmann, D.H. & Greiner, J. 2014, *A&A*, 563, A2
- Hernanz, M. & Sala, G. 2002, *Science*, 298, 393
- Hertz, P., Bailyn, C.D., Grindlay, J.E., Garcia, M.R., Cohn, H. & Lugger, P.M. 1990, *ApJ*, 364, 251
- Hickman, R., Wheatley, P., Marsh, T.R., Dhillon, V.S., Littlefair, S., Gänsicke, B. 2009, Poster paper presented at the European Week of Astronomy and Space Sciences, 20–23 April 2009, University of Hertfordshire, UK, F-P07 (<http://star.herts.ac.uk/ewass/>)
- Hoogerwerf, R., Brickhouse, N.S. & Mauche, C.W. 2004, *ApJ*, 610, 411
- Hubeny, I. 1990, *ApJ*, 351, 632
- Hubeny, I. 1994, in “Interacting binary stars: a symposium held in conjunction with the 105th Meeting of the Astronomical Society of the Pacific, San Diego State University, 13–15 July 1993,” *ASP Conf. Ser* 56, ed. A.W. Shafter, 3
- Ibarra, A., Kuulkers, E., Osborne, J.P., Page, K., Ness, J.U., Saxton, R.D., Baumgartner, W., Beckmann, V., Bode, M.F., Hernanz, M., Mukai, K., Orio, M., Sala, G., Starrfield, S. & Wynn, G.A. 2009, *A&A*, 497, L5
- Ishida, M. 1991, Ph.D. Thesis, University of Tokyo
- Ishida, M., Morio, K. & Ueda, Y. 2004, *ApJ*, 601, 1088
- Ishida, M., Okada, S., Hayashi, T., Nakamura, R., Terada, Y. Mukai, K. & Hamaguchi, K. 2009, *PASJ*, 61, S77
- Itoh, K., Okada, S., Ishida, M. & Kunieda, H. 2006, *ApJ*, 639, 397
- Jahoda, K., Swank, J.H., Giles, A.B., Stark, M.J., Strohmayer, T., Zhang, W. & Morgan, E.H. 1996, *Proc SPIE*, 2808, 59
- Jansen, F., Lumb, D., Altieri, B., Clavel, J., Ehle, M., Erd, M., Gabriel, C., Guainazzi, M., Gondoin, P., Much, R., Munoz, R., Santos, M., Schartel, N., Texier, D. & Vacanti, G. 2001, *A&A*, 365, L1.
- Joshi, A., Pandey, J.C., Singh, K.P. & Agrawal, P.C. 2016, *ApJ*, 830, A56
- Kahabka, P. & van den Heuvel, E.P.J. 1997, *ARA&A*, 35, 69
- Karowska, M., Schlegel, E., Hack, W., Raymond, J.C. & Wood, B.E. 2005, *ApJ*, 623, L137
- Karowska, M., Gaetz, T.J., Carilli, C.L., Hack, W., Raymond, J.C. & Lee, N.P. 2010, *ApJ*, 710, L132
- Kennea, J.A., Mukai, K., Sokoloski, J.L., Luna, G.J.M., Tueller, J., Markwardt, C.B. & Burrows, D.N. 2009, *ApJ*, 701, 1992
- King, A.R. & Williams, G.A. 1985, *MNRAS*, 215, 1p
- King, A.R. & Watson, M.G. 1987, *MNRAS*, 227, 205
- King, A.R. & Lasota, J.-P. 1991, *ApJ*, 378, 674
- King, A.R. 2000, *ApJ*, 541, 306
- Kitaguchi, T., An, H., Beloborodov, A.M., Gotthelf, E.V., Hayashi, T., Kaspi, V.M., Rana, V.R., Boggs, S.E., Christensen, F.E., Craig, W.W., Hailey, C.J., Harrison, F.A., Stern, D. & Zhang, W.W. 2014, *ApJ*, 782, A3
- Knigge, C., Baraffe, I. & Patterson, J. 2011, *ApJS*, 194, A28
- Kraft, R.P., Mathews, J. & Greenstein, J.L. 1962, *ApJ*, 136, 312
- Krauss, m.I., Chomiuk, L., Rupen, M., Roy, N., Mioduszewski, A.J., Sokoloski, J.L., Nelson, T., Mukai, K., Bode, M.F., Eyres, S.P.S. & O’Brien, T.J. 2011, *ApJ*, 739, L6
- Kuijpers, J. & Pringle, J.K. 1982, *A&A*, 114, L4
- Lamb, D.Q. & Masters, A.R. 1979, *ApJ*, 234, L117
- Lasota, J.-P., Kuulkers, E. & Charles, P. 1999, *MNRAS*, 305, 473
- Lasota, J.-P. 2001, *NewAR*, 45, 449
- Leutenegger, M.A., Paerels, F.B.S., Kahn, S.M. & Cohen, D.H. 2006, *ApJ*, 650, 1096
- Li, K.L., Kong, A.K.H., Charles, P.A., Lu, T.-N., Bartlett, E.S., Coe, M.J., McBride, V., Rajoelimanana, A., Udalski, A., Masetti, N. & Franzen, T. 2012, *ApJ*, 761, A99
- Liebert, J., Bergeron, P. & Holberg, J.B. 2003, *AJ*, 125, 348
- Linnell, A.P., Godon, P., Hubeny, I. Sion, E.M. & Szkody, P. 2007, *ApJ*, 662, 1204

- Liu, F.K., Meyer, F., Meyer-Hofmeister, E. & Burwitz, V. 2008, *A&A*, 483, 231
- Lo, K.K., Farrell, S., Murphy, T. & Gaensler, B.M. 2014, *ApJ*, 786, 20
- Lopes de Oliveira, R., Motch, C., Haberl, F., Negueruela, I. & Janot-Pacheco, E. 2006, *A&A*, 454, 265
- Lubow, S.H. & Shu, F.H. 1975, *ApJ*, 198, 383
- Luna, G.J.M. & Costa, R.D.D. 2005, *A&A*, 435, 1087
- Luna, G.J.M. & Sokoloski, J.L. 2007, *ApJ*, 671, 741
- Luna, G.J.M., Montez, R., Sokoloski, J.L., Mukai, K. & Kastner, J.H. 2009, *ApJ*, 707, 1168
- Luna, G.J.M., Raymond, J.C., Brickhouse, N.S., Mauche, C.W., Proga, D., Steeghs, D. & Hoogerwerf, R. 2010, *ApJ*, 711, 1333
- Luna, G.J.M., Sokoloski, J.L., Mukai, K. & Nelson, T. 2013, *A&A*, 559, A6
- Luna, G.J.M., Raymond, J.C., Brickhouse, N.S., Mauche, C.W. & Suleimanov, V. 2015, *A&A*, 578, A15
- Marsh, T.R. & Steeghs, D. 2002, *MNRAS*, 331, L7
- Marsh, T.R., Gänsicke, B.T., Hümmerich, S., Hamsch, F.-J., Bernhard, K., Lloyd, C., Breedt, E., Stanway, E.R., Steeghs, D.T., Parsons, S.G., Toloza, O., Schreiber, M.R., Jonker, P.G., van Roestel, J., Kupfer, T., Pala, A.F., Dhillon, V.S., Hardy, L.K., Littlefair, S.P., Aungwerojwit, A., Arjyotha, S., Koester, D., Bochinski, J.J., Haswell, C.A., Frank, P. & Wheatley, P.J. 2016, *Nature*, 537, 374
- Mason, K.O. 1985, *SpSciRev*, 40, 99
- Mason, P.A. & Gray, C.L. 2007, *ApJ*, 660, 662
- Matt, G., de Martino, D., Gänsicke, B.T., Negueruela, I., Silvotti, R., Bonnet-Bidaud, J.-M., Mouchet, M. & Mukai, K. 2000, *A&A*, 358, 177
- Matt, G. 2004, *A&A*, 423, 495
- Mauche, C.W., Raymond, J.C. & Mattei, J.A. 1995, *ApJ*, 446, 842
- Mauche, C.W. 1999, in “Annapolis Workshop on Magnetic Cataclysmic Variables,” ASP Conf Ser 157, eds. C. Hellier & K. Mukai, 157
- Mauche, C.W. & Raymond, J.C. 2000, *ApJ*, 541, 924
- Mauche, C.W., Liedahl, D.A. & Fournier, K.B. 2001, *ApJ*, 560, 992
- Mauche, C.W. & Robinson, E.L. 2001, *ApJ*, 562, 508
- Mauche, C.W. 2002, in “Continuing the Challenge of EUV Astronomy: Current Analysis and Prospects for the Future,” ASP Conf Ser. 264, eds. S. Howell, J. Dupuis, D. Golombek, F. Walter & J. Cullison, 75
- Mauche, C.W., Liedahl, D.A. & Fournier, K.B. 2003, *ApJ*, 588, L101
- Mauche, C.W. 2004, *ApJ*, 610, 422
- Mauche, C.W., Wheatley, P.J., Long, K.S., Raymond, J.C. & Szkody, P. 2005, in “The Astrophysics of Cataclysmic Variables and Related Objects,” ASP Conf Ser. 330, eds. J.-M. Hamury & J.-P. Lasota, 355
- Mauche, C.W. 2006, *MNRAS*, 369, 1983
- Mauche, C.W. 2009, *ApJ*, 706, 130
- McGowan, K.E., Priedhorsky, W.C. & Trudolyubov, S.P. 2004, *ApJ*, 601, 1100
- Meyer, F. & Meyer-Hofmeister, E. 1994, *A&A*, 288, 175
- Miller-Jones, J.C.A., Sivakoff, G.R., Knigge, C., Cörding, E.G., Templton, M. & Waagen, E.O. 2013, *Science*, 340, 950
- Mitsuda, K. et al. 2007, *PASJ*, 59, S1
- Mohamed, S. & Podsiadlowski, Ph. 2007, *ASPC*, 372, 397.
- Mukai, K. 1988, *MNRAS*, 232, 175
- Mukai, K. & Shiokawa, K. 1993, *ApJ*, 418, 863
- Mukai, K., Wood, J.H., Naylor, T., Schlegel, E.M. & Swank, J.H. 1997, *ApJ*, 475, 812
- Mukai, K. 1999, *ASP Conf. Ser.* 157, 33
- Mukai, K. & Ishida, M. 2001, *ApJ*, 551, 1024
- Mukai, K., Kallman, T., Schlegel, E., Bruch, A., Handler, G. & Kemp, J. 2001, *ASP Conf. Ser.* 251, 90
- Mukai, K., Kinkhabwala, A., Peterson, J. R., Kahn, S. M. & Paerels, F. 2003, *ApJ*, 586, L77
- Mukai, K. & Orio, M. 2005, *ApJ*, 622, 602
- Mukai, K., Ishida, M., Kilbourne, C. et al. 2007, *PASJ*, 59, 177
- Mukai, K., Orio, M. & Della Valle, M. 2008, *ApJ*, 667, 1248
- Mukai, K., Zietsman, E. & Still, M. 2009, *ApJ*, 707, 652
- Mukai, K., Rana, V., Bernardini, F. & de Martino, D. 2015, *ApJLett*, 807, L30
- Mukai, K., Luna, G.J.M., Cusumano, G., Segreto, A., Munari, U., Sokoloski, J.L., Lucy, A.B., Nelson, T. & Nuñez, N.E. 2016, *MNRASL*, 461, L1
- Munari, U., Dallaporta, S. & Cherini, G. 2016, *NewA*, 47, 7
- Muno, M.P., Baganoff, F.K., Bautz, M.W., Brandt, W.N., Broos, P.S., Feigelson, E.D., Garmire, G.P., Morris, M.R., Ricker, G.R. & Townsley, L.K. 2003, *ApJ*, 589, 225
- Muno, M.P. et al. 2009, *ApJS*, 181, 110
- Mürset, U., Wolff, B. & Jordan, S. 1997, *A&A*, 319, 201
- Mushotzky, R.F. & Szymkowiak, A.E. 1988, in “Cooling flows in clusters and galaxies; Proceedings of the NATO Advanced Research Workshop, Cambridge, England, June 22-26, 1987,” Kluwer Academic Publishers, Dordrecht, Netherlands, p53
- Narayan, R. & Popham, R. 1993, *Nature*, 362, 820
- Naylor, T., Bath, G.T., Charles, P.A., Hassall, B.J.M., Sonneborn, G., van der Woerd, H. & van Paradijs, J. 1988, *MNRAS*, 231, 237
- Naylor, T. & la Dous, C. 1997, *MNRAS*, 290, 160

- Nelson, T., Orio, M., Cassinelli, J.P., Still, M., Leibowitz, E. & Mucciarelli, P. 2008, *ApJ*, 673, 1067
- Nelson, T., Mukai, K., Orio, M., Luna, G.J.M. & Sokolowski, J.L. 2011, *ApJ*, 737, A7
- Nelson, T., Donato, D., Mukai, K., Sokolowski, J. & Chomiuk, L. 2012, *ApJ*, 748, A43
- Nelson, T., Chomiuk, L., Roy, N., Sokolowski, J.L., Mukai, K., Krauss, M.I., Moduszewski, A.J., Rupen, M.P. & Weston, J. 2014, *ApJ*, 785, A78
- Ness, J.-U., Starrfield, S., Burwitz, V., Wichmann, R., Hauschildt, P., Drake, J.J., Wagner, R.M., Bond, H.E., Krautter, J., Orio, M., Hernanz, M., Gehr, R.D., Woodward, C.E., Butt, Y., Mukai, K., Balman, S. & Truran, J.W. 2003, *ApJ*, 594, L127
- Ness, J.-U., Osborne, J.P., Dobrotka, A., Page, K.L., Drake, J.J., Pinto, C., Detmers, R.G., Schwarz, G., Bode, M.F., Beardmore, A.P., Starrfield, S., Hernanz, M., Sala, G., Krautter, J. & Woodward, C.E. 2011, *ApJ*, 733, A70
- Ness, J.-U., Osborne, J.P., Henze, M., Dobrotka, A., Drake, J.J., Ribeiro, V.A.R.M., Starrfield, S., Kuulkers, E., Behar, E., Hernanz, M., Schwarz, G., Page, K.L., Beardmore, A.P. & Bode, M.F. 2013, *A&A*, 559, A50
- Ness, J.-U., Beardmore, A.P., Osborne, J.P., Kuulkers, E., Henze, M., Piero, A.L., Drake, J.J., Dobrotka, A., Schwarz, G., Starrfield, S., Kretschmar, P., Hirsch, M. & Wilms, J. 2015, *A&A*, 578, A39
- Nichols, J.S., DePasquale, J., Kellogg, E., Anderson, C.S., Sokolowski, J. & Pedelty, J. 2007, *ApJ*, 660, 651
- Norton, A.J. & Watson, M.G. 1989, *MNRAS*, 237, 853
- Norton, A.J., Hellier, C., Beardmore, A.P., Wheatley, P.J., Osborn, J.P. & Taylor, P. 1997, *MNRAS*, 289, 362
- Norton, A.J., Butters, O.W., Parker, T.L. & Wynn, G.A. 2008, *ApJ*, 672, 524
- Nucita, A.A., Maiolo, B.M.T., Carpano, S., Belanger, G., Coia, D., Guainazzi, M., de Paolis, F. & Ingrassio, G., 2009, *A&A*, 504, 973
- Nucita, A.A., Kuulkers, E., Maiolo, B.M.T., de Paolis, F., Ingrassio, G., Vetrugno, D 2011, *A&A*, 536, A75
- Núñez, N.E., Nelson, T., Mukai, K., Sokolowski, J.L. & Luna, G.J.M. 2016, *ApJ*, 824, A23
- Orio, M., Nelson, T., Bianchini, A., Di Mille, F. & Harbeck, D. 2010, *ApJ*, 717, 739
- Orio, M., Behar, E., Gallagher, J., Bianchini, A., Chiosi, E., Luna, G.J.M., Nelson, T., Rauch, T. Schaefer, B.E. & Tofflemire, B. 2013, *MNRAS*, 429, 1342
- Orio, M., Mukai, K. & Della Valle, M. 2016, *ATel*, 8625
- Osborne, J.P., Bonnet-Bidaud, J.-M., Bowyer, S., Charles, P.A., Chiappetti, L., Clarke, J.T., Henry, J.P., Hill, G.J., Kahn, S., Maraschi, L., Mukai, K., Treves, A. & Vrtillek, S. 1986, *MNRAS*, 221, 823
- Osborne, J.P., Beuermann, K., Charles, P., Maraschi, L., Mukai, K. & Treves, A. 1987, *ApJ*, 315, L123
- Osborne, J.P., Page, K.L., Beardmore, A.P., Bode, M.F., Goad, M.R., O'Brien, T.J., Starrfield, S., Rauch, T., Ness, J.-U., Krautter, J., Schwarz, G., Burrows, D.N., Gehrels, N., Drake, J.J., Evans, A. & Eyres, S.P.S. 2011, *ApJ*, 727, A124
- Page, K.L., Osborne, J.P., Evans, P.A., Wynn, G.A., Beardmore, A.P., Starling, R.L.C., Bode, M.F., Ibarra, A., Kuulkers, E., Ness, J.-U. & Schwarz, G.J. 2010, *MNRAS*, 401, 121
- Page, K.L., Osborne, J.P., Wagner, R.M., Beardmore, A.P., Shore, S.N., Starrfield, S. & Woodward, C.E. 2013, *ApJ*, 768, L26
- Page, K.L., Osborne, J.P., Kuin, N.P.M., Henze, M., Walter, F.M., Beardmore, A.P., Bode, M.F., Darnley, M.J., Delgado, L., Drake, J.J., Hernanz, M., Mukai, K., Nelson, T., Ness, J.-U., Schwarz, G.J., Shore, S.N., Starrfield, S. & Woodward, C.E. 2015, *MNRAS*, 454, 3108
- Pagnotta, A. & Zurek, D. 2016, *MNRAS*, 458, 1833
- Pandel, D., Córdova, F.A., Shirey, R.E., Ramsay, G., Cropper, M., Mason, K.O., Much, R. & Kilkenney, D. 2002, *MNRAS*, 332, 116
- Pandel, D., Córdova, F.A., Mason, K.O. & Priedhorsky, W.C. 2005, *ApJ*, 629, 396
- Parker, T.L., Norton, A.J. & Mukai, K. 2005, *A&A*, 439, 213
- Parmar, A.N., White, N.E., Giommi, P. & Gottwald, M. 1986, *ApJ*, 308, 199
- Patterson, J. 1981a, *Nature*, 292, 810
- Patterson, J. 1981b, *ApJS*, 45, 517
- Patterson, J., Beuermann, K., Lamb, D.Q., Fabbiano, G., Raymond, J.C., Swank, J. & White, N.E. 1984, *ApJ*, 279, 785
- Patterson, J. & Raymond, J.C. 1985a, *ApJ*, 292, 535
- Patterson, J. & Raymond, J.C. 1985b, *ApJ*, 292, 550
- Patterson, J. 1994, *PASP*, 106, 209
- Patterson, J., Richman, H., Kemp, J. & Mukai, K. 1998, *PASP*, 110, 403
- Patterson, J. & Knigge, C. 2017, *PASP*, in preparation
- Pietsch, W., Fliri, J., Freyberg, M.J., Haberl, F., Riffeser, A. & Sala, G. 2005, *A&A*, 442, 879
- Pinto, C., Ness, J.-U., Verbunt, F., Kaastra, J.S., Costantini, E. & Detmers, R.G. 2012, *A&A*, 543, A134
- Popham, R. & Narayan, R. 1995, *ApJ*, 442, 337

- Pratt, G.W., Hassall, B.J.M., Naylor, T. & Wood, J.H. 1999, *MNRAS*, 307, 413
- Pratt, G.W., Mukai, K., Hassall, B.J.M., Naylor, T. & Wood, J.H. 2004, *MNRAS*, 348, L49
- Predehl, P. & Schmitt, J.H.M.M. 1995, *A&A*, 293, 889
- Press, W.H. & Rybicki, G.B. 1989, *ApJ*, 338, 277
- Pretorius, M.L., Knigge, C., O'Donoghue, D., Henry, J.P., Gioia, I.M. & Mullis, C.R. 2007, *MNRAS*, 382, 1279
- Pretorius, M.L. & Knigge, C. 2012, *MNRAS*, 419, 1442
- Pretorius, M.L., Knigge, C. & Schwöpe, A.D. 2013, *MNRAS*, 432, 570
- Pretorius, M.L. & Mukai, K. 2014, *MNRAS*, 442, 2580
- Priedhorsky, W., Marshall, F.J. & Hearn, D.R. 1987, *A&A*, 173, 95
- Pringle, J.E. & Webbink, R.F. 1975, *MNRAS*, 172, 493
- Pringle, J.E. 1977, *MNRAS*, 178, 195
- Ramsay, G., Mason, K.O., Cropper, M., Watson, M.G. & Clayton, K.L. 1994, *MNRAS*, 270, 692
- Ramsay, G., Cropper, M., Hellier, C. & Wu, K. 1998, *MNRAS*, 297, 1269
- Ramsay, G., Poole, T., Mason, K., Córdoba, F., Priedhorsky, W., Breeveld, A., Much, R., Osborne, J., Pandel, D., Potter, S., West, J. & Wheatley, P. 2001, *A&A*, 365, L288
- Ramsay, G. & Cropper, M. 2004, *MNRAS*, 347, 497
- Ramsay, G., Cropper, M., Wu, K., Mason, K.O., Córdoba, F.A., & Priedhorsky, W. 2004, *MNRAS*, 350, 1373
- Ramsay, G., Hakala, P., Wu, K., Cropper, M., Mason, K.O., Córdoba, F.A. & Priedhorsky, W. 2005, *MNRAS*, 357, 49
- Ramsay, G., Groot, P.J., Marsh, T., Nelemans, G., Steeghs, D. & Hakala, P. 2006, *A&A*, 457, 623
- Ramsay, G. & Cropper, M. 2007, *MNRAS*, 379, 1209
- Ramsay, G., 2008, *MNRAS*, 384, 687
- Ramsay, G., Wheatley, P.J., Norton, A.J., Hakala, P. & Baskill, D. 2008, *MNRAS*, 387, 1157
- Ramsay, G., Sokoloski, J.L., Luna, G.J.M. & Nuñez, N.E., 2016, *MNRAS*, 461, 3599
- Reimer, T.W., Welsh, W.F., Mukai, K. & Ringwald, F.A. 2008, *ApJ*, 678, 276
- Reis, R.C., Wheatley, P.J., Gänsicke, B.T. & Osborne, J.P. 2013, *MNRAS*, 430, 1994
- Revnivtsev, M., Sazonov, S., Gilfanov, M., Churazov, E., & Sunyaev, R. 2006, *A&A* 452, 169
- Revnivtsev, M., Sazonov, S., Churazov, E., Forman, W., Vikhlinin, A. & Sunyaev, R. 2009, *Nature*, 458, 1142
- Rosen, S.R., Mason, K.O., Mukai, K. & Williams, O.R. 1991, *MNRAS*, 249, 417
- Rosen, S.R. 1992, *MNRAS*, 254, 493
- Rosen, S.R., Webb, N.A., Watson, M.G. et al. 2016, *A&A*, 590, A1
- Rothschild, R. E., Gruber, D. E., Knight, F. K., Matteson, J. L., Nolan, P. L., Swank, J. H., Holt, S. S., Serlemitsos, P. J., Mason, K. O. & Tuohy, I. R. 1981, *ApJ*, 250, 723
- Sahai, R., Sanz-Forcada, J., Sánchez Contreras, C. & Stute, M. 2015, *ApJ*, 810, A77
- Sambruna, R.M., Parmar, A.N., Chiappetti, L., Maraschi, L. & Treves, A. 1994, *ApJ*, 424, 947
- Scargle, J.D. 1982, *ApJ*, 263, 835
- Schlegel, E.M., Shipley, H.V., Rana, V.R., Barrett, P.E. & Singh, K.P. 2014, *ApJ*, 797, A38
- Schmidt, G.D. & Stockman, H.S. 1991, *ApJ*, 371, 749
- Schreiber, M.R., Hameury, J.-M. & Lasota, J.-P. 2003, *A&A*, 410, 239
- Schwarz, R., Schwöpe, A.D., Staude, A., Rau, A., Hasinger, G., Urrutia, T. & Motch, C. 2007, *A&A*, 473, 511
- Schwarz, G.J., Ness, J.-U., Osborne, J.P., Page, K.L., Evans, P.A., Beardmore, A.P., Walter, F.M., Hilton, L.A., Woodward, C.E., Bode, M., Starrfield, S. & Drake, J.J. 2011, *ApJS*, 197, A31
- Schwöpe, A., Schwarz, R., Sirk, M. & Howell, S.B. 2001, *A&A*, 375, 419
- Shaviv, G. & Wehrse, R. 1986, *A&A*, 159, L5
- Silber, A.D. 1992, Ph.D. Thesis, Massachusetts Institute of Technology
- Sion, E.M., Cheng, F.-H., Huang, M., Hubeny, I. & Szkody, P. 1996, *ApJ*, 471, L41
- Smith, R.K. & Hughes, J.P. 2010, *ApJ*, 718, 583
- Sokoloski, J.L. & Bildsten, L. 1999, *ApJ*, 517, 919
- Sokoloski, J.L., Kenyon, S.J., Epsley, B.R., Keyes, C.D., McCandliss, S.R., Kong, A.K.H., Aufdenberg, J.P., Filippenko, A.V., Li, W., Brocksopp, C., Kaiser, C.R., Charles, P.A., Rupen, M.P. & Stone, R.P.S. 2006, *ApJ*, 636, 1002
- Sokoloski, J.L., Luna, G.J.M., Mukai, K. & Kenyon, S.J. 2006, *Nature*, 442, 276
- Sokoloski, J.L. & Bildsten, L. 2010, *ApJ*, 723, 1188
- Solheim, J.-E. 2010, *PASP*, 122, 1133
- Strohmayr, T.E. 2004, *ApJ*, 608, L53
- Strohmayr, T.E. 2008, *ApJ*, 679, L109
- Suleimanov, V., Revnivtsev, M. & Ritter, H. 2005, *A&A*, 435, 191
- Szkody, P., Long, K.S., Sion, E.M. & Raymond, J.C. 1996, *ApJ*, 469, 834
- Takei, D., Tsujimoto, M., Kitamoto, S., Ness, J.-U., Drake, J.J., Takahashi, H. & Mukai, K. 2009, *ApJ*, 697, L54
- Takei, D., Drake, J.J., Yamaguchi, H., Slane, P., Uchiyama, Y. & Katsuda, S. 2015, *ApJ*, 801, A92
- Tanaka, Y., Inoue, H. & Holt, S.S. 1994, *PASJ*, 46, L37

- Taylor, B.G., Andresen, R.D., Peacock, A. & Zobl, R. 1981, *SSRv*, 30, 479
- Terada, Y., Ishida, M., Makishima, K., Imanari, T., Fujimoto, R. Matsuzaki, K. & Kaneda, H. 2001, *MNRAS*, 328, 112
- Terada, Y., Ishida, M. & Makishima, K. 2004, *PASJ*, 56, 523
- Thorstensen, J.R., Lépine, S. & Shara, M. 2008, *AJ*, 136, 2107
- Trümper, J. 1983, *AdSpR*, 2, 241.
- Tueller, J., Baumgartner, W.H., Markwardt, C.B., et al. 2010, *ApJS*, 186, 378
- Turner, M.J.L., Thomas, H.D., Patchett, B.E., Reading, D.H., Makishima, K., Ohashi, T., Dotani, T., Hayashida, K., Inoue, H., Kondo, H., Koyama, K., Mitsusa, K., Ogawara, Y., Takano, S., Awaki, H., Tawara, Y & Nakamura, N. 1989, *PASJ*, 41, 345
- Uthas, H., Knigge, C. & Steeghs, D. 2010, *MNRAS*, 409, 237
- Valyavin, G., Shulyak, D., Wade, G.A., Antonyuk, K., Zharikov, S.V., Galazutdinov, G.A., Plachinda, S., Bagnulo, S., Fox Machado, L., Alvarez, M., Clark, D.M., Lopez, L.M., Hiriart, D., Han, I., Jeon, Y.-B., Zurita, C., Mujica, R., Burlakova, T., Szeifert, T. & Burenkov, A. 2014, *Nature*, 515, 88
- van den Berg, M., Grindlay, J., Laycock, S., Hong, J., Zhao, P., Koenig, X., Schlegel, E.M., Cohn, H., Lugger, P., Rich, R.M., Dupree, A.K., Smith, G.H. & Strader, J. 2004, *ApJ*, 647, L135
- van Teeseling, A., Drake, J.J., Drew, J.E., Hoare, M.G. & Verbunt, F. 1995, *A&A*, 300, 808
- van Teeseling, A., Beuermann, K. & Verbunt, F. 1996, *A&A*, 315, 467
- Vaytet, N.M.H., O'Brien, T.J. & Bode, M.F. 2007, *ApJ* 665, 654
- Wada, Q., Tsujimoto, M., Ebisawa, K. & Hayashi, T. 2017, *PASJ*, in press
- Warner, B. 1989, *IBVS*, 3383
- Warner, B. 1995, *Cataclysmic Variable Stars* (Cambridge: Cambridge University Press
- Warner, B. 2002, in "Classical Nova Explosions," *AIP Conf. Proc.* 637, eds. M. Hernanz & J. José, 3
- Warwick, R.S., Turner, M.J.L., Watson, M.G. & Willingale, R. 1985, *Nature*, 317, 218
- Weisskopf, M.C., O'Dell, S.L. & van Speybroeck, L.P 1996, *Proc. SPIE* 2085, 2
- Welsh, W.F., Horne, K. & Gomer, R. 1998, *MNRAS*, 298, 285
- Weston, J.H.S., Sokoloski, J.L., Metzger, B.D., Zheng, Y., Chomiuk, L., Krauss, M.I., Linford, J.D., Nelson, T., Mioduszewski, A.J., Rupen, M.P., Finzell, T. & Mukai, K. 2016a, *MNRAS*, 457, 887
- Weston, J.H.S., Sokoloski, J.L., Chomiuk, L., Linford, J.D., Nelson, T., Mukai, K., Finzell, T., Mioduszewski, A.J., Rupen, M.P. & Walter, F.M. 2016b, *MNRAS*, 460, 2687
- Wheatley, P.J., Mauche, C.W. & Mattei, J.A. 2003, *MNRAS*, 345, 49
- Wheatley, P.J. & West, R.G. 2003, *MNRAS*, 345, 1009
- Wijngaarden, M.J.P., Gourdji, K., Oostrum, L.C. & Henrichs, H.F. 2016, *Astronomers Telegram*, No. 9634
- Williams, G.A., King, A.R. & Brooker, J.R.E. 1987, *MNRAS*, 266, 725
- Williams, G. 2003, *PASP*, 115, 618
- Wilms, J., Allen, A. & McCray, R. 2000, *ApJ*, 542, 914
- Winkler, C., Courvoisier, T.J.-L., Di Cocco, G., Gehrels, N., Giménez, A., Grebenev, S., Hermsen, W., Mas-Hesse, J.M., Lebrun, F., Lund, N., Palumbo, G.G.C., Paul, J., Roques, J.-P., Schnopper, H., Schönfelder, V., Sunyaev, R., Teegarden, B., Ubertini, P., Vedrenne, G. & Dean, A.J. 2003, *A&A*, 411, L1
- Wynn, G.A. & King, A.R. 1992, *MNRAS*, 255, 83
- Xu, X.-J., Wang, Q.D. & Li, X.-D. 2016, *ApJ*, 818, A136
- Yamauchi, S., Nobukawa, K.K., Nobukawa, M., Uchiyama, H. & Koyama, K. 2016, *PASJ*, 68, A59
- Yoshida, K., Inoue, H. & Osaki, Y. 1992, *PASJ*, 44, 537
- Yuasa, T., Nakazawa, K., Makishima, K., Saitou, K., Ishida, M., Ebisawa, K., Mori, H. & Yamada, S. 2010, *A&A*, 520, A25
- Yuasa, T., Makishima, K. & Nakazawa, K. 2012, *ApJ*, 753, A129
- Zemko, P., Orio, M., Mukai, K. & Shugarov, S. 2014, *MNRAS*, 445, 869
- Zemko, P., Mukai, K. & Orio, M. 2015, *ApJ*, 807, A61